Determining the Effects of Duct Fittings on Volumetric Air flow Measurements

by

CRAIG HICKMAN

B.S., Kansas State University, 2004

A THESIS

submitted in partial fulfillment of the requirements for the degree

MASTER OF SCIENCE

Department of Mechanical and Nuclear Engineering
College of Engineering

KANSAS STATE UNIVERSITY
Manhattan, Kansas

2010

Approved by:

Major Professor
B. Terry Beck

Abstract

The purpose of the research was to quantify the influence of several duct disturbances on volumetric flow rate measurements and use these in developing guidelines for field technicians. This will assist the field technicians in making more accurate volumetric air flow measurements in rectangular ducts during a test and balance operation.

Multiple duct sizes, fittings, probes, traverse algorithms, and locations upstream and downstream of the disturbances are used to compare a variety of situations. The two traverse algorithms used are the log-Tchebycheff and equal area methods. Two upstream and five downstream locations are tested for each duct configuration. Two air velocity probes are used for local velocity measurements on each traverse: a pitot-static probe and a hot wire anemometer. A nozzle bank and Air Flow Measurement Station are used as the flow measurement standards for comparison with each traverse.

This paper discusses the setup and initial results of ASHRAE 1245-RP. Data collected subsequent to this thesis will complete the balance of results and will be collected and analyzed by other researchers. Results will be summarized and presented in a way which allows technicians to use it in the field for more accurate balancing results.

Table of Contents

List of Figures

List of Tables

Acknowledgements

I would like to thank ASHRAE's Technical Committees, TC 1.2, Instruments and Measurements, and TC 7.7, Testing and Balancing, for initiation of the research project (ASHRAE 1245-RP). I would also like to thank the project monitoring subcommittee (PMS) for their support on the project. The following members served on the PMS: Frank Spevak, Jim Clarke, Andy Nolfo, Gaylon Richardson, and Charlie Wright . Specifically I would like to thank Gaylon Richardson and Andy Nulfo for organizing the donation of the blower and variable frequency drive used by the project. I would like to thank TSI Inc. for donation of the measurement probes used to perform the traverse measurements. A thank you also goes to Ronaldo Maghirang for the use of the nozzle chamber used in the measurements. Finally I would like to thank my supervisory committee: B. Terry Beck, Bruce Babin, and Steve Eckels for their continued support over the course of the project.

CHAPTER 1 - Introduction

The purpose of the research was to quantify the influence of several duct disturbances on volumetric flow rate measurements and use these in developing guidelines for field technicians. This paper discusses the setup and initial results of ASHRAE 1245-RP. Data collected subsequent to this thesis will complete the balance of results and will be collected and analyzed by other researchers. Results will be summarized and presented in a way which allows technicians to use it in the field for more accurate balancing results.

1.1 Background and Relevant Literature

Current methods of making volumetric air flow measurements in the field are prone to a number of known inaccuracies. As field technicians are required to take measurements in non-ideal circumstances, these inaccuracies in the air flow measurements will exist. These situations are unavoidable due to physical limitations caused by the construction of building duct systems. This usually means that measurements are taken closer to a disturbance than would normally be desirable. These measurements are used in the test and balancing procedures associated with HVAC systems designed to meet comfort and air quality requirements. The data gathered in this project will be used in an attempt to quantify the error caused by the distance from a disturbance to a given air flow measurement (traverse) location.

A duct traverse can be performed as an acceptable method of measuring volumetric air flow rate. According to ASHRAE Standard 111-1988 qualified technicians can obtain accuracies of 5% to 10% in good conditions. When good conditions don't exist errors can be greater than +/-10%. For ASHRAE 1245-RP two duct traverse algorithms were used which are the log-Tchebycheff and equal area methods. According to (MacFerren, E., 1999) the equal area method is almost exclusively used in the United States and many test and balance contractors acknowledge that there is little difference between the two methods in terms of contract cost, labor, and time. There has been some controversy over which method is more accurate. It has been the conclusion by the majority of the HVAC industry, and the recommendation of ASHRAE standard 111-1988, that the log-Tchebycheff traversing method yields a more accurate assessment of volumetric flow rate than the equal area method. One possible explanation for this

is that the log-Tchebycheff method uses points closer to the wall of the duct, and thus is better at quantifying wall friction effects. (MacFerren, E., 1999) supports these conclusions finding that the equal area method consistently produces errors from 5% to 9% and up to 20% above actual air flow. This project investigated this issue in an attempt to confirm or deny the conclusion that the equal area method consistently produces a bias error compared to log-Tchebycheff.

Duct traverses aren't always possible considering upstream duct length requirements and other physical limitations. It is common that air flow measurements are made with rotating vane anemometers on diffusers, grill faces, or coil faces of an HVAC system. The use of vane anemometers has been the topic of previous research [13-24]. Several influences were uncovered which significantly add to the inaccuracy of these measurements including turbulence levels, probe size, sensitivity to probe location, and non-uniform velocity profiles.

This research followed the guidelines of three standards for conducting measurements. The first is ASHRAE Standard 111-1988 which is used for the balancing of HVAC systems and describes the log-Tchebycheff method. The log-Tchebycheff method is also described in the ASHRAE Fundamentals Handbook and (ISO 3966, 1977). The equal area method is described in the (AABC, 2002) standard and also in the ASHRAE Fundamentals Handbook. The final standard is ASHRAE Standard 120-1999 which describes the measurement of air flow by use of nozzles or orifice plates. Standard 120 will be used for calculation of volumetric air flow at the nozzle bank which is the standard that all traverse measurements will be compared to.

1.2 Testing

Testing was to be done with three duct sizes upstream of the disturbance. These include 24" x 24", 48" x 12", and 28" x 14". The effects of four disturbances were to be evaluated in this research. These include a 90^o mitered easy bend elbow, 90^o and 60^o rectangular-to-rectangular concentric transitions, and a 90^o diverging tee with 45^o entry. Prior to the submittal of this thesis, data was collected for the 24" x 24" upstream duct size. The impact of these flow disturbances were determined by comparing the results of duct traverses to a flow measurement standard. The measurement standard used was a nozzle bank for all duct configurations. Configurations using a tee as the duct disturbance required second measurement standard in conjunction with the nozzle bank. An Air Flow Measurement Station (FMS) was used as the second standard. The traverses were conducted at several locations upstream and downstream of

each disturbance. The traverses were conducted in a similar manner to that which a field technician would use but with some changes to improve consistency. These additional measures were meant to limit the potential of bias errors caused by variations in traverse methods between researchers.

While distance from a disturbance is the main focus of the project, other causes of error were considered. The issues to be investigated include the affect of the traverse method and the type of probe. For ASHRAE 1245-RP the traverse algorithms used were log-Tchebycheff and equal area. The project also compared two probe types to investigate any bias one may have over the other. The probes used to perform the traverses were a pitot-static probe and a thermal anemometer. It should further be noted that the probes used were typical of the probes actually in use by field engineers used in test and balance operations. Four velocities of 600, 1200, 1800, and 2400 fpm were to be tested in each of the duct sizes and aspect ratios. This thesis discusses results for a 24" x 24" upstream duct. The rest of the measurements for ASHRAE 1245-RP will come later from different researchers and include the upstream duct sizes of 48" x 12" and 28" x 14".

CHAPTER 2 - Experimental Facility

Except in the tee testing, the general layout of the experimental facility consists of three main components: (1) a blower, (2) a multi-nozzle chamber, (3) duct configurations under test. A fourth component was used for the duct configurations with the diverging tee fitting. This component was a Flow Measurement Station (FMS), used for measurements of air flow in the main line of the tee fitting configuration while traverses were taken in the branch line of each tee. Figure 2.1 and Figure 2.2 are schematics of the general test site and layout for the different duct disturbances. Figures 2.3 and 2.4 are pictures of the general test setup. Other equipment needed were velocity probes, pressure transducers, temperature sensors, a humidity sensor, a manometer, a computer and data acquisition equipment, and devices to hold the probes in the correct position of the duct.

There were several requirements of the facility which made it difficult to find a suitable place to conduct the tests. A large footprint was required. The duct configurations, including the nozzle bank chamber, and blower resulted in a total length in excess of 80 ft. The width requirement was more than 25 ft. The blower used for the project also required access to 3 phase power. Other requirements for the test facility environment included a location with stable ambient conditions and a level surface for assembly and operation of the duct configurations.

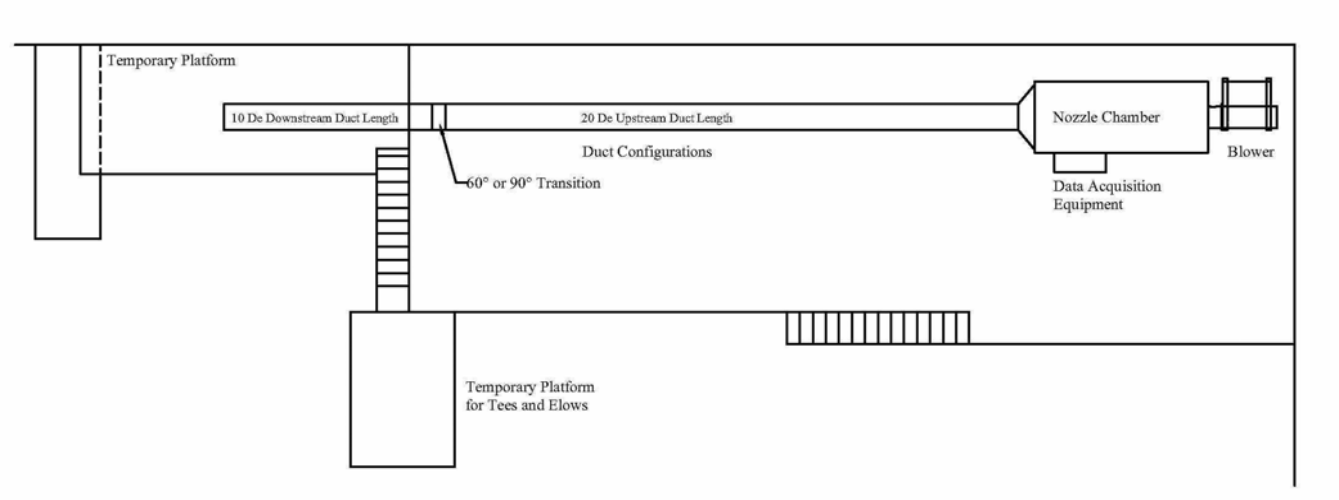

(a) Transitions

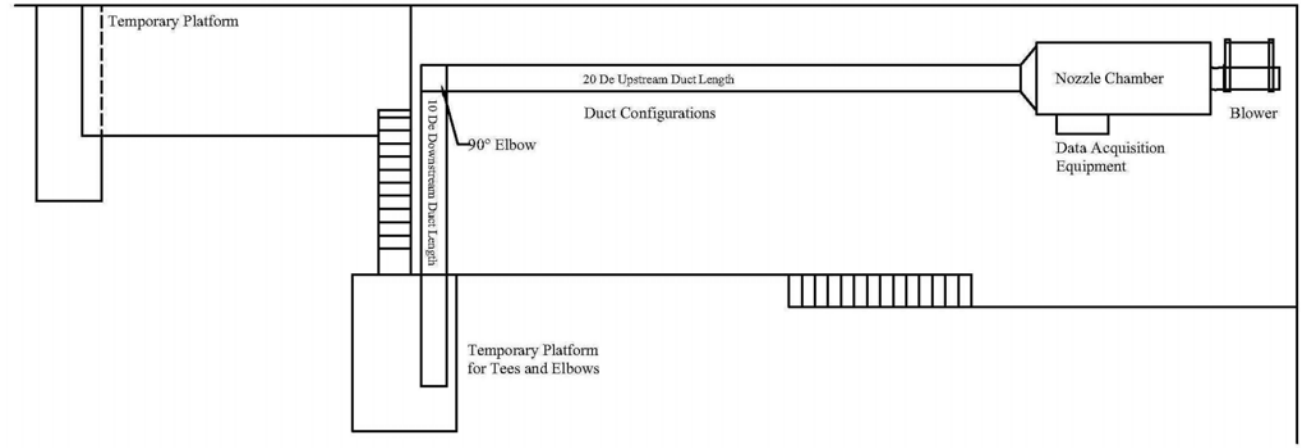

(b) Elbows

Figure 2.1 General Test Area (a) Transitions and (b) Elbows

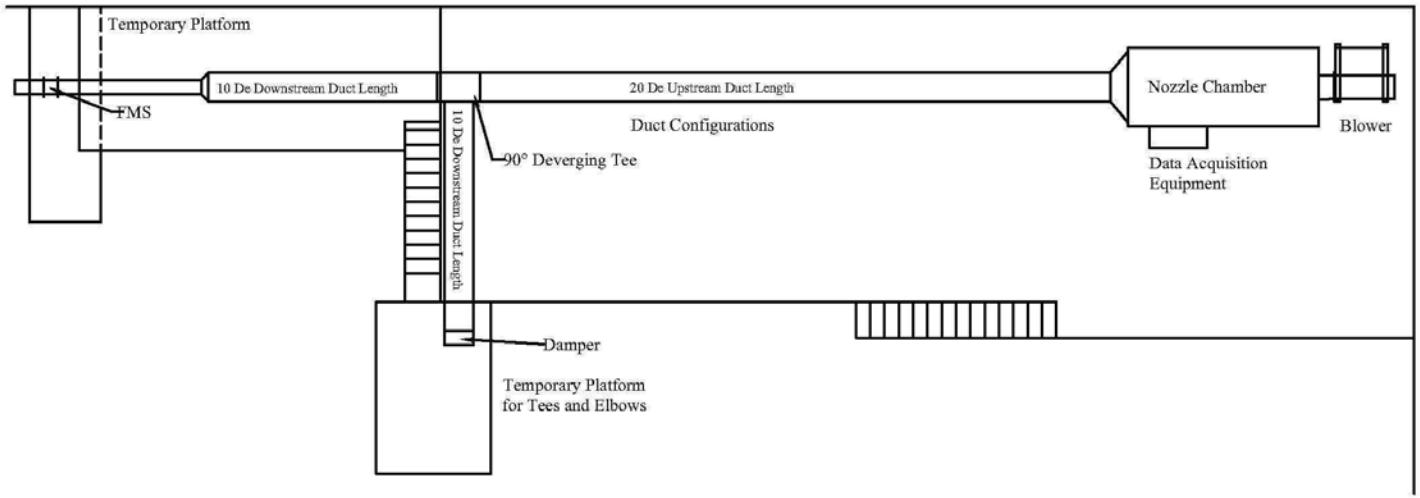

Figure 2.2 General Test Area (Tees)

Figure 2.3 General Test Site 1

Figure 2.4 General Test Site 2

2.1 Blower

The maximum flow rate requirement of 9600 SCFM required a large capacity blower. It was determined that at the maximum flow rate the blower would have to provide a static pressure head of approximately 8 inches of water in order to overcome losses in the system. A Greenheck 30 BISW-41-55 backward inclined blower was donated for use on this facility. The blower was powered by a Saftronics C10 Vector AC Drive. This variable frequency drive allows for the adjustment of flow rate. The blower was capable of being run with multiple voltages including 460, 230 and 208 volts 3 phase. The voltage available at the location was 208 volts. The adjustment of the VFD frequency setting was done manually by the researcher.

2.2 Nozzle Bank Flow Measurement Standard

For this research a nozzle bank chamber was used as the flow measurement standard for comparison with all other volumetric flow measurements in particular comparison with the traversing methods. The nozzle bank was also used for calibration of the flow measurement station (FMS) device. The nozzle bank chamber has three major functions: (1) to connect to and receive flow from the blower, (2) to measure the air flow rate, and (3) to distribute the flow uniformly to the particular duct configuration being used. (Heber et al., 1991) describes the construction of the nozzle chamber. The nozzle chamber was constructed in compliance with AMCA Standard 210-85.

A detailed schematic of the chamber is shown in Figure 2.5 below and pictures are available in Figures 2.9 and 2.10. (Heber et al., 1991) describes the chamber as a baffled multi-nozzle chamber. The flow chamber consists of five upstream flow diffuser screens, a nozzle bank containing nine nozzles, and three downstream diffuser screens. The chamber was constructed with 0.75" thick plywood and 1" angle iron framing. (Heber et al., 1991) discusses sealing of the chamber but recommended rechecking of the chamber seals after transportation, which was necessary for this application. Seal tests were performed on the chamber, as well as, on a representative duct configuration. More information about the seal test is given in Appendix A.

Diffuser screens are used to distribute and straighten the flow in the nozzle chamber. The diffuser screens are round-wire, square-mesh screens. The location of diffuser screens is based

on the equivalent diameter (De) of the chamber. These distances are shown in Figure 2.5 below. De is calculated from the inside height and width of the chamber as follows:

$$D_e = \sqrt{\frac{4(\text{width})(\text{height})}{\pi}} \quad \textbf{(1)}$$

(Heber et al., 1991) makes note of the AMCA Standard 210-85 requirement that the maximum velocity 0.1De downstream of the diffusers shall not exceed the average velocity by more than 25% when the maximum velocity is more than 2m/s (400 fpm). And that this requirement is not enforced at lower velocities.

The nozzle bank consists of nine aluminum-spun nozzles. Their nominal dimensions are available in Table 2.1 and their layout over the duct cross-section is presented in Figure 2.7. A picture of the nozzle bank is available in Figure 2.11. For the nozzles exact dimensions and uncertainties measured by the researchers see Table 5.1 and Table 5.2. The nozzle bank was used to determine the flow rate. The pressure drop across the nozzle bank was measured by means of two Piezometer rings which detect the static pressure differential. Each ring is made of copper tube and contains four pressure taps, one on each side of the chamber. The static pressure given from each ring represents the average of these four static pressure taps. There is a Piezometer ring on each side of the nozzle bank as well as one in front of the downstream diffuser screens. This third ring was used in Heber's work but was not needed for the current research. The dimensions of the pressure taps are shown in Figure 2.6.

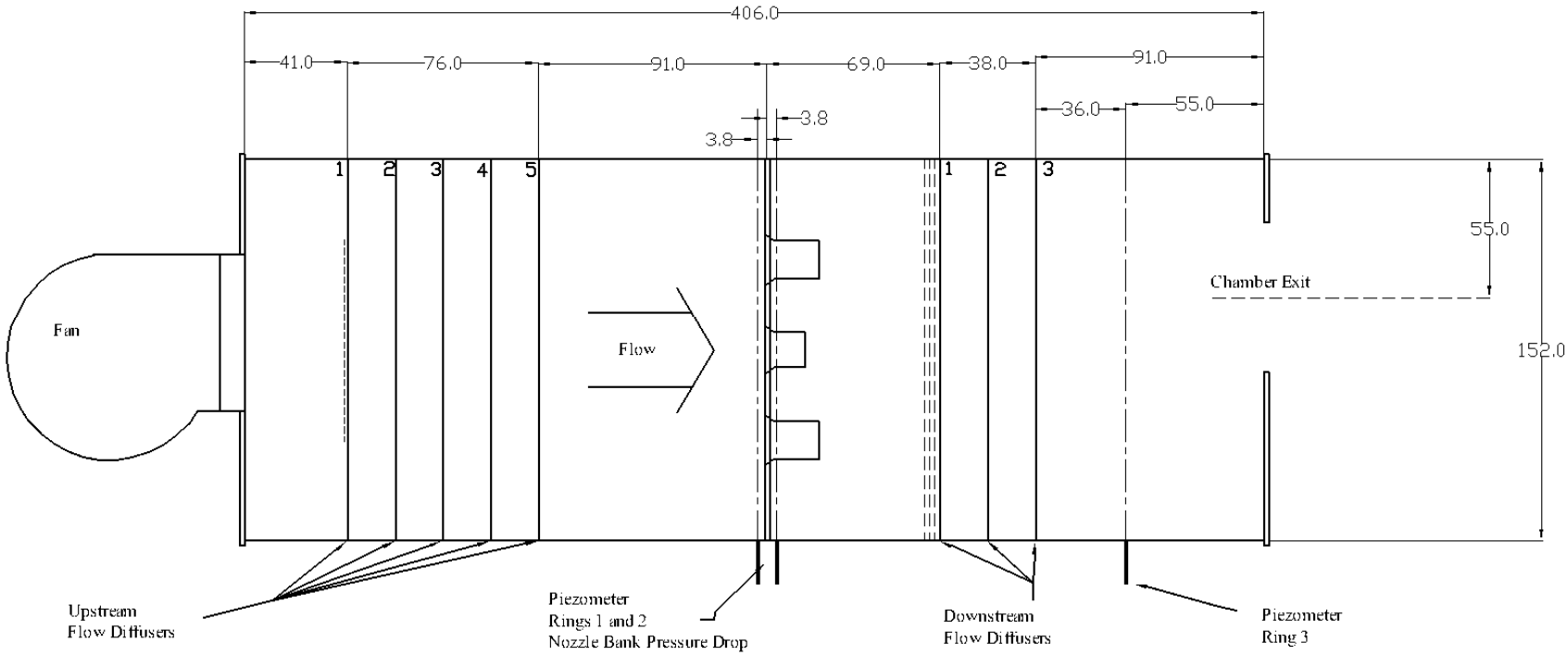

Note: Dimensions in cm

Figure 2.5 Nozzle Chamber based on (Heber et al., 1991)

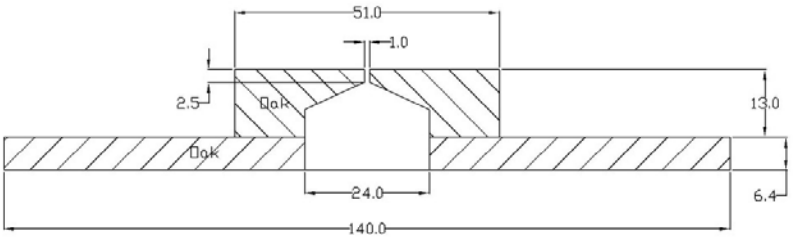

Note: Dimensions in mm

Figure 2.6 Pressure Tap based on (Heber et al., 1991)

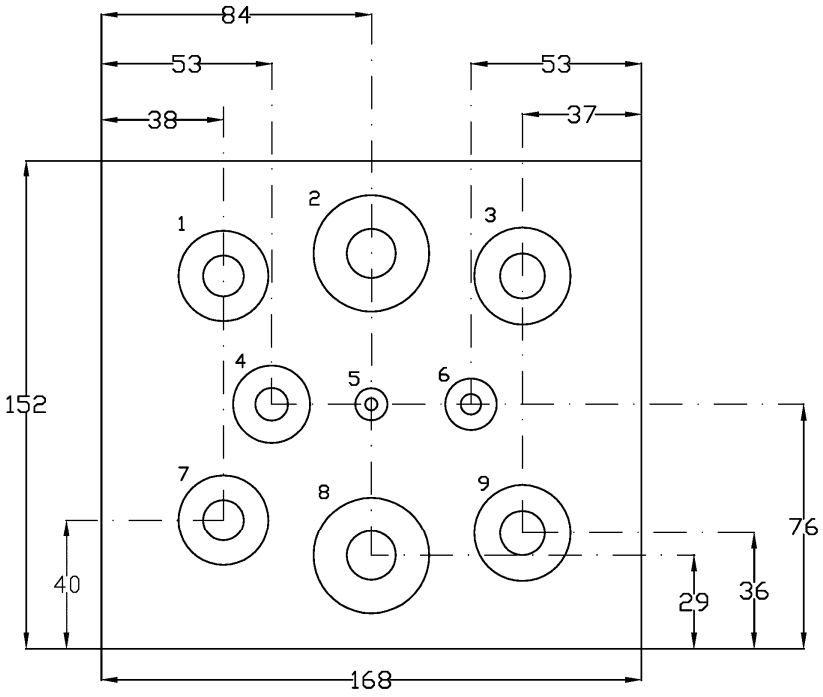

Note: Dimensions in cm

Figure 2.7 Nozzle Layout based on (Heber et al., 1991)

Table 2.1 Nozzle Dimensions

Nozzle	Diameter		Area
	Inches	cm	cm^2
1	5.000	12.700	126.68
2	6.000	15.240	182.41
3	5.500	13.970	153.28
4	4.000	10.160	81.07
5	1.600	4.064	12.97
6	2.500	6.350	31.67
7	5.000	12.700	126.68
8	6.000	15.240	182.41
9	5.500	13.970	153.28

Some alterations to the facility were required for the research. First of all the opening from the chamber to the duct needed to be enlarged. This was due to the large duct test section to be tested. The opening was made significantly larger than the duct and a transition was built to attach the duct to the chamber. The larger transition was implemented to reduce the pressure drop caused by the chamber exit and provide as little disturbance to the exiting flow as possible. A second alteration was made to the opening at the inlet of the chamber to accommodate the new blower. The new 9,600 CFM blower required a larger opening at the chamber entrance. So as not to constrict the flow at the blower exit, the opening in the chamber was made the same size as the blower exit area. Flex duct was used to connect the blower to the chamber. A schematic similar to Figure 2.5 with these changes made is presented in Figure 2.8 below. Pictures of the nozzle chamber are presented in Figure 2.9 and Figure 2.10.

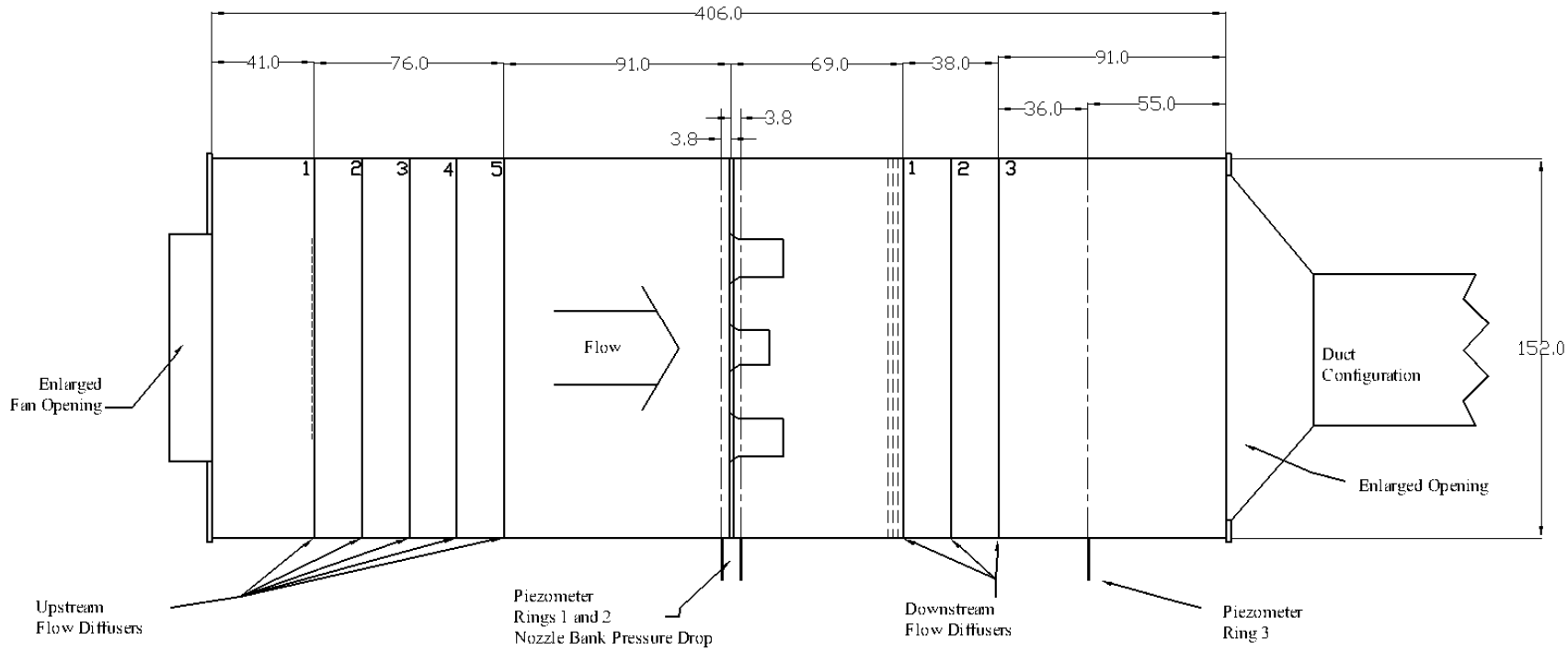

Note: Dimensions in cm

Figure 2.8 Altered Nozzle Chamber

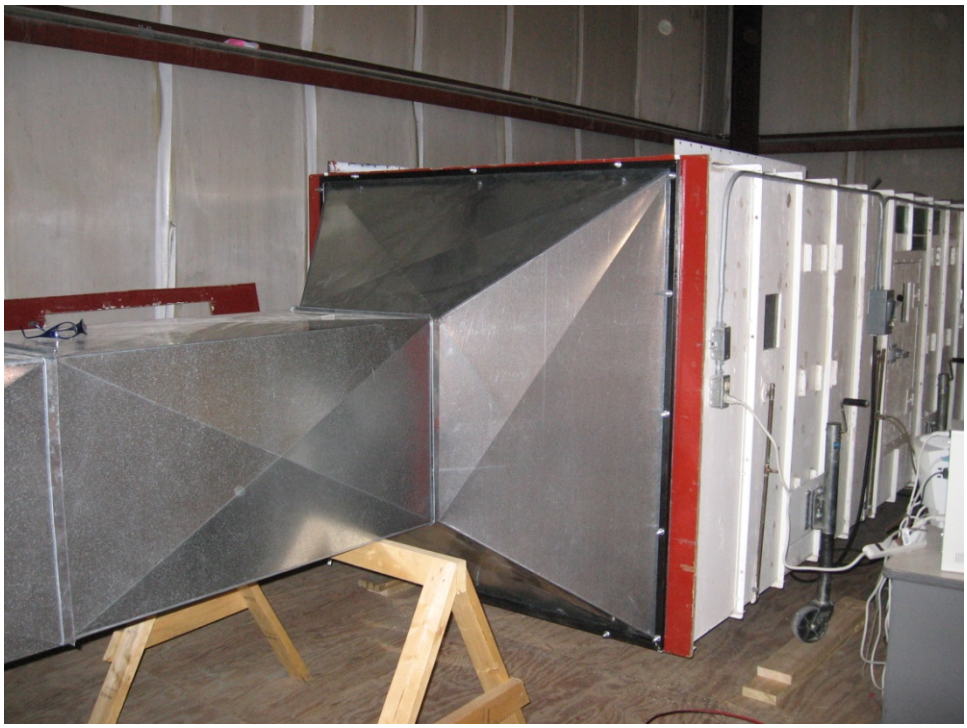

Figure 2.9 Nozzle Chamber 1

Figure 2.10 Nozzle Chamber 2

Figure 2.11 Nozzle Bank

ASHRAE 1245-RP required compliance with ASHRAE standard 120 and the test facility modifications described above were constructed in compliance with AMCA standard 210-85. It was necessary to show that these nozzle bank chamber modifications were in compliance with both standards. Chamber requirements for each standard are presented in the list below:

1. Pressure Tap Size

   Dimensions from Figure 2.6 show that we are compliant with both standards.

   a. ASHRAE standard 120

      1.5 mm (0.059 in) preferred, 3 mm (0.118 in) maximum

   b. AMCA standard 210

      0.060 in (1.52 mm) preferred, 0.125 in (3.18 mm) maximum

   c. Current Test Chamber

      1.0 mm (0.039 in)

2. Flow Settling Means (Diffusers)

   Maximum velocity shall not exceed average velocity by more than 25% for velocities greater than 2 m/s (400 fpm).

   a. ASHRAE standard 120

      Requirement at 0.2 D_e downstream of screen

   b. AMCA standard 210

      Requirement at 0.1 D_e downstream of screen

c. Current Test Chamber

   Because AMCA standard 210 is the stricter standard we are also compliant with ASHRAE standard 120. Also the average velocity of 349 fpm at 9600 cfm in the nozzle chamber is less than 400 fpm.

3. Nozzle Location

   For both ASHRAE Standard 120 and AMCA 210 the following criteria apply:

   a. Nozzle centerlines should be at least 1.5 throat diameters away from all chamber walls
   b. The minimum distance between centers of any two nozzles should be at least 3 throat diameters of the largest nozzle.

The modified nozzle bank meets the requirements listed above for both standards. Therefore it represents a suitable means of measuring flow rate for the current ASHRAE 1245-RP project and was used as the flow measurement standard for comparison with all other measurements.

2.3 Air Flow Measurement Station (FMS)

When measurements were conducted using the diverging tee duct configurations, an additional standard measurement of flow was required. Duct configurations are discussed in detail in section *2.4 Duct Configurations and Fabrication* below. The reason for the addition of a second standard was to facilitate accurate measurement of the branch line flow rate. The tee branch line flow rate was determined from the difference between the nozzle bank total flow rate and the FMS flow, with this flow measurement station installed in the main line of the tee.

The flow measurement station used for the current project was a Paragon Controls FE 1500 Air Flow Measurement Station. Pictures of the FMS are available in Figures 2.12 and 2.13 below. The measurement station has a cross section of 1' x 1'. It uses two 9/16" tubes with total and static pressure ports along the tube. The tubes work like Pitot tubes and the average total and static pressures along the tubes are used to determine the dynamic pressure and thus the average velocity. Manufacturers specifications suggest a +/-2% of flow rate accuracy. A separate in-line calibration of the FMS was performed prior to use in the ASHRAE 1245-RP tee testing. The results of the calibration are discussed in section *5.5 Flow Measurement Station Uncertainty*.

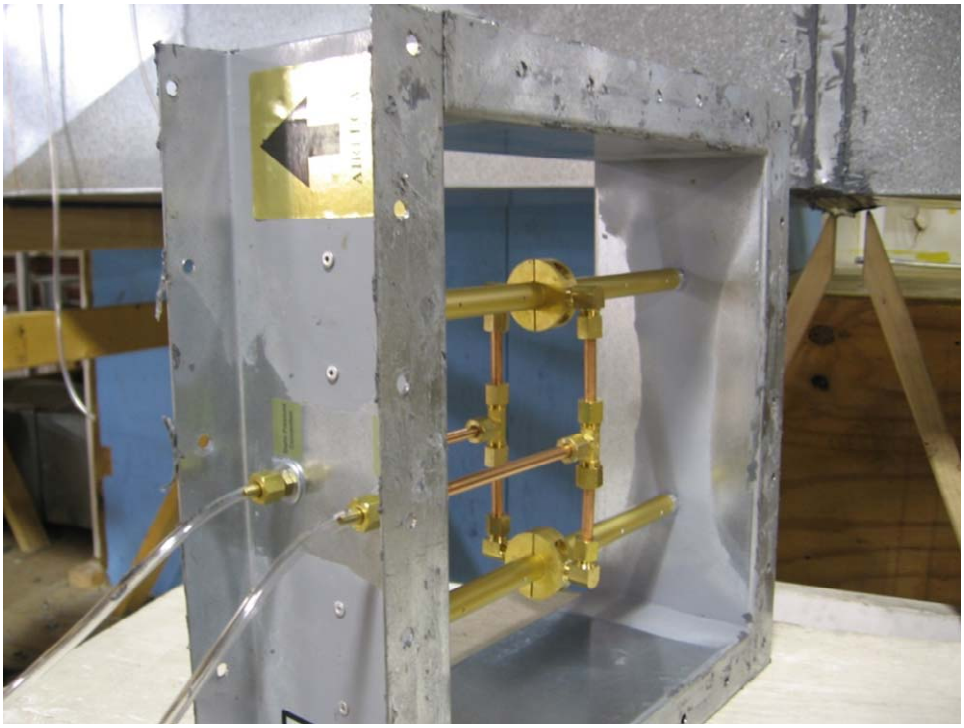

Figure 2.12 FMS 1

Figure 2.13 FMS 2

2.4 Duct Configurations and Fabrication

Several duct configurations were used in the current research. All ducts were constructed from #24 gauge galvanized steel in compliance with (SMACNA, 1995). Some of the configurations were used to check equipment and the procedure the researchers planned to use. Other configurations were for the data comparisons needed to achieve the goal of the project. The required lengths of all ducts were determined in the same manner. These lengths depend on the hydraulic diameter of the duct used, or alternately the equivalent diameter. The equivalent diameter was given in Equation (1). All duct lengths associated with ASHRAE 1245-RP were required to be specified in terms of equivalent diameter. D_e isn't the traditional hydraulic diameter but rather an equivalent diameter of a circle that has the same area as the duct. The true hydraulic diameter is based on the wetted parameter of the duct. The upstream duct length in each case was at least 20 equivalent diameters. The downstream duct length was always 10 equivalent diameters.

Data was collected on several duct configurations. This included various duct sizes, shapes, and the addition of multiple disturbances. Three duct sizes were used upstream of the disturbances. These include 24" z 24", 48" x 12", and 28" x 14". Each upstream duct size had its own set of disturbances and downstream conditions. Table 2.2 contains a summary of the duct configurations along with the duct disturbances to be investigated by ASHRAE 1245-RP.

For each duct size, a straight section of duct was needed to evaluate the setup, equipment, instrumentation, and general measurement procedure being used in the research. The duct contained no disturbances and was the length of the appropriate upstream and downstream lengths based on the upstream duct equivalent diameter. Data was collected at the proper locations upstream and downstream of a theoretical disturbance, or in other words the reference plane where the disturbance was to be introduced. The traverses ideally should produce negligible error in the flow measurement at these reference planes because plenty of undisturbed duct length existed upstream and therefore, the flow should be accentually fully-developed at these locations.

In addition to the straight duct tests each duct size had multiple disturbances. The 24" x 24" duct had four disturbances; 90^o elbow which included turning vanes and maintained the original duct size, 60^o and 90^o transitions which took the duct from its original 24" x 24" size down to 24" x 12", and a 90^o diverging tee with a 45^o branch entry. The tee also reduced the

duct size to 24” x 12” in both the main and branch lines. A picture of the tee is available in Figure 2.14 below. The measurements with the tee included three subsets of measurements which varied the branch to common line flow ratio (Qb/Qc). For diverging tees the branch line flow rate (Qb) is measured in the tee’s offshoot section of the duct and the common flow rate (Qc) is measured in the upstream section of duct. Data was taken with Qb/Qc ratios of 0.2, 0.4, and 0.6.

Figure 2.14 Tee

The 48” x 12” and 28” x 14” duct will have the 90^{o} elbow and 90^{o} tee configurations but will not have the transitions. Like the 24” x 24” duct, the elbow maintains the size of the upstream duct. The tees have the same downstream duct size for all configurations as well as the same flow ratios Qb/Qc. The 48” x 12” and 28” x 14” duct configurations to be investigated were not part of this thesis.

Table 2.2 Duct Configurations

Upstream Duct Configuration			Disturbance	Downsteam Duct Configuration			
Duct Size in x in	D_h in	Duct Length ft		Duct Size in x in	D_h in	Duct Length ft	Q_b / Q_c
24 x 24	27.1	45.1	60° Transition	24 x 12	19.1	16.0	Not applicable
24 x 24	27.1	45.1	90° Transition	24 x 12	19.1	16.0	Not applicable
24 x 24	27.1	45.1	90° Bend	24 x 24	27.1	22.6	Not applicable
24 x 24	27.1	45.1	Tee	24 x 12	19.1	16.0	0.2, 0.4, 0.6
48 x 12	27.1	45.1	90° Bend	48 x 12	27.1	22.6	Not applicable
48 x 12	27.1	45.1	Tee	24 x 12	19.1	16.0	0.2, 0.4, 0.6
28 x 14	22.3	37.2	90° Bend	28 x 14	22.3	18.6	Not applicable
28 x 14	22.3	37.2	Tee	24 x 12	19.1	16.0	0.2, 0.4, 0.6

Note: Equivalent Diameter D_e is defined as $D_e = \sqrt{\frac{4(\text{width})(\text{height})}{\pi}}$

One additional duct configuration was used. Its purpose was to evaluate the leakage in the system. If there is significant leakage from the nozzle bank (where the actual flow rate is computed) to the measurement location it needs to be quantified. The test simply uses the initial 24" x 24" checkout duct setup with the addition of an end cap. This setup ideally yields a theoretical flow rate of 0 SCFM; however, some finite reading was to be expected. The actual leakage flow rate produced was measured at the nozzle bank. A more extensive discussion of the seal testing is given in appendix A.

CHAPTER 3 - Flow Rate Determination

The volumetric air flow rate needed to be determined at the nozzle chamber, duct traverses, and the flow measurement station when a tee disturbance was used. The measurements included air property measurements as well as others depending on the measurement type. For the nozzle chamber and FMS the primary measurement for determining the flow rate was a pressure measurement. For the traverses it was local air velocity measurements. The methods of determining the flow rate as well as a discussion of the air properties required are presented below. Example calculations are available in Appendix E. Much of the data was taken with a Hewlett Packard 34970A Data Acquisition / Switch Unit and computer equipped with LabView software. The LabView software was also used to perform calculations required to determine the flow rate for both the nozzle bank and FMS. The Hewlett Packard 34970A was able to store some data in its output buffer. This was used to do some signal averaging internally and reduce the size of the output file. LabView was able to capture the average of several points from the Hewlett Packard 34970A and store those averages in a text file rather than storing each individual reading. Pictures of the LabView front panels and block diagrams are available in Appendix F.

3.1 Air Properties

The primary air properties required for the calculation of volumetric air flow measurement are the air viscosity and density. The air viscosity can be assumed a function of dry bulb temperature only. For ASHRAE 1245-RP the viscosity was calculated with Equation 5 of ASHRAE Standard 120 section 9. The air density can be determined several ways requiring the measurement of one or more air properties including dry bulb temperature, pressure, and humidity. The humidity can be obtained by various methods including the measurement of the wet bulb temperature, relative humidity, or dew point temperature. The simplest way would be to use the ideal gas law and assume the air is dry. The most accurate way to calculate the air density would be to use the dry bulb temperature and pressure along with the humidity measurement. This is the method ASHRAE 1245-RP used.

The calculation of density including humidity effects is more complicated than the ideal gas assumptions for dry air. It is also more accurate and is therefore recommended for density calculations where high degrees of accuracy are required such as for the nozzle bank used in ASHRAE 1245-RP. The humidity can be determined by measurement of dry bulb temperature along with the measurement of wet bulb temperature, relative humidity, or the dew point temperature. ASHRAE Standard 120 section 9 Equations 1 through 3 use the wet bulb temperature for determining humidity effects on density. If measurements of relative humidity or dew point temperature are used the ASHRAE Fundamentals Handbook or ASHRAE Standard 41.6-1994 can be used as a reference for density calculations. ASHRAE 1245-RP required ASHRAE Standard 120 as the source for nozzle bank measurements; however, as discussed in section *3.1.4 Air density Accuracy Verification* other sources can be used for density calculation as long as the maximum error in density doesn't exceed 0.5%. ASHRAE 1245-RP measured the relative humidity rather than the wet bulb temperature and therefore used the equations of ASHRAE Fundamentals Chapter 6 were used as the source for determining air density for the nozzle bank and FMS. A correction to the density was required for the nozzle bank because the pressure was greater in the chamber than in the general test area. The correction is made with Equation 4 of ASHRAE Standard 120 section 9. The temperature correction isn't required because the temperature is measured in the nozzle chamber rather than the general test area. The individual air properties of barometric pressure, dry bulb temperature, and relative humidity required for the calculation were made with the following instruments. A full listing of instrument specifications is available in Appendix D.

3.1.1 Barometric Pressure

The barometric pressure was recorded with a mercury barometer with a scale readability of 0.01" hg. Adjustments were made for changes in the density of mercury due to change in temperature.

3.1.2 Temperature

The wet bulb and dry bulb temperatures were measured with a TSI Velocicalc model 8347. This wet bulb temperature was used for the 60^{o} and 90^{o} transitions on the 24" x 24" upstream duct. The wet bulb temperature wasn't actually measured but calculated internally by the meter from the relative humidity and dry bulb. Standard 120 section 6.9 specifies

thermometers must have accuracy and scale readability of +/- 0.5 ^{o}C. The Velocicalc unit has an accuracy of +/- 0.3 ^{o}C + 0.03 ^{o}C/ ^{o}C for change in instrument temperature from 25 ^{o}C and a resolution of 0.1 ^{o}C. After the 60^{o} and 90^{o} transitions an Omega 44000 series 5,000 ohm thermistor was implemented. Its measurements were taken continuously with the Hewlett Packard 34970A Data Acquisition / Switch Unit and computer equipped with LabView software. The thermistor has an interchangeability of +/-0.2^{o}C.

3.1.3 Humidity

The relative humidity was first measured before and after each test with the TSI Velocicalc model 8347. This was done for the 60^{o} and 90^{o} transitions on the 24" x 24" upstream duct. After that a HyCal model IH-3602 sensor was used and placed in the flow stream just upstream of the nozzle bank for continuous measurement. Measurements from the HyCal sensor were taken with the Hewlett Packard 34970A Data Acquisition / Switch Unit. The Velocicalc device has an accuracy of +/-3% relative humidity. The accuracy for the HyCal sensor at 25^{o}C and 5 Vdc excitation is $\pm 2.0\%$ RH . At the time of this project the humidity sensor was a few years old. Due to this the factory calibration was no longer accurate. A calibrations was performed which resulted in an increase in uncertainty. The calibration was done with a TSI 8347 anemometer; therefore, the uncertainty in the HyCal sensor could be no better than the 8347. From the calibration data the random uncertainty in the data and the accuracy of the DVM used in the calibration are shown to be negligible from table 3.1 below. The absolute uncertainty for either the TSI probe or HyCal sensor is given below. Calibrations curves are available in Appendix C.

$U_{RH} = \pm 3.0\%$ RH

Table 3.1 HyCal Humidity Sensor Uncertainty

Random Uncertainty	TSI 8347 Uncertainty	DVM Uncertainty		Total Uncertainty
% RH	% RH	Volts	%RH	% RH
0.1	3.0	0.001	0.0003	3.0

3.1.4 Air Density Accuracy Verification

Due to the facts that ASHRAE Standard 120 gives a wet bulb temperature specification and our anemometer probe gives relative humidity accuracy it is necessary to show that we are compliant with Standard 120 regardless. Also, it is necessary to show that our use of the ASHRAE Fundamentals method of determining density is compliant with standard 120. The TSI 8347 anemometer uses the procedure of ASHRAE Fundamentals chapter 6 to calculate wet bulb temperature. ASHRAE Fundamentals actually calculates the adiabatic saturation temperature rather than wet bulb temperature but these are very similar. Standard 120 section 9 specifies that other means can be used to calculate density as long as the error in the density calculated does not exceed 0.5%. Also it can be shown that Equations 11, 28, and 22 from ASHRAE Fundamentals Chapter 6 can be combined to obtain Equation 3 from Standard 120 section 9. The main difference in the calculations is in determining the partial vapor pressure.

Table 3.2 shows that by calculating the density using AHRAE Fundamentals or by using ASHRAE standard 120 produces an error or difference between them of much less than 0.5%. Values of temperature (T), relative humidity (φ), and barometric pressure (P) were varied from a min to max and a value in the middle. Also, Table 3.3 shows that the relative humidity specification of +/- 3% is also sufficient. This table uses 20% relative humidity as an expected value. The table shows that the relative humidity must change by about 50% relative humidity to affect the density for ASHRAE Fundaments by 0.5%. This would be very similar to the affect on Standard 120 because as table 3.2 showed the densities are very close. The calculations were done over a range of temperatures expected at the data collection site. The barometric pressure used was a typical value measured at the site.

Table 3.2 Comparison of Air Density Calculation

Ambient Conditions				Wet Bulb	Air Density kg / m^3		Difference
Condition	T °C	Φ	P kPa	T* °C	ρ_{ASHRAE}	$\rho_{std\ 120}$	$\rho_{ASHRAE} - \rho_{std\ 120}$
min t, min Φ, min P	10	0.100	95.00	1.12	1.1682	1.1681	-0.009%
min t, max Φ, min P	10	0.700	95.00	7.29	1.1648	1.1650	0.017%
min t, min Φ, max P	10	0.100	101.50	1.45	1.2482	1.2481	-0.008%
min t, max Φ, max P	10	0.700	101.50	7.38	1.2448	1.2449	0.008%
max t, min Φ, min P	32	0.100	95.00	13.85	1.0825	1.0828	0.028%
max t, max Φ, min P	32	0.700	95.00	27.21	1.0702	1.0703	0.009%
max t, min Φ, max P	32	0.100	101.50	14.30	1.1567	1.1569	0.017%
max t, max Φ, max P	32	0.700	101.50	27.29	1.1444	1.1445	0.009%
Middle	21	0.400	98.25	13.00	1.1591	1.1593	0.016%

Table 3.3 Relative Humidity Effect on Air Density

Ambient Conditions			Wet Bulb	Air Density	Density Change
T °C	Φ	P kPa	T* °C	ρ_{ASHRAE} kg / m3	$\rho_{new} - \rho_{old}$
20	0.200	98.00	9.08	1.1625	
20	0.300	98.00	10.69	1.1614	0.09%
20	0.100	98.00	7.38	1.1635	-0.09%
20	0.700	98.00	16.37	1.1572	0.46%
15	0.200	98.00	5.77	1.1832	
15	0.100	98.00	4.40	1.1840	-0.07%
15	0.300	98.00	7.09	1.1825	0.06%
15	0.700	98.00	11.85	1.1793	0.33%
25	0.200	98.00	12.31	1.1423	
25	0.100	98.00	10.23	1.1437	-0.12%
25	0.300	98.00	14.25	1.1409	0.12%
25	0.700	98.00	20.89	1.1353	0.62%

3.1.5 Standard Air Density

Volumetric air flow measurements for all measurements needed to be based on a standard air density. The correction to standard density is discussed in section *3.5 Correction to Standard Air Density*. Standard conditions used are the following:

$P_{Standard}$ = Standard Pressure (29.92 inches of mercury)

$T_{Standard}$ = Standard Temperature (70° F)

3.2 Nozzle Bank Flow Measurement Standard

An ASME nozzle bank was used to determine the standard volumetric air flow rate for comparison with the experimental results obtained from duct traverse methods. The volumetric air flow rate through the ASME nozzle bank was calculated using the method presented in ASHRAE Standard 120. Standard 120 section 9 presents the equations and the procedure for all parameters involved in the determination of flow rate. Measurements taken at the nozzle chamber were used to calculate the flow rate. Some of these include air property measurements discussed in the previous section. Uncertainties of flow rate calculation are discussed in detail in Chapter 5.

The volumetric flow rate Q for the chamber can be computed from standard 120 section 9 Equations 16 and 17.

$$\dot{m} = 1.414 Y_n \sqrt{\rho_1 \Delta P_{s,\,1-2}} \, \Sigma(C_n A_n) \qquad \textbf{(2)}$$

$$Q = \frac{1000\dot{m}}{\rho_1} \quad \textbf{(3)}$$

Where

Q=	Volumetric Flow Rate
$\dot{m}$ =	Mass Flow Rate
Y_n =	Nozzle Expansion Factor
ρ_1 =	Air Density in Test Chamber
$\Delta P_{s,\,1-2}$ =	Static Pressure Drop Across Nozzle Bank
C_n =	Discharge Coefficient for Nozzle n
A_n =	Area of Nozzle n

These equations can be combined to obtain a single equation for the volumetric flow rate.

$$Q = 1414 Y_n \sqrt{\frac{\Delta P_{s,\,1-2}}{\rho_1}} \Sigma(C_n A_n) \quad \textbf{(4)}$$

The above formulas give the flow in actual units as opposed to standard units, the desired units for the project. The conversion from actual to standard units is discussed in section *3.5 Correction to Standard Air Density*. The air density was discussed in section 3.1. The other variables are discussed below.

3.2.1 Nozzle Expansion Factor

The expansion factor and discharge coefficient are calculated from Standard 120 as well. The expansion factor is a function of Alpha ratio, Beta ratio, and the specific heat ratio and is calculated with Equation 8 of Standard 120 section 9. The Alpha ratio is the ratio of nozzle exit pressure to nozzle approach pressure and is determined with Equation 6 of Standard 120 section 9. The Beta ratio is the ratio of nozzle throat diameter to approach duct diameter and can be assumed 0 for a chamber (ASHRAE Standard 120). The specific heat ratio can be taken as 1.402 (ASHRAE Standard 120). In our case the expansion factor is the same for all nozzles.

3.2.2 Nozzle Discharge Coefficient

In order to compute the discharge coefficient for each nozzle the Reynolds Number must also be calculated. The process of determining the discharge coefficient involves an iterative

process. An initial estimate of the Reynolds Number must first be computed. The equation for this estimate is similar to the actual version of the equation with some assumptions made. Equation 12 of Standard 120 section 9 is used for the initial estimate. With an initial estimate of the Reynolds Number the iterative process can be performed to obtain the discharge coefficients. Equations 11 and 13 of Standard 120 section 9 are used for the iterative process. Nozzles of different size will have a unique discharge coefficient; therefore, this process including initial estimate of Reynolds Number must be performed for each nozzle of different size. Nozzles with the same diameter will have the same discharge coefficient. In the chamber used there are 9 nozzles available for use; however, there are only 6 unique sizes.

It was necessary to determine the number of iterations necessary to converge to an accurate discharge coefficient. Values of Reynolds number and discharge coefficient were calculated for all nozzles with multiple iterations. Temperature and flow rate were adjusted with minimal effect. These adjustments had very little impact on the % change in Cn. The smaller temperatures and smaller flow rates increased the % change slightly but only a couple hundredths of a percent. The percent change from iteration 0 to iteration 1 is barely significant anyway. The second iteration from 1 to 2 is very small and insignificant. The calculations are presented in Table 3.4 showing that a single iteration is sufficient.

Table 3.4 Discharge Coefficient Convergence

Nozzle	Diameter		Initial Estimate		Iteration 1			Iteration 2		
Number	inches	meters	Re	Cn	Re	Cn	Change in C_n	Re	Cn	Change in C_n
1	5.000	0.1270	252037.3	0.9835	270986.6	0.9840	0.05%	271114.2	0.9840	0.0003%
2	6.000	0.1524	302444.8	0.9846	325558.6	0.9851	0.04%	325700.5	0.9851	0.0003%
3	5.500	0.1397	277241.1	0.9841	298268.7	0.9845	0.05%	298403.6	0.9845	0.0003%
4	4.000	0.1016	201629.9	0.9820	216450.8	0.9825	0.05%	216562.5	0.9825	0.0004%
5	1.600	0.0406	80651.9	0.9735	85835.2	0.9742	0.07%	85897.4	0.9742	0.0008%
6	2.500	0.0635	126018.7	0.9781	134751.0	0.9787	0.06%	134834.5	0.9787	0.0006%
7	5.000	0.1270	252037.3	0.9835	270986.6	0.9840	0.05%	271114.2	0.9840	0.0003%
8	6.000	0.1524	302444.8	0.9846	325558.6	0.9851	0.04%	325700.5	0.9851	0.0003%
9	5.500	0.1397	277241.1	0.9841	298268.7	0.9845	0.05%	298403.6	0.9845	0.0003%

3.2.3 Static Pressure

The pressure drop across the nozzle bank was measured using an Omega PX653 pressure transducer. A power supply was used to supply the pressure transducer with a 24 volt excitation voltage. The output voltage of the pressure transducer was recorded with the Hewlett Packard 34970A Data Acquisition / Switch Unit.

The static pressure at the nozzle bank inlet was also needed for a pressure correction to the air density discussed in section *3.1 Air Properties*. This static pressure at the nozzle bank inlet was measured with different pressure transducers at different points in the project. The transducer voltages were both measured with the Hewlett Packard 34970A Data Acquisition / Switch Unit. The pressure was first measured with the same Omega PX653 pressure transducer as the pressure drop. This device was used for the 60^o and 90^o transitions on the 24" x 24" upstream duct. The pressure was measured before and after each test. After the 60^o and 90^o transitions an additional pressure transducer was purchased to measure nozzle inlet static pressure. The new pressure transducer is a Setra model 264 with the 0.25% optional accuracy.

In order to meet ASHRAE Standard 120 compliance, the pressure must be measured with an accuracy of +/- 1.0% of reading. The PX653 and Setra 264 have accuracies based on best fit line (BFL) of 0.25% full scale output (FSO). It was noticed the pressure transducers didn't quite follow the calibration provided by the manufacturer. A calibration was done following the guidelines in Standard 120 section 6.2.5.1. The description and results of these calibrations are available in appendix C. With a full scale output of 10" W.C. our uncertainty is 0.25" W.C.. This means that to obtain an accuracy of less than 1.0% of reading we must maintain a pressure drop across the nozzles of 2.5" W.C. or larger.

3.3 Air Flow Measurement Station

The air flow measurement station (FMS) used was a Paragon Controls FE-1500 Air Flow Measurement Station. It was 1 ft square and used pitot probe type pressure measurement for determining the average velocity pressure. It used two horizontal tubes containing holes for capturing the average total pressure and static pressure which can be used to determine the average velocity pressure. The velocity pressure was measured with a Setra 264 similar to that used to measure static pressure drop across the nozzle bank discussed in section *3.2.3 Static Pressure*. Two transducers were required one with a pressure range of 0" to 0.5" W.C. and one with a range of 0" to 5" W.C.. The Setra pressure transducers have accuracies based on a best fit line (BFL) of 0.25% FSO. The velocity pressure can then be converted to a velocity. The air density determined in section *3.1 Air Properties* for the general test area is used for determining the velocity from the velocity pressure. It is assumed the temperature and humidity are relatively constant through the duct and that the density at the FMS is significantly close to the density in

the general test area near the nozzle chamber. The FMS is at about 2 ft from the end of the duct system and the pressure is close to ambient; therefore, the barometric pressure can be used for determining the air density and the density correction for pressure required for the nozzle bank isn't necessary. In theory the averaging in the FMS accurately represents the average velocity pressure in the duct. With this assumption the average velocity would be determined by the following equation:

$$V_{FMS} = \sqrt{\frac{2P_v}{\rho_o}} \quad \textbf{(5)}$$

Where

V_{FMS} = Average Velocity at FMS

P_v = Average Velocity Pressure at FMS

ρ_o = Air Density in General Test Area

The flow rate then can be determined by multiplying the average velocity by the duct area of the FMS.

The above discussion is with the assumption the FMS accurately represents the average velocity pressure. It was noticed by ASHRAE 1245-RP that this assumption might not hold for all sizes and aspect ratios of flow measurement stations. A calibration was performed on the FMS used by this project. The calibration uses the following relationships for calculations.

$$P_v = C\frac{1}{2}\rho_o V_{FMS}^{\wedge 2} \quad \textbf{(6)}$$

$$Re = \frac{\rho_o d_{tube} V_{FMS}}{\mu_o} \quad \textbf{(7)}$$

Rearranging and substituting gives:

$$Re = \frac{\rho_o d_{tube}}{\mu_o}\left(\frac{2P_v}{C\rho_o}\right)^{\frac{1}{2}} \quad \textbf{(8)}$$

Where

$$C = f\left(Re\right) \quad \textbf{(9)}$$

And

C= FMS Flow Coefficient

Re = Reynolds Number based on Tube Diameter

μ_o = Viscosity in General Test Area

d_{tube} = Diameter of Tubes inside the FMS

In the case of ASHRAE 1245-RP an area ratio is used to help explain some of the reason the FMS was giving readings far off of theoretical. The reduced area due to the tubes in the air stream was on the same order of magnitude as the error in flow rate. The following relationship was established:

$$C = C^* A_{ratio}{}^2 \tag{10}$$

Where

$$A_{ratio} = \frac{\text{FMS Area}}{\text{FMS Area - Tube Area}} \tag{11}$$

The area ratio is constant and just used to explain the error of the FMS. The calibration resulted in the following relationships for the flow coefficient:

$$C^* = -1.36\ e-4\left(\frac{Re}{10^3}\right)^2 + 8.20e-3\left(\frac{Re}{10^3}\right) + 9.06997e-1 \tag{12}$$

An iterative process with Equations 8 and 12 can be used to determine the Reynolds number and flow coefficient. An initial guess of the Reynolds number is determined from the measured velocity pressure at the FMS assuming a flow coefficient of 1. Once the iterations yield significantly small changes in Reynolds number, the final average velocity is obtained by rearranging Equation 7 to solve for V_{FMS}.

$$V_{FMS} = \frac{Re\mu_o}{\rho_o d_{tube}} \tag{13}$$

3.4 Flow Measurement by Duct Traverses

The traverse measurement of flow rate is simply an average of several velocities in a particular traverse algorithm. At each point in the traverse the local velocity is measured. The number of traverse points is determined by the duct size and algorithm being used. To obtain the flow rate the average velocity must be multiplied by the duct area. For ASHRAE 1245-RP the measurements were done using two probes and two traverse algorithms.

3.4.1 Log-Tchebycheff and Equal Area Algorithms

In the case of ASHRAE 1245-RP the traverse algorithms used were log-Tchebycheff and equal area. The log-Tchebycheff traverse algorithm was obtained from ASHRAE Standard 111-1988 and is also made available in the ASHRAE Fundaments Handbook and (ISO 3966, 1977). The equal area traverse algorithm was obtained from (AABC, 2002). A summary of all traverse points for each duct size is available in table 3.5 below.

Table 3.5 Traverse Points

Duct Size inch x inch	Traverse Algorithm	Horizontal Locations (inches) from side of duct	Vertical Locations (inches) from bottom of duct
24 x 24	Log-Tchebycheff Equal Area	1.8, 6.9, 12, 17.1, 22.2 3, 9, 15, 21	1.8, 6.9, 12, 17.1, 22.2 3, 9, 15, 21
48 x 12	Log-Tchebycheff Equal Area	2.5, 9.7, 17.6, 24, 30.4, 38.3, 45.5 4, 12, 20, 28, 36, 44	0.9, 3.5, 6, 8.5, 11.1 2, 6, 10
28 x 14	Log-Tchebycheff Equal Area	2.1, 8.1, 14, 19.9, 25.9 2.8, 8.4, 14, 19.6, 25.2	1.0, 4.0, 7, 10.0, 13.0 2.3, 7, 11.7
24 x 12	Log-Tchebycheff Equal Area	1.8, 6.9, 12, 17.1, 22.2 3, 9, 15, 21	0.9, 3.5, 6, 8.5, 11.1 2, 6, 10

3.4.2 Measurement Plane Locations

Measurements were taken downstream of the nozzle chamber to simulate balancing tests performed in the field by technicians. The measurements were taken at several locations upstream and downstream of each disturbance. The locations are based on the equivalent diameter of the duct. The equivalent diameter is determined from Equation 1 in Chapter 2. The upstream locations for all duct sizes are 1 and 3 De. The downstream locations for all duct sizes are 1, 2, 3, 5, and 7.5 De. The flow rates measured at these different locations can be compared to the nozzle bank to determine the closest location to the disturbance giving accurate results. Also, corrections can potentially be generated to assist field technicians in obtaining accurate results when measurements have to be taken at an undesirable distance from a disturbance.

3.4.3 Local Air Velocity Measurements

The measurement of air velocity at a specific point in an air stream can be done with several devices. These include rotating vane anemometers, thermal anemometers, pitot-static

probes, and others. This paper will focus on the two used by ASHRAE 1245-RP, a thermal anemometer and a pitot-static probe.

3.4.3.1 Pitot-static Probe

Pitot-static probes are used in conjunction with a pressure measurement device measuring the difference between the total pressure and static pressure at each point in the airstream. The pressure measurement device used in ASHRAE 1245-RP was an Alnor EBT 720 electronic balancing tool. Pictures of the pitot-static probe and EBT 720 are available in Figures 3.1 and 3.2 below. The main source of error for this measurement is with the pressure sensor and air property measurement. This is typically provided by the manufacturer, although in many cases a calibration must be performed to insure accurate measurement. The EBT 720 is also a pressure transducer and can measure pressure directly, but was specifically designed with software to be used for air velocity measurement with a pitot-static probe. It also has capability to measure air properties. The device was calibrated for velocity measurement and therefore the manufacturer provides accuracies for velocity measurement. The accuracy of the EBT 720 is +/- 3.0% of reading for velocity. Most pressure transducers would only provide accuracies for pressure which would need to be combined with air properties to obtain the uncertainty in velocity. The EBT 720 has the capability to record multiple points and display the average of those points. Recording the average of multiple points reduces the random uncertainty in the measurement which was done for this research. It was necessary to determine how many points to average to significantly reduce the uncertainty without adding too much time to the measurement process. Each point takes about 10 seconds. With lots of points and tests to perform this can add up to a significant increase in measurement time. A test was performed to look into the random uncertainty in the measurement for different numbers of averaged points. Figure 3.3 shows the reduction of random uncertainty for increased number of points recorded. From this plot the researchers decided to record the average of 4 points. This provides a significant reduction in random uncertainty with a manageable amount of time added.

Figure 3.1 Pitot-static Probe

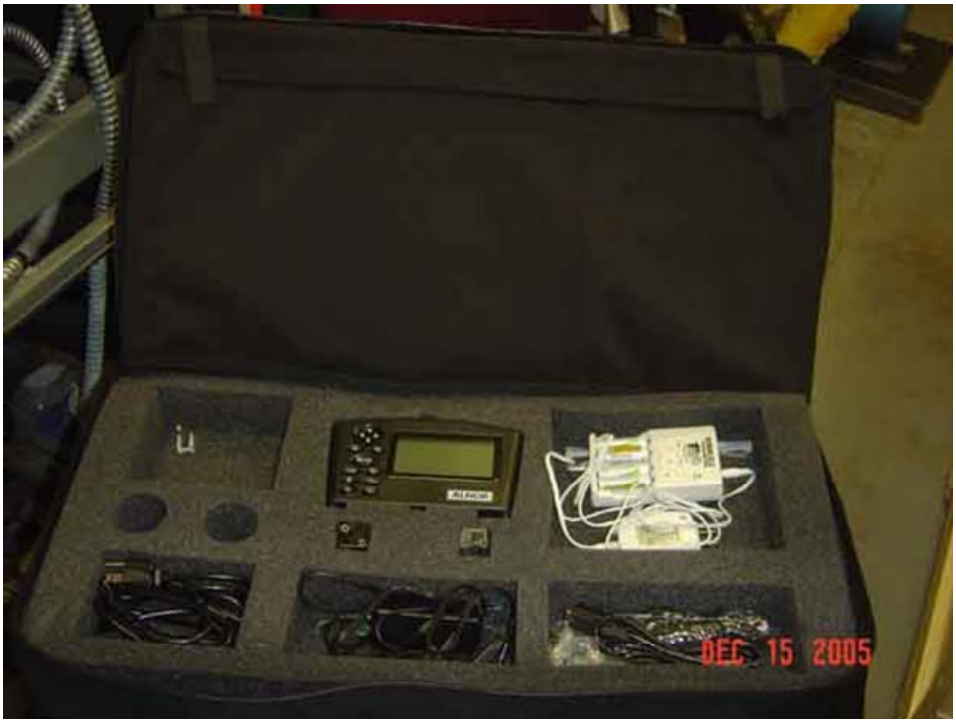

Figure 3.2 EBT 720 Electronic Balancing Tool

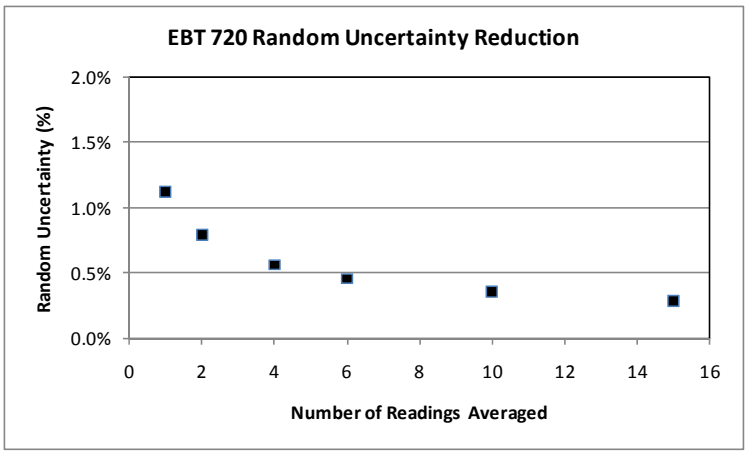

Figure 3.3 EBT 720 Reduction in Random Uncertainty

3.4.3.2 Thermal Anemometer

Unlike the pitot-static probe this probe does not measure pressure. Thermal anemometers or hot wire probes use heat transfer to measure air flow. The velocity is related to the convective heat transfer on the probe's wire. The heat transfer is measured from the power input required to keep the wire at a constant temperature. The accuracy of the probe is typically provided by the manufacturer. ASHRAE 1245-RP used a TSI VelociCalc model 8347 air velocity meter. The accuracy of the 8347 is +/- 3.0% of reading. A picture of the meter is available in Figure 3.4 below. This anemometer is capable of provided a 10 second average of 1 reading per second so the averaging of multiple points discussed above for the EBT 720 isn't necessary for this device.

Figure 3.4 TSI VelociCalc Model 8347 Anemometer

3.5 Correction to Standard Air Density

Volumetric air flow measurements needed to be based on a standard air density. Reporting the results based on a standard density gives the flow rate the air would have been had it been at standard temperature and pressure. This gives an easy way to compare results of various atmospheric conditions. Corrections to the standard air density are made based on the ideal gas law with the equation below. Standard temperature and pressure were defined in section *3.1.5 Standard Air Density*.

$$SCFM = ACFM \left(\frac{P_{Actual}}{P_{Standard}} \right) \left(\frac{T_{Standard}}{T_{Actual}} \right) \quad \textbf{(14)}$$

Where

SCFM = Volumetric Air Flow Rate at standard density

ACFM = Volumetric Air Flow Rate at actual density

P_{Actual} = Actual Pressure

T_{Actual} = Actual Temperature

This correction must be performed for both the nozzle bank and FMS measurements. The probes used for traversing the ducts can perform this correction internally and don't require a separate correction. The Alnor EBT 720 can perform the correction internally; however, the temperature probe must be used with the EBT 720 in order to accurately make this correction. The TSI VelociCalc model 8347 reports the velocity in standard units (SFPM) with no action or further correction required.

CHAPTER 4 - Experimental Procedure

This chapter describes test procedures for all measurements taken by ASHRAE 1245-RP. These include measurements of air properties, pressures, and velocities. Measurements needed to be taken to determine flow rates in 3 major locations. These include the nozzle chamber, flow measurement station, and traverses. A procedure was also required for accuracy verification of the velocity and pressure probes used.

4.1 Nozzle Chamber Measurement Procedure

Some measurements were taken manually before and after each test while others were measured with a Hewlett Packard 34970A Data Acquisition / Switch Unit and computer equipped with LabView software. LabView was also used to calculate all other variables needed to determine the flow rate for the nozzle bank and FMS and print the output to a file. See Chapter 3 for more information on the measured parameters and calculations. The HP 34970A was used to do some averaging. Two LabView files were created, one for setting the flow rate and one for taking the actual data. The reason for the two is that the file for taking actual data can do more averaging while the other can do less averaging but give faster indicator updates. This simply allows for shorter setup times while still providing plenty of averaging for the actual data.

The nozzle bank allowed for nozzles to be plugged and therefore raise the pressure drop across the nozzles. Nozzles were plugged with test plugs and/or non-porous inflatable balls. The nozzle pressure drop and inlet static pressure needed to be larger than 2.5" water column in order to achieve desired accuracy in the pressure reading. This was discussed n more detail in Chapter 3. A summary of nominal flow rates used by the project and the nozzles required to be plugged to achieve those flow rates is available in Table 4.1.

Table 4.1 Nozzles Plugged

Nominal Flow Rate	Nozzles Plugged
SCFM	Nozzle Number
9600	None
7200	None
6533	2
4900	2, 8
4800	2, 8
3600	1, 3, 7, 9
3267	1, 3, 4, 7, 9
2400	2, 3, 4, 7, 8
1633	1, 2, 4, 7, 8, 9
1200	2, 3, 4, 7, 8, 9

For each traverse at each location a single basic procedure was used. The basic procedure for performing calculations at the nozzle bank is the following:

1. Plug appropriate nozzles.
2. Take all manual measurements required before a test.
3. Run the LabView file for setting the flow rate and adjust fan speed until desired flow rate is achieved.
4. Run the LabView file for actual data collection until the current traverse is complete. Note: equal area traverses were done right after log-Tchebycheff but separate files were created.
5. Take all manual measurements required after a test.

This basic procedure is consistent throughout the project; however, the procedure may vary some due to changes made by other researchers during the project. This may include implementation of new probes or sensors requiring less manual measurements before and after each test. For example after the 60° and 90° transitions relative humidity and temperature measurements were recorded with LabView and no longer required before and after each test. Also this procedure only includes measurements at the nozzle bank. Other additions to the overall procedure may include adjustments of a damper for tee measurement.

4.2 Flow Measurement Station Procedure

Along with the basic procedure additional steps will be included when using the tee disturbance. An additional pressure transducer is used at the end of the main line on the Flow Measurement Station. The specific pressure transducer to use depends on the velocity being measured. Pressure transducers with different ranges were used depending on the velocity being

measured. This is to insure good uncertainty in the measurement. The appropriate pressure transducer needs to be implemented before the test. In addition to selecting a pressure transducer the Qb/Qc ratio needed to be adjusted. This is done during step 3 above along with the flow rate adjustment. To accomplish this, a damper at the end of the branch line is adjusted.

4.3 Traverse Measurement Procedure

The traverse procedure simply involved taking a velocity measurement at each traverse point in Table 3.5. This is done at each location and each velocity. The two probes needed to somehow be positioned at these locations and their accuracies needed to be checked periodically to insure they were working properly. This is discussed below.

4.3.1 Probe Positioning Procedure

A device was built to position the probes in the proper position for the log-Tchebycheff and equal area algorithms. Holes could be drilled to insure proper placement along the x axis of the duct. To insure the probes were in the center, a template was used with holes marking the proper log-Tchebycheff and equal area horizontal locations. A line was drawn across the duct in the proper location in terms of the number of equivalent diameters up or downstream of the disturbance, the center of the duct was marked, and the templates' center was aligned with the center of the duct. To insure proper placement in the vertical direction each probe was equipped with a bracket which allowed it to be screwed into a vertical aluminum column. There was a hole in the column for each point in the log-Tchebycheff and equal area traverse patterns. The holes in the column provide proper placement of the probes relative to a center hole on the column. The column with the probe being used then needed to be centered such that the center of the probe was in the center of the duct. To do this the column was placed above the center horizontal location of the duct. A wood dowel with a mark at the duct's nominal center height and 1/8" inch marks on either side of the center mark was used to measure the duct height. The probe was also marked only with 1/16" inch marks. The probe was placed in the center position on the column and adjusted until its center was in the actual center of the duct. The probe was then secured with its bracket.

The column was attached to a frame which was positioned on the duct. Figure 4.1 is a schematic of the device using the pitot-static probe and pictures are available in Figures 4.2 and 4.3. A different column needed to be constructed for each vertical duct size because the log-

Tchebycheff and equal area holes are different for different sizes of duct. The device could be moved along the duct to each measurement location up and downstream of the disturbance. The column could be swapped for different duct sizes. At each measurement location holes were drilled according to the appropriate duct size and x locations summarized in Table 3.5.

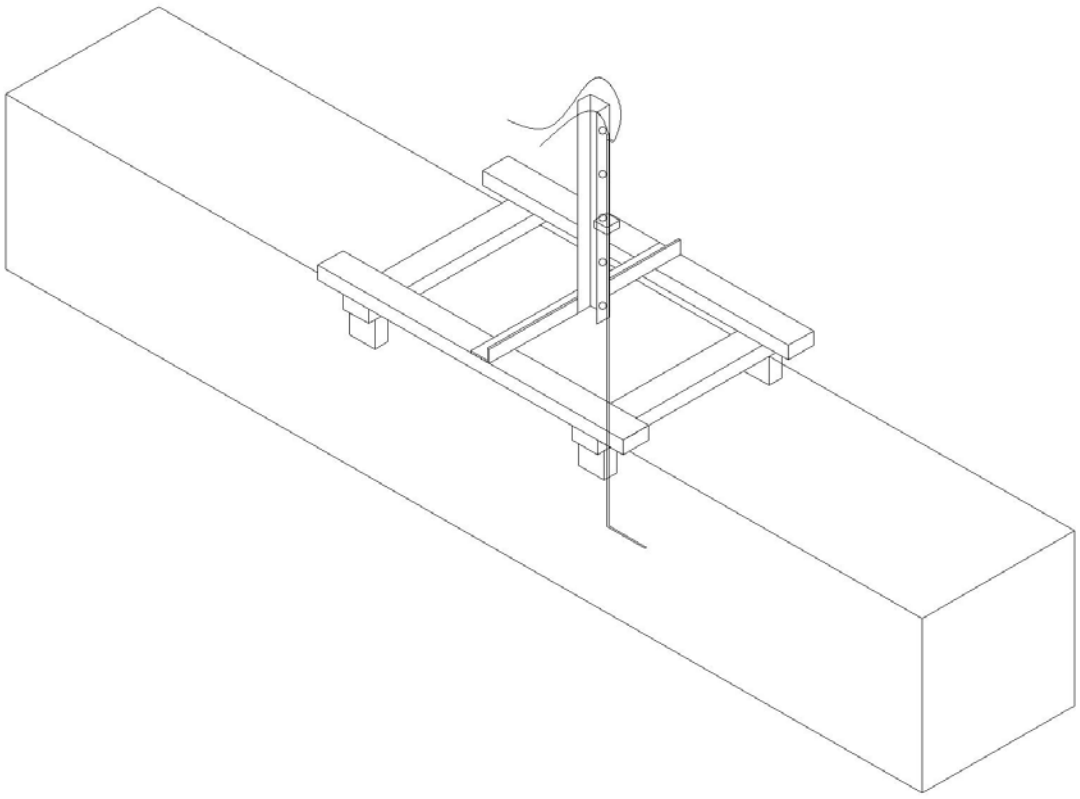

Figure 4.1 Pitot-static Probe Setup

Figure 4.2 Pitot-static Probe Picture 1

Figure 4.3 Pitot-static Probe Picture 2

4.3.2 Probe Specification Compliance Procedure

A procedure needed to be implemented to insure that both the thermal anemometer and EBT 720 were working properly. This was done by the use of a water micromanometer. Ideally all three instruments would be used simultaneously and the pitot-static probe would be placed in the same point of the flow stream as the anemometer. Several limitations exist preventing performing this ideal procedure. The probes cannot be in the same spot at the same time because of physical constraints. The probes cannot be tested independently because the anemometer doesn't measure pressure, and therefore cannot be used in conjunction with the micromanometer. Because of these constraints the following describes the procedure used.

The pitot-static probe is supported by the usual means with the probe holder setup as in Figure 4.1 above. The probe was placed in the center of the flow stream 3 De upstream of the disturbance. The pitot-static probe was then connected to the EBT 720 in conjunction with the micromanometer and readings of each were taken. Four readings of pressure and velocity were taken and averaged. The pitot-static probe was then removed. In order to make the transition to the anemometer as fast as possible the probe holder was not moved. The anemometer was placed at 3 De. The anemometer was extended the proper distance to reach the center of the duct and supported by a board spanning the base of the holder and by hand. A 10 second average with the anemometer was then taken. There is a schematic of the pitot-static probe setup in Figure 4.1 above and a schematic of the anemometer being used in Figure 4.4 below. Other than for this specification test, when a traverse with the anemometer was conducted the anemometer would be supported by the column rather than the board.

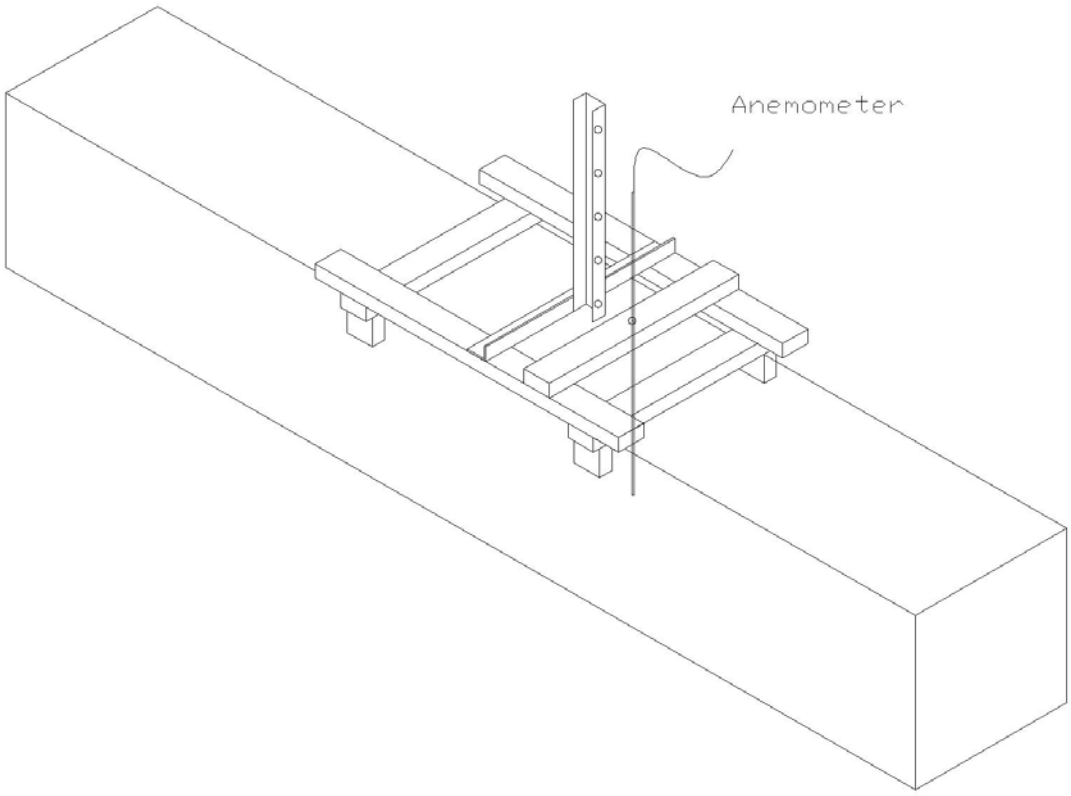

Figure 4.4 Anemometer Setup

This procedure was conducted each time a new duct configuration was built or within no less than a week of a test. Table 4.2 shows the dates of these tests. If each probe's measurements fell within their accuracy specifications, the probes were working properly. If, however, they fell outside of that range further investigation needed to be done. This may include doing the procedure over or a more elaborate calibration check. The procedure was conducted at two velocities for each probe. The velocity wasn't exactly the same on each test but was kept approximately the same by setting the VFD the same. A summary of when these checks were conducted while this researcher was in charge of conducting tests is presented below in.

Table 4.2 Probe Specification Checks (Passed)

Date	EBT 720 VFD Settings		VelociCalc 8347(A) VFD Settings	
6/26/2006	30	50	30	50
7/14/2006	30	50	30	50
7/20/2006	30	50	30	50
7/27/2006	30	50	30	50
10/26/2006	18	34	18	34
10/31/2006	18	34	18	34
11/7/2006	18	34	18	34
11/14/2006	18	34	18	34
11/30/2006	18	34	18	34
12/8/2006	18	34	18	34
12/19/2006	18	34	18	34
1/2/2007	18	34	18	34
1/11/2007	18	34	18	34
1/19/2007	18	34	18	34
1/31/2007	18	34	18	34
2/7/2007	18	34	18	34
2/15/2007	18	34	18	34
2/23/2007	18	34	18	34
3/8/2007	18	34	18	34
3/27/2007	18	34	18	34
4/9/2007	18	34	18	34
4/16/2007	18	34	18	34

CHAPTER 5 - Experimental Uncertainty

Chapter 3 identified the methods for measuring the air flow rate used in ASHRAE 1245-RP. A nozzle bank was selected as the standard to base all measurement comparisons on. The nozzle bank was selected for its low uncertainty, large flow range capability, and ease of use with a data acquisition system. A Flow Measurement Station was used as a second standard when there are multiple paths for air to flow. Duct traverses were used for air flow measurements in the duct. The uncertainties in these three measurement types must be determined to form a valid basis of comparison between the measurements which depend on the instruments used to make the measurements. A full listing of instrument specifications is available in Appendix D. Along with the accuracies and precision of all measurements being taken a sensitivity analysis combined with the root mean square method was performed on all calculations. The analysis was performed in the following manner, assuming a generic equation of the following form:

$$A = f\left(B, C\right) \tag{15}$$

Where A, B, and C represent the variables being analyzed and could be anything. There could be more or fewer variables. From a sensitivity analysis the absolute error in the variable A is:

$$E_A = \frac{\partial A}{\partial B} E_B + \frac{\partial A}{\partial C} E_C \tag{16}$$

The uncertainty in A is determined from the root mean square method.

$$U_A = \left(\left(\frac{\partial A}{\partial B} U_B \right)^2 + \left(\frac{\partial A}{\partial C} U_C \right)^2 \right)^{\frac{1}{2}} \tag{17}$$

This type of analysis was used on all calculations where a sensitivity analysis was required to determine the propagation of errors through the equations. The uncertainties for the calculations discussed in Chapter 3 are presented below.

5.1 Air Property Uncertainties

As discussed in chapter 3 the primary air properties required for the calculation of volumetric air flow measurement are the air viscosity and density. The uncertainties in these two parameters are influenced by the other properties measured to obtain them. The methods by which these other properties are measured greatly affect their uncertainties. The air viscosity can be assumed a function of dry bulb temperature only; therefore, the uncertainty is directly related to the uncertainty in the dry bulb temperature measurement. The air density can be determined several ways requiring the measurement of one or more air properties including dry bulb temperature, pressure, and humidity. The humidity can be obtained by various methods including the measurement of the wet bulb temperature, relative humidity, or dew point temperature. For this project the density is a function of the following variables from ASHRAE Fundamentals.

$$\rho_o = f\left(P, P_w, T, R_{da}\right) \tag{18}$$

Where

P = Barometric Pressure

P_w = Partial Vapor Pressure

T = Dry Bulb Temperature

R_{da} = Gas Constant for Dry Air

And from a sensitivity analysis the uncertainty in density is:

$$U_{\rho_o} = \left(\left(\frac{\partial \rho_o}{\partial P} U_P \right)^2 + \left(\frac{\partial \rho_o}{\partial P_w} U_{P_w} \right)^2 + \left(\frac{\partial \rho_o}{\partial T} U_T \right)^2 + \left(\frac{\partial \rho_o}{\partial R_{da}} U_{R_{da}} \right)^2 \right)^{\frac{1}{2}} \tag{19}$$

The gas constant can be assumed to have negligible error. The accuracy of the pressure and temperature measurement was discussed in chapter 3 section 1. From the ASHRAE Fundamentals Handbook the partial vapor pressure is a function of the following variables.

$$P_w = f\left(\phi, P_{ws}(T)\right) \tag{20}$$

Where

ϕ = Relative Humidity

$P_{ws}(T)$ = Saturation Pressure

And the uncertainty is the following:

$$U_{P_w} = \left(\left(\frac{\partial P_w}{\partial \phi} U_\phi \right)^2 + \left(\frac{\partial P_w}{\partial P_{ws}(T)} U_{P_{ws}(T)} \right)^2 \right)^{\frac{1}{2}} \quad \textbf{(21)}$$

The accuracy of the relative humidity measurement was discussed in chapter 3 section 1 and the saturation pressure is a function of temperature only and a sensitivity analysis can be used to determine the effect of temperature on it.

5.2 Nozzle Bank Flow Uncertainty

The calculation of volumetric air flow rate through a nozzle bank can be determined using ASHRAE Standard 120 or a similar AMCA standard such as AMCA Standard 210-1985. For ASHRAE 1245-RP ASHRAE Standard 120 was chosen as the standard for volumetric flow rate through a nozzle bank. Calculations of the flow rate taken from this standard are discussed in chapter 3. The following discusses the uncertainties associated with those calculations.

The flow rate is a function of the following variables from Equation 3 in chapter 3.

$$Q = f\left(Y_n, \Delta P_{s,\,1-2}, \rho_1, C_n, A_n\right) \quad \textbf{(22)}$$

From the sensitivity analysis the following equation for the absolute uncertainty in flow rate is obtained.

$$U_Q = \left(\begin{array}{l} \left(\frac{\partial Q}{\partial Y_n} U_{Y_n} \right)^2 + \left(\frac{\partial Q}{\partial \Delta P_{s,\,1-2}} U_{\Delta P_{s,\,1-2}} \right)^2 + \left(\frac{\partial Q}{\partial \rho_1} U_{\rho_1} \right)^2 \\ + \sum_{n=1}^{N} \left(\frac{\partial Q}{\partial C_n} U_{C_n} \right)^2 + \left(\frac{\partial Q}{\partial A_n} U_{A_n} \right)^2 \end{array} \right)^{\frac{1}{2}} \quad \textbf{(23)}$$

In order to further analyze the flow rate uncertainty the absolute uncertainty for each variable must also be analyzed. Each one will also have its own independent variables which must be analyzed until we get down to the measured variables discussed in chapter 3. The uncertainty in the air density was discussed in section 5.1. The accuracy of the static pressure drop across the nozzles was discussed in chapter 3. The other uncertainties are evaluated below.

5.3.2 Nozzle Expansion Factor Uncertainty

The expansion factor is a function of the following three variables discussed in chapter 3.

$$Y_n = f(\alpha, \beta, \gamma) \quad \textbf{(24)}$$

Where

α = Alpha Ratio

β = Beta Ratio

γ = Specific Heat Ratio

In this case the uncertainties of the other variables aren't necessary. The relative uncertainty in the expansion factor is determined by the following equation from (ASME MFC 3M, 1989).

$$\mu_{Y_n} = \frac{2\Delta P_{s,\,1-2}}{P_{s1}} \ \% \quad \textbf{(25)}$$

Where

P_{s1} = Static Pressure at Nozzle Inlet

5.3.3 Discharge Coefficient Uncertainty

An appropriate uncertainty in the discharge coefficient isn't clear from ASHRAE Standard 120. Other sources were looked at as a reference for an appropriate discharge coefficient uncertainty. These include (AMCA Standard 210, 1985), (ASME MFC 3M, 1989), and (ISO 5168, 1978) none of which resulted in a definite conclusion. AMCA Standard 210-1985 references a tolerance of 1.2% for the discharge coefficients used in that standard. The curve fit equations used in this standard are not the same as ASHRAE Standard 120 so this isn't necessarily appropriate the discharge coefficient used in this research; However, it seems reasonable that the discharge coefficient equations of ASHRAE Standard 120 would have a similar uncertainty. One other standard is being looked into which might discuss the uncertainty of the discharge coefficient used in ASHRAE Standard 120. This is ISO Standard 5167-1.

5.3.4 Nozzle Area Uncertainty

The nozzle areas are calculated using the nozzle diameter. The uncertainty depends on the nozzle diameter measurement uncertainty. Measurements of all nozzle diameters in the nozzle bank were taken to verify their nominal values and determine the uncertainties in the dimensions. The nominal dimensions were used in calculations of flow rate at the nozzle bank. The measurements were taken from three plains at equal angles apart inside the nozzles. The first

was vertical. The following two were at 60° angles in opposite directions from the first. Three readings were taken at each plain. The measurements are presented in Table 5.1.

Table 5.1 Nozzle Diameter Measurements

	Nozzle Number								
Position	1	2	3	4	5	6	7	8	9
Vertical	5.0070	5.9654	5.5048	3.9950	1.6029	2.5053	5.0003	6.0045	5.5018
	5.0045	6.0075	5.5049	3.9947	1.6085	2.5044	5.0014	6.0120	5.4998
	4.9978	6.0023	5.5046	3.9985	1.5997	2.5063	4.9984	6.0072	5.5003
Rotated 60° Clockwise	4.9875	5.9874	5.4864	3.9810	1.5985	2.5009	5.0124	5.9881	5.5081
	4.9835	5.9980	5.5020	3.9775	1.5966	2.4980	5.0120	6.0161	5.5151
	4.9938	6.0002	5.5015	3.9739	1.5976	2.5005	5.0115	6.0078	5.5119
Rotated 60° Counter Clockwise	5.0082	5.9974	5.5100	3.9970	1.6076	2.5034	4.9964	5.9954	5.5052
	5.0039	5.9890	5.5112	3.9949	1.6062	2.5024	4.9932	6.0023	5.5021
	5.0034	5.9960	5.5114	3.9973	1.6018	2.5019	4.9932	6.0081	5.5050

Standard deviations and uncertainties were determined from the measurements of each nozzle. Table 5.2 summarizes these uncertainties. The uncertainties in the diameter measurements varied from 0.22% to a maximum of 0.64%. Therefore, an uncertainty of 0.64% in nozzle diameter was used for all nozzles. This is to simplify calculations of uncertainty while using a conservative uncertainty estimate.

Table 5.2 Nozzle Diameter Uncertainty

	Nozzle Number								
	1	2	3	4	5	6	7	8	9
Nominal Dimension	**5.00**	**6.00**	**5.50**	**4.00**	**1.60**	**2.50**	**5.00**	**6.00**	**5.50**
Average	4.9988	5.9937	5.5041	3.9900	1.6022	2.5026	5.0021	6.0046	5.5055
Standard Deviation	0.0088	0.0123	0.0076	0.0096	0.0044	0.0026	0.0079	0.0085	0.0053
t-value	2.306	2.306	2.306	2.306	2.306	2.306	2.306	2.306	2.306
Uncertainty inches	**2.04E-02**	**2.83E-02**	**1.76E-02**	**2.22E-02**	**1.02E-02**	**5.98E-03**	**1.82E-02**	**1.96E-02**	**1.22E-02**
Uncertainty m	**5.17E-04**	**7.19E-04**	**4.46E-04**	**5.64E-04**	**2.60E-04**	**1.52E-04**	**4.63E-04**	**4.98E-04**	**3.11E-04**
Uncertainty %	**0.41%**	**0.47%**	**0.32%**	**0.56%**	**0.64%**	**0.24%**	**0.36%**	**0.33%**	**0.22%**
Max Uncertainty	**0.64%**								

5.4 Traversing Algorithm Uncertainties

The flow rate of a traverse is discussed in chapter 3 section 3.4. There is an uncertainty associated with the average velocity, duct area, and methods by which the traverse is performed. The first two of these (average velocity and duct area) can be obtained from a sensitivity analysis. The combination of these uncertainties yields the following equation for the uncertainty in the traverse:

$$U_{Q_{Traverse}} = \left(\left(\frac{\partial Q_{Traverse}}{\partial A_{duct}} U_{A_{duct}} \right)^2 + \sum_{n=1}^{M} \left(\frac{\partial Q_{Traverse}}{\partial V_n} U_{V_n} \right)^2 + U_{Traverse}{}^2 \right)^{\frac{1}{2}} \quad \textbf{(26)}$$

Where

$Q_{Traverse}$ = Volumetric Flow Rate of Traverse

A_{duct} = Nominal Area of Duct

V_n = Local velocity at point n

M = Number of Traverse Points

$U_{Traverse}$ = Uncertainty in Traverse Methods

The constant M depends on the traverse algorithm being used. For ASHRAE 1245-RP this was either log-Tchebycheff or equal area. M also depends on the duct dimensions. Log-Tchebycheff and equal area traverse algorithms are available in ASHRAE Standard 111-1988 and the ASHRAE Fundamentals Handbook. Equal area algorithms are also available in (AABC, 2002). The uncertainty in the local velocity measurement of each point in the traverse depends on the method that velocity is measured. Local velocity measurements were discussed in chapter 3 and +/-3% of reading can be obtained for probes used in this project. The uncertainty in the duct area and traverse methods must be discussed in more detail.

5.4.1 Duct Area Uncertainty

The uncertainty in the area of the duct can have a much larger impact on the uncertainty of the flow rate than may be first realized. The uncertainty in the duct area is affected by the tolerance on duct manufacturing. The nominal area of the duct is calculated with the nominal height and width of the duct. An estimate of the uncertainty can then be obtained assuming the angles of the rectangular duct are at 90^o. Additional error could be present due to variations in duct shape including duct bowing and leaning. The uncertainty in duct area is the following with the assumption that it is a function of the duct dimensions only.

$$U_{A_{duct}} = \left(\left(\frac{\partial A_{duct}}{\partial Width} U_{Width} \right)^2 + \left(\frac{\partial A_{duct}}{\partial Height} U_{Height} \right)^2 \right)^{\frac{1}{2}} \quad \textbf{(27)}$$

With a typical duct dimension tolerance of ±0.25 inches and 2 ft x 1 ft duct dimensions it can quickly be seen that this uncertainty can be as high as 2% or more.

5.4.2 Traverse Methods

Many things can affect the uncertainty in the traverse method. It's largely dependent on the methods used to perform the traverse. As an example this paper will look at uncertainty effects in the methods used by ASHRAE 1245-RP. Many of these would be present in most methods; however, the value of the uncertainty could vary. Things that could affect the uncertainty include but are not limited to the following:

- Probe Positioning
- Longitudinal Placement
- Vertical Placement
- Probe Tilt
- Probe Twist
- Duct Dimensions
- Duct Shape

Assumptions must be made in order to determine this uncertainty. Appropriate assumptions were still being looked into at the submittal of this thesis.

5.5 Flow Measurement Station Uncertainty

Air flow measurement stations typically will have an uncertainty specification provided by the manufacturer; however, the device may not have been tested for all variations of the device sold. For example the flow measurement station used by ASHRAE 1245-RP was a 1 ft x 1 ft device which was not tested by the manufacturer. The manufacturer had tested other sizes of flow measurement stations. With accuracy verification test performed by the researchers of ASHRAE 1245-RP it was determined that the device required a calibration. When compared to the nozzle bank the FMS was far outside the 2% of air flow manufacturer spec. The uncertainty of the device should be determined based on this new calibration. The calibration was discussed in chapter 3.

The uncertainty is a function of the FMS duct area and the average velocity through the duct.

$$U_{Q_{FMS}} = \left(\left(\frac{\partial Q_{FMS}}{\partial V_{FMS}} U_{V_{FMS}} \right)^2 + \left(\frac{\partial Q_{FMS}}{\partial A_{duct}} U_{A_{duct}} \right)^2 \right)^{\frac{1}{2}} \quad \textbf{(28)}$$

Where

Q_{FMS} = Flow Rate through FMS

The uncertainty analysis for the average velocity is slightly more complicated because the flow coefficient and Re depend on each other. A sensitivity analysis was performed to obtain the uncertainty in FMS flow rate. The absolute uncertainty in the average velocity at the FMS is obtained from a sensitivity analysis on Equation 12 of chapter 3.

$$U_{V_{FMS}} = \left(\left(\frac{\partial V_{FMS}}{\partial Re} U_{Re} \right)^2 + \left(\frac{\partial V_{FMS}}{\partial \rho_o} U_{\rho_o} \right)^2 + \left(\frac{\partial V_{FMS}}{\partial \mu_o} U_{\mu_o} \right)^2 + \left(\frac{\partial V_{FMS}}{\partial d_{tube}} U_{d_{tube}} \right)^2 \right)^{\frac{1}{2}} \quad \textbf{(29)}$$

The absolute error in the Re is determined from Equation 6 of chapter 3.

$$E_{Re} = \frac{\partial Re}{\partial P_v} E_{P_v} + \frac{\partial Re}{\partial C} E_C + \frac{\partial Re}{\partial \rho_o} E_{\rho_o} + \frac{\partial Re}{\partial \mu_o} E_{\mu_o} + \frac{\partial Re}{\partial d_{tube}} E_{d_{tube}} \quad \textbf{(30)}$$

From Equation 11 of chapter 3 the error in the flow coefficient is dependent on the Re and the random error associated with the calibration and is the following:

$$E_C = \frac{\partial C}{\partial Re} E_{Re} + E_{Rand} \quad \textbf{(31)}$$

Combining these equations gives a final error and uncertainty in the Re of the following:

$$E_{Re} = \frac{1}{1 - \frac{\partial Re}{\partial C}\frac{\partial C}{\partial Re}} * \left(\frac{\partial Re}{\partial C} E_{Rand} + \frac{\partial Re}{\partial P_v} E_{P_v} + \frac{\partial Re}{\partial \rho_o} E_{\rho_o} + \frac{\partial Re}{\partial \mu_o} E_{\mu_o} + \frac{\partial Re}{\partial d_{tube}} E_{d_{tube}} \right) \quad \textbf{(32)}$$

$$U_{Re} = \frac{1}{1 - \frac{\partial Re}{\partial C}\frac{\partial C}{\partial Re}} * \left(\begin{array}{l} \left(\frac{\partial Re}{\partial C} U_{Rand} \right)^2 + \left(\frac{\partial Re}{\partial P_v} U_{P_v} \right)^2 + \left(\frac{\partial Re}{\partial \rho_o} U_{\rho_o} \right)^2 \\ + \left(\frac{\partial Re}{\partial \mu_o} U_{\mu_o} \right)^2 + \left(\frac{\partial Re}{\partial d_{tube}} U_{d_{tube}} \right)^2 \end{array} \right)^{\frac{1}{2}} \quad \textbf{(33)}$$

The random uncertainty in the flow coefficient depends on the standard deviation of the data collected in the calibration. The calibration of ASHRAE 1245-RP resulted in the curve fit in Figure 5.1 and deviations of the flow coefficient C* in Figure 5.2.

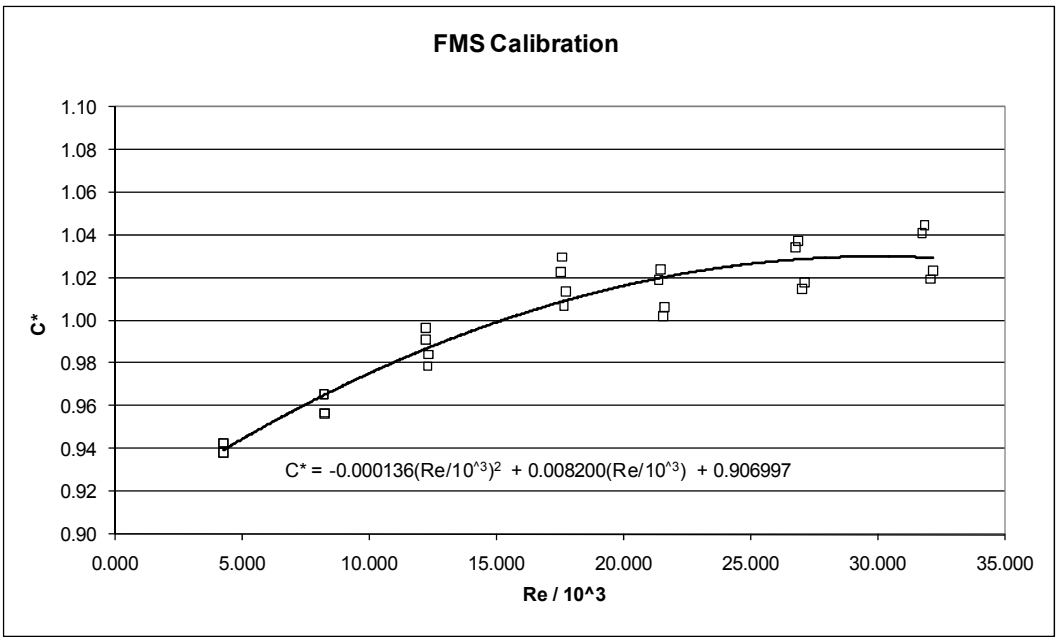

Figure 5.1 FMS Flow Coefficient Calibration Curve

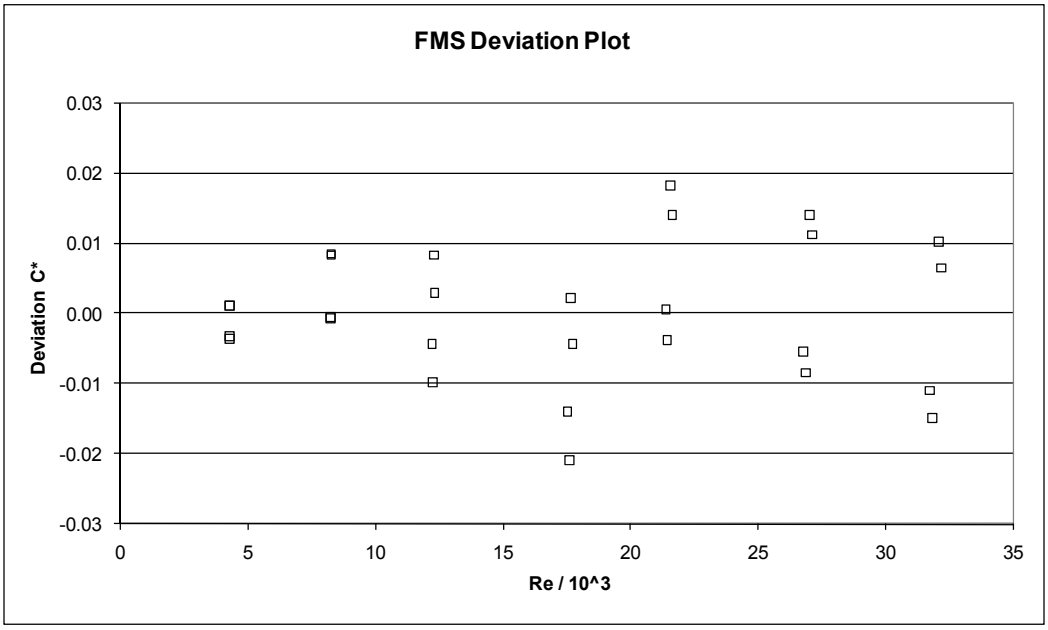

Figure 5.2 FMS Calibration Coefficient Deviation Plot

These deviations resulted in the following random uncertainty in the flow coefficient C*.

$U_{Rand} = \pm 0.02$

Because the area ratio used in Equation 9 of chapter 3 is a constant and does not change, the random uncertainty in C and C* are the same.

CHAPTER 6 - Experimental Data and Analysis

This thesis analyzes data collected for the 24" x 24" duct. This includes the disturbances 60^o transition, 90^o transition, 90^o elbow, and 90^o diverging tee. In addition to this there were measurements taken in a straight section of duct with no disturbance, used to show that the system is working properly and to have a basis to compare all other data to. The velocities to be tested were specified in the downstream duct to be 600, 1200, 1800, and 2400 fpm with the exception of the tee measurements. The velocities for the tee were to be the same only specified to be in the upstream duct. This is because if specified to be in the downstream duct the highest velocity with the lowest branch to common line flow ratio would produce a very large and unobtainable flow rate.

The purpose of the analysis is to make some comparisons and determine if there are significant changes between them for which conclusions could be drawn. The comparisons made are the following:

- Measurement Location: Distance from the Disturbance
- Traverse Algorithm: Log-Tchebycheff and Equal Area
- Measurement Probe: Pitot-static Probe and Anemometer

The comparisons made will be between the traverse data for each case and the flow measurement standard. For non-tee measurements this is the nozzle bank. For the tee measurements this is the nozzle bank along with the flow measurement station. The duct traverses represent an idealization of the measurements that technicians would take in the field. It is desired to quantify the error in the traverse measurements. Error is defined as a comparison of the traverse flow rate and the actual flow rate or standard, and is defined as:

$$\text{Error} = \frac{Q_{SCFM}(\text{Traverse}) - Q_{SCFM}(\text{Standard})}{Q_{SCFM}(\text{Standard})} 100\% \quad \textbf{(34)}$$

For tees the standard is defined as:

$$Q_{SCFM}(\text{Standard}) = Q_{SCFM}(\text{Nozzle Bank}) - Q_{SCFM}(\text{FMS}) \quad \textbf{(35)}$$

For all other measurements it is defined as:

$$Q_{SCFM}(\text{Standard}) = Q_{SCFM}(\text{Nozzle Bank}) \quad \textbf{(36)}$$

The traverse data was collected on data sheets, hard copies later transferred to a computer for analysis. The data sheets contain all relevant information including log-Tchebycheff and equal area traverse velocities, barometric pressure, VFD setting, number of nozzles plugged and others. Some changes in what parameters were collected were made over the course of the project due to slight improvements in the procedure. For example after the 60° and 90° transitions an additional pressure transducer was purchased and nozzle inlet pressure no longer needed to be recorded before and after each test. The sheets also contain information describing which test the sheet pertains to for organization and file maintenance purposes. An example of a data sheet for the 90^{o} Elbow is presented in Figures 6.1 and Figure 6.2 below.

Measurement Data

Tester	Craig
Date	4/12/2007
Location	
# Diameters	1
Upstream / Downstream	Upstream
Duct Size	2 x 2
Disturbance	90^{o} Elbow
Intended	
Flow Rate (SCFM)	9600
Mean Velocity (SFPM)	2400
Anemometer / Pitot	Anemometer

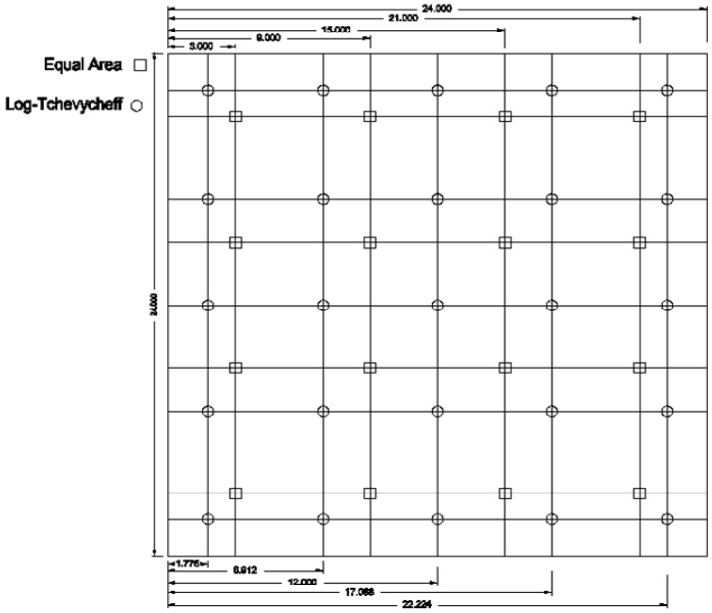

Figure 6.1 90^{o} Elbow Data Sheet page 1

Initial Conditions				
Barometric Pressure "hg	29.09	Frequency hz	52.20	
Barometer Temperature °C	75.00	Nozzles Plugged	None	
Barometric Pressure kPa	98.09			
		Log-Tchebycheff		
2185	2290	2255	2340	2255
2240	2640	2665	2695	2400
2265	2625	2720	2730	2490
2200	2485	2460	2575	2350
2030	2095	2040	2270	2070
		Equal Area		
2370	2435	2425	2440	
2340	2710	2740	2585	
2380	2590	2605	2555	
2285	2190	2350	2275	
Final Conditions				
Barometric Pressure "hg	29.08			
Barometer Temperature °C	75.00			
Barometric Pressure kPa	98.05			

Figure 6.2 90^{o} Elbow Data Sheet page 2

The flow rates for the nozzle bank and FMS were calculated with LabView software and printed to a file. Once all the traverse, FMS, and nozzle bank measurements had been made the comparison process began. The error previously mention was calculated for all duct sizes, duct disturbances, duct location, traverse algorithm, velocity, and probe combinations. The results of the calculation of error are presented in plots comparing the error at each location upstream and downstream of the disturbance. There is a plot for each velocity for a total of 4 plots for each duct size and disturbance combination. Results for both probes as well as log-Tchebycheff and equal area traverse data are presented in the same plot. Appendix B contains these plots along with summary tables for all duct configurations taken up to the submission of this thesis. An example of the summary and plot is in Figure 6.3 below.

6.1 No Disturbance (Straight Duct) Analysis

The duct with no disturbance had 20 De of upstream duct length and 10 De of downstream duct length and should produce fully developed turbulent flow. Measurements should be scattered around an error of 0 within the uncertainty of the measurements. The

assumption of fully developed flow is confirmed from Figures 6.3 and 6.4 below. Measurement profiles at 3 De upstream and 7.5 De downstream of the theoretical disturbance, had there been one, are shown. It appears from the plots that the flow profile isn't changed very much between the locations and the flow profile is fairly symmetrical, although they appear to be slightly skewed. This suggests that the flow is fully developed or close to it.

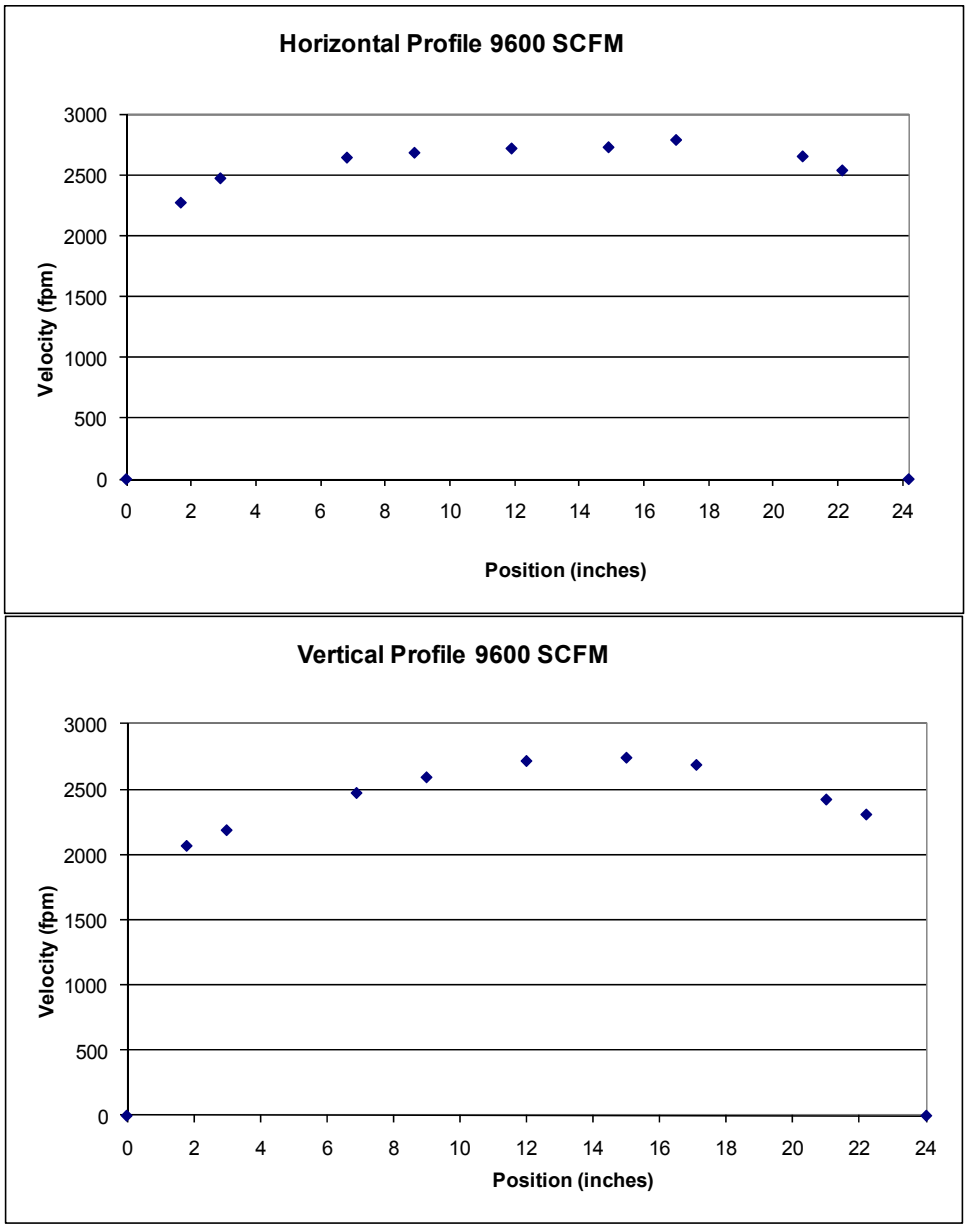

Figure 6.3 Velocity Profiles 3 De Upstream

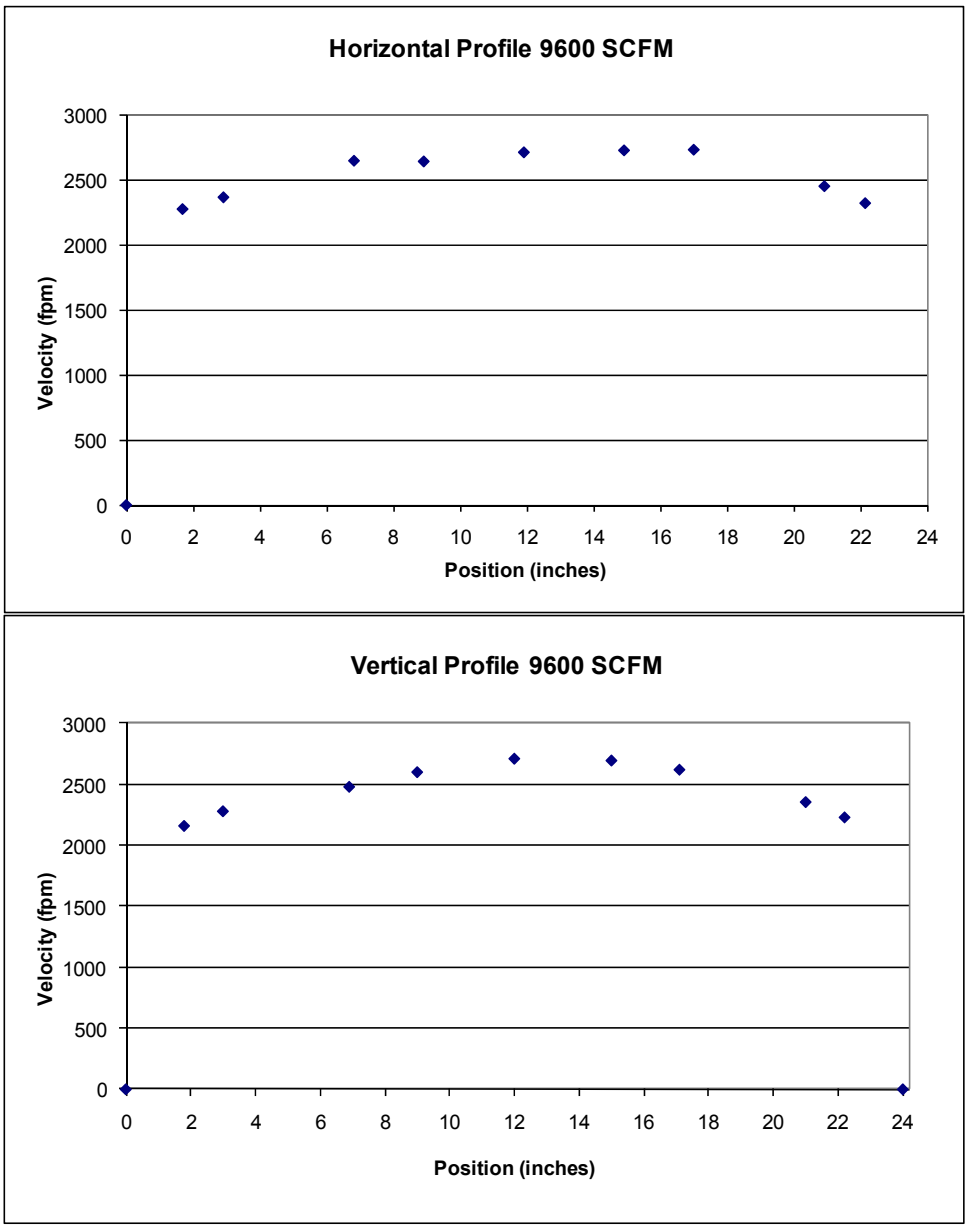

Figure 6.4 Velocity Profiles 7.5 De Downstream

Based on the discussion in Chapter 5, a 1.6% traverse uncertainty estimate was calculated for the 24" x 24" duct. This is based on the +/-3% accuracy of the probes being primarily random uncertainty with small bias error and a +/-0.25" duct dimension tolerance. It doesn't include uncertainty in all aspects of the traverse such as proper probe placement because these are still being investigated. From Figure 6.5 below it appears the two probes are obtaining the same reading within this uncertainty. This suggests that the assumption that the probe accuracy is primarily random uncertainty is appropriate and the bias error of the probes is small. An initial

estimate of the uncertainty in the nozzle bank was also performed which gave an uncertainty between 0.75% and 1.75% depending on flow rate. This was based on an assumption of a 1.0% uncertainty in the nozzle discharge coefficient with is still under investigation. The error or difference between the traverses and the nozzle bank for the log-Tchebycheff measurements appear to be scattered around 0 for all measurement locations and within the uncertainties of the nozzle bank and traverse. This suggests that log-Tchebycheff is an accurate measurement technique when a fully developed flow exists. The equal area data errors appear to be higher than the log-Tchebycheff errors for both probes. From Figure 6.5 it appears that the differences between the two are about 3 to 4% on average. This is consistent over all measurement locations upstream and downstream of the theoretical disturbance location.

Measurement Location	Pitot Probe						Anemometer					
	Log-T			Equal Area			Log-T			Equal Area		
De	Q(Standard) SCFM	Traverse SCFM	Error %	Q(Standard) SCFM	Traverse SCFM	Error %	Q(Standard) SCFM	Traverse SCFM	Error %	Q(Standard) SCFM	Traverse SCFM	Error %
-3	4770	4817	0.97	4774	4974	4.19	4793	4750	-0.89	4788	4900	2.33
-1	4798	4808	0.21	4790	4977	3.89	4795	4786	-0.18	4791	4953	3.37
0	1200 SFPM Straight Duct											
1	4807	4839	0.68	4817	5035	4.54	4802	4777	-0.52	4802	5013	4.39
2	4796	4833	0.77	4795	4991	4.08	4806	4903	2.02	4810	5161	7.31
3	4798	4812	0.30	4795	4980	3.86	4795	4748	-0.99	4798	4928	2.70
5	4812	4899	1.81	4818	5093	5.69	4794	4810	0.34	4791	4991	4.18
7.5	4796	4742	-1.14	4784	4910	2.63	4797	4703	-1.97	4795	4914	2.48

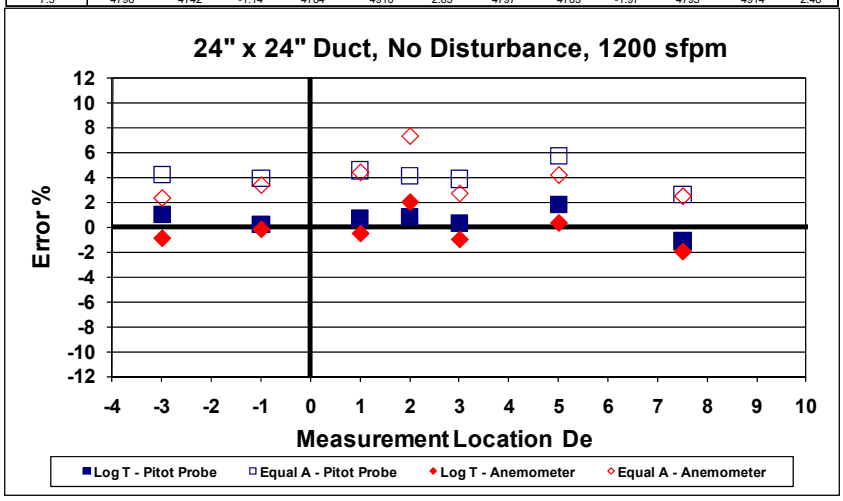

Figure 6.5 No Disturbance 1200 SFPM Data Example

6.2 Single Flow Path Disturbance Analysis

The single flow path disturbances include the 60^o transition, 90^o transition, and 90^o elbow. Examples of data plots for these disturbances are available in Figures 6.6 through 6.8 below. All data for the tests can be reviewed in Appendix B. As in the straight duct, it was noticed that the equal area errors are about 3 to 4% higher on average than the log-Tchebycheff

errors for all three disturbances. Also, it appears there is no significant difference between the probe types for any disturbance. For the 90° elbow the error differences between measurement locations were consistent and no significant differences are apparent for the effect of measurement location on traverse measurement. For the transitions there appears to be an upward trend in error the further downstream of the disturbance a measurement was taken. This is evident at the 5 De and 7.5 De locations. A possible explanation of this is that for these two locations the traverse plain was at a duct seam. It is believed that boundary layer affects from the seam could possibly have affected the traverse measurements. The reason this trend is apparent on the transition measurements and not the elbow is that the downstream duct size for the transitions is different; therefore, the De and measurement locations are different and the seam is not located so close to a measurement location. The 90° elbow and straight duct have a 24" x 24" downstream duct and the transitions have a 24" x 12" downstream duct.

Measurement Postion	Pitot Probe						Anemometer					
	Log-T			Equal Area			Log-T			Equal Area		
De	Q(Standard) SCFM	Traverse SCFM	Error %	Q(Standard) SCFM	Traverse SCFM	Error %	Q(Standard) SCFM	Traverse SCFM	Error %	Q(Standard) SCFM	Traverse SCFM	Error %
-3	2403	2420	0.68	2410	2537	5.29	2396	2428	1.34	2395	2525	5.45
-1	2399	2382	-0.72	2397	2480	3.48	2401	2397	-0.18	2402	2491	3.69
0	1200 SFPM 60° Transition											
1	2406	2398	-0.32	2405	2505	4.13	2393	2345	-2.03	2399	2442	1.79
2	2406	2434	1.14	2407	2507	4.13	2406	2370	-1.51	2408	2432	1.00
3	2398	2364	-1.39	2397	2431	1.42	2402	2357	-1.90	2403	2440	1.54
5	2398	2422	0.99	2394	2488	3.92	2381	2399	0.76	2379	2475	4.04
7.5	2402	2465	2.62	2405	2567	6.71	2400	2449	2.05	2401	2569	6.99

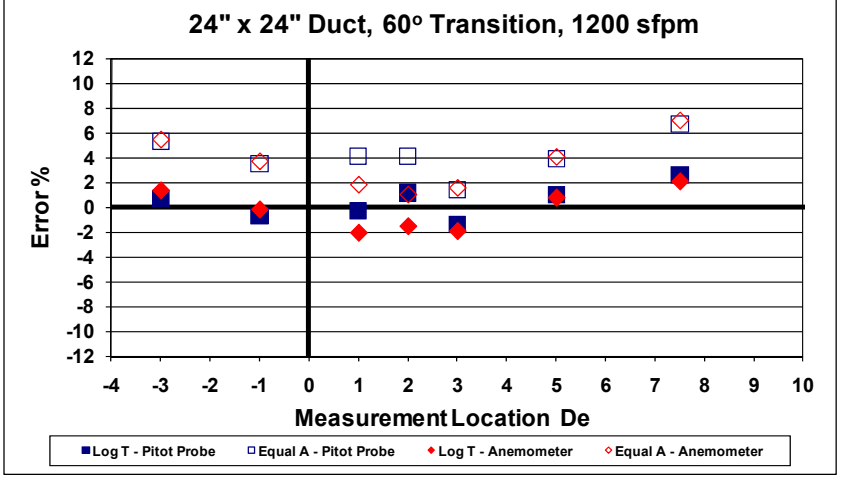

Figure 6.6 60° Transition 1200 SFPM Data Example

Measurement Location	Pitot Probe						Anemometer					
	Log-T			Equal Area			Log-T			Equal Area		
De	Q(Standard) SCFM	Traverse SCFM	Error %	Q(Standard) SCFM	Traverse SCFM	Error %	Q(Standard) SCFM	Traverse SCFM	Error %	Q(Standard) SCFM	Traverse SCFM	Error %
-3	2395	2421	1.06	2395	2522	5.33	2391	2407	0.71	2394	2526	5.51
-1	2408	2395	-0.54	2412	2522	4.56	2402	2404	0.06	2404	2504	4.15
0	1200 SFPM 90° Transition											
1	2403	2428	1.04	2405	2524	4.96	2406	2384	-0.91	2409	2473	2.67
2	2406	2431	1.06	2409	2507	4.09	2403	2365	-1.58	2402	2452	2.05
3	2413	2383	-1.22	2409	2440	1.25	2406	2348	-2.40	2413	2442	1.19
5	2400	2448	1.99	2396	2521	5.19	2395	2446	2.14	2390	2525	5.64
7.5	2400	2458	2.42	2400	2567	6.94	2393	2430	1.55	2387	2526	5.80

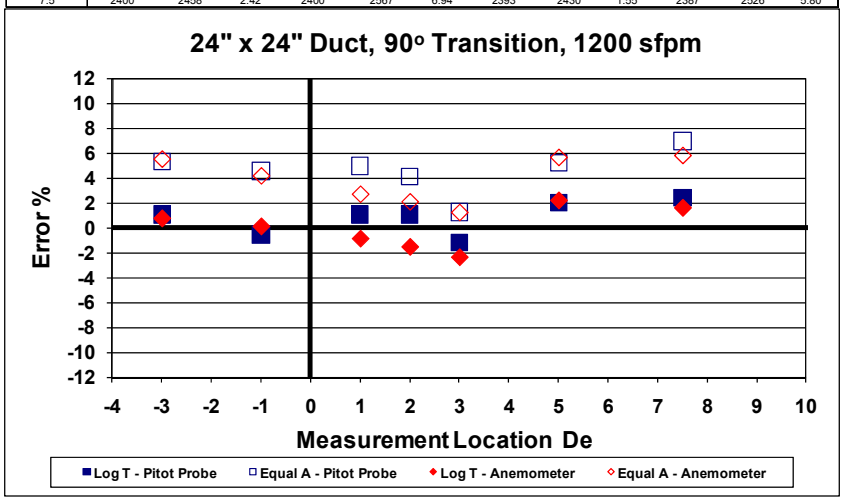

Figure 6.7 90° Transition 1200 SFPM Data Example

Measurement Location	Pitot Probe						Anemometer					
	Log-T			Equal Area			Log-T			Equal Area		
De	Q(Standard) SCFM	Traverse SCFM	Error %	Q(Standard) SCFM	Traverse SCFM	Error %	Q(Standard) SCFM	Traverse SCFM	Error %	Q(Standard) SCFM	Traverse SCFM	Error %
-3	4794	4855	1.28	4788	5012	4.68	4794	4883	1.85	4793	5023	4.80
-1	4790	4785	-0.11	4791	4942	3.15	4802	4748	-1.12	4807	4910	2.14
0	1200 SFPM 90° Elbow											
1	4789	4718	-1.47	4779	4925	3.06	4785	4645	-2.93	4758	4800	0.87
2	4789	4824	0.74	4779	4952	3.62	4807	4880	1.51	4813	5019	4.28
3	4787	4770	-0.35	4764	4930	3.47	4797	4787	-0.21	4789	4943	3.20
5	4812	4933	2.51	4807	5099	6.07	4804	4828	0.49	4802	4920	2.46
7.5	4796	4759	-0.79	4796	4948	3.15	4794	4712	-1.70	4790	4900	2.30

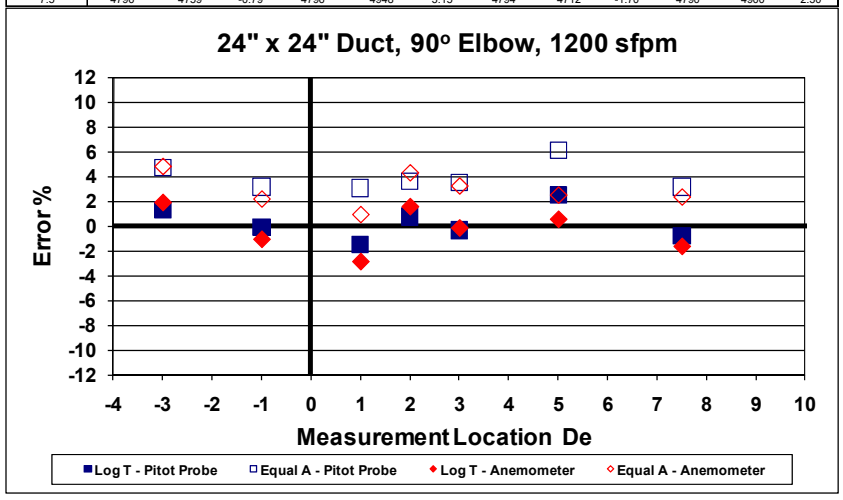

Figure 6.8 90° Elbow 1200 SFPM Data Example

6.3 Multiple Flow Path (Tee) Disturbance Analysis

Up to the submittal of this thesis only one multiple flow path disturbance had been tested which was the diverging tee on the 24" x 24" upstream duct. The velocity targets of 600, 1200, 1800, and 2400 fpm are the same as the single flow path measurements; however, for a Qb/Qc ratio of 0.2 the highest velocity couldn't be achieved because of pressure drop and fan limitations. It was decided by the ASHRAE committee to allow 2100 fpm to be used for this measurement instead. The results of the tee measurements are much more unusual than the single path disturbances especially with a lower branch to common line flow ratio. The lowest branch to common line flow ratio (Qb/Qc = 0.2) produced anomalous results for locations close to the tee exit. Specifically locations of 1 and 2 equivalent diameters from the disturbance were greatly affected. This is believed to be partially due to "negative velocity pressure readings" due to non-parallel flows and even reverse flows as the air moves into the branch of the tee where the measurements are taken. Of course a "negative velocity pressure" doesn't make since. These readings simply mean that the static pressure port on the pitot-static probe is experiencing a higher pressure than the stagnation port due to the air swirling. An example of a datasheet containing the negative readings obtained is available in Figures 6.10 and 6.11 below. The anemometer and pitot-static probe are both unidirectional devices and do not account for air swirling or reverse flow back toward the tee. This could also be affecting other measurements with other flow ratios and measurement locations but was most noticeable for the 0.2 ratio. (Beck et al, 2010) discusses errors from pitot-static probe readings when reverse or perpendicular flows are present. Figure 6.9 illustrates the conclusions for the paper where a flow coefficient for the pitot-static probe is defined as in Equations 37 and 38.

$$C_p = \frac{\Delta P}{\frac{1}{2}\rho U_\infty^2} \quad \textbf{(37)}$$

$$\Delta P = P_{stagnation} - P_{static} \quad \textbf{(38)}$$

The figure shows that completely reverse flow would be likely to produce a reading of 0 and closer to perpendicular flows would tend to produce the negative readings which appear in the data.

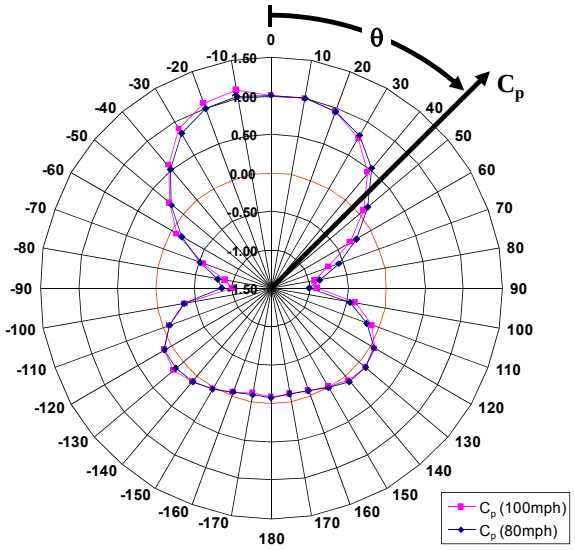

Figure 6.9 Pitot Probe Flow Coefficient Variation

In general it is more difficult to draw conclusion from the tee data. It is evident that the tee is creating a significant amount of flow measurement difficulties. Figures 6.12 through 6.14 are examples of data collected for each Qb/Qc ratio. Many errors exceed the limits of the plots but it can be seen from the tables that errors reach levels close to 60%. The remaining data is available in Appendix B. The bias between log-Tchebycheff and equal area algorithms as well as consistency between probe types is still present for the majority of the measurements upstream of the disturbance, which indicates that the results are consistent with the single flow path measurements.

Measurement Data	
Tester	Lance Basgall
Date	5/1/2008
Location	
# Diameters	1 Dh
Upstream / Downstream	Downstream
Duct Size	2 x 1
Disturbance	90° Tee
Intended	
Flow Rate (SCFM)	7200
Mean Velocity (SFPM)	720
Anemometer / Pitot	Pitot Probe

Figure 6.10 90° Tee Qb/Qc = 0.2 Datasheet 1

Initial Conditions				
Barometric Pressure "hg	28.4	Qb / Qc	0.20	
Barometer Temperature °F	85	Frequency hz	53.11	
Barometric Pressure kPa	95.70	Nozzles Plugged	None	
		Log-Tchebycheff		
-469	-211	1360	1169	2129
-491	-330	676	949	2094
-457	-274	322	882	2089
-465	-274	1044	1016	2083
-470	83	1446	1792	2040
		Equal Area		
-393	486	1242	1976	
-471	68	422	1966	
-417	729	1217	2035	
Final Conditions				
Barometric Pressure "hg	28.4			
Barometer Temperature °F	87			
Barometric Pressure kPa	95.71			

Figure 6.11 90° Tee Qb/Qc = 0.2 Datasheet 2

Measurement Location	Pitot Probe						Anemometer					
	Log-T			Equal Area			Log-T			Equal Area		
De	Q(Standard) SCFM	Traverse SCFM	Error %	Q(Standard) SCFM	Traverse SCFM	Error %	Q(Standard) SCFM	Traverse SCFM	Error %	Q(Standard) SCFM	Traverse SCFM	Error %
-3	4781	4697	-1.77	4765	4862	2.04	4778	4789	0.23	4796	5144	7.24
-1	4806	4695	-2.31	4788	4840	1.08	4774	4685	-1.87	4789	4894	2.19
0	1200 SFPM 90° Tee Qb/Qc 0.2											
1	949	747	-21.26	949	577	-39.22	971	1436	47.80	971	1340	37.93
2	955	910	-4.74	955	793	-17.04	988	1088	10.05	988	990	0.18
3	929	960	3.35	929	961	3.37	993	1062	6.96	993	999	0.61
5	983	984	0.03	983	1011	2.77	992	1024	3.24	992	999	0.77
7.5	960	944	-1.71	960	977	1.73	979	1061	8.28	979	984	0.46

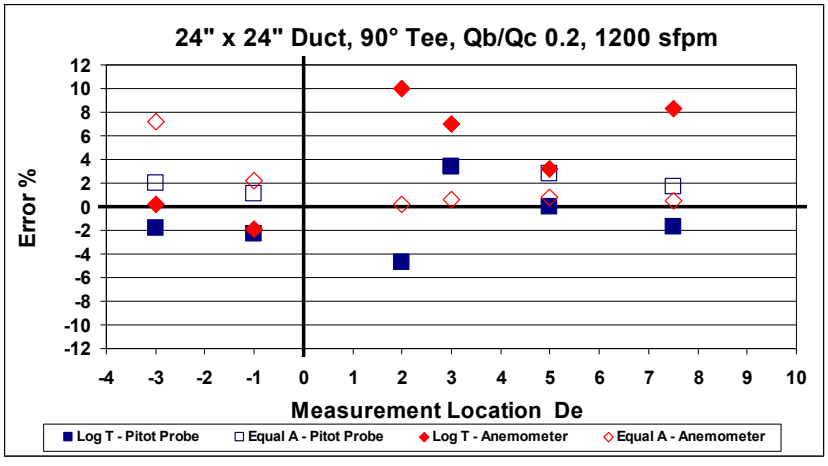

Figure 6.12 90° Tee Qb/Qc = 0.2 1200 SFPM Data Example

Measurement Location	Pitot Probe						Anemometer					
	Log-T			Equal Area			Log-T			Equal Area		
De	Q(Standard) SCFM	Traverse SCFM	Error %	Q(Standard) SCFM	Traverse SCFM	Error %	Q(Standard) SCFM	Traverse SCFM	Error %	Q(Standard) SCFM	Traverse SCFM	Error %
-3	4785	4730	-1.16	4795	4908	2.35	4792	6650	38.78	4782	5044	5.48
-1	4804	4742	-1.29	4785	4873	1.84	4803	4766	-0.76	4792	4879	1.81
0	1200 SFPM 90° Tee Qb/Qc 0.4											
1	1920	1857	-3.29	1920	1935	0.79	1901	2043	7.49	1901	1994	4.91
2	1920	1997	4.01	1920	1953	1.70	1939	1966	1.38	1939	1890	-2.52
3	1918	2001	4.34	1918	2023	5.44	1917	2062	7.59	1917	2069	7.96
5	1916	1971	2.87	1916	1973	2.99	1916	2030	5.95	1916	2007	4.76
7.5	1945	2004	3.05	1945	2036	4.71	1916	2108	9.98	1916	2026	5.69

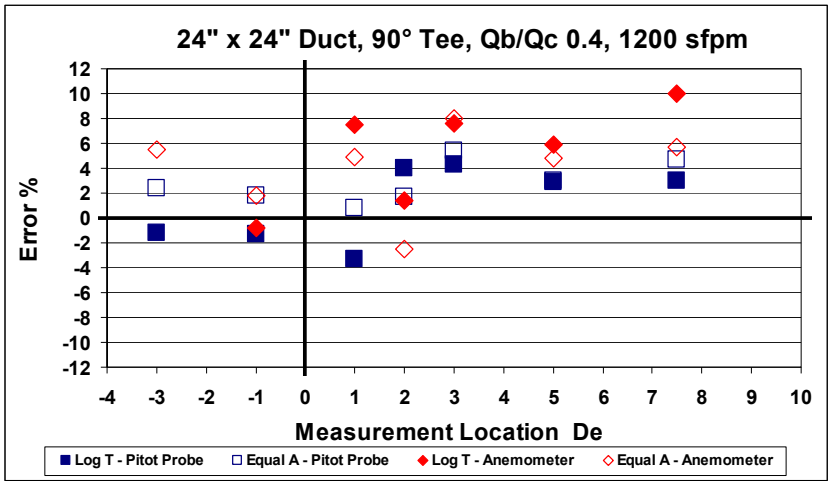

Figure 6.13 90° Tee, Qb/Qc = 0.4, 1200 SFPM Data Example

Measurement Location	Pitot Probe						Anemometer					
	Log-T			Equal Area			Log-T			Equal Area		
De	Q(Standard) SCFM	Traverse SCFM	Error %	Q(Standard) SCFM	Traverse SCFM	Error %	Q(Standard) SCFM	Traverse SCFM	Error %	Q(Standard) SCFM	Traverse SCFM	Error %
-3	4788	4769	-0.41	4792	4937	3.01	4795	4780	-0.31	4771	4924	3.21
-1	4794	4762	-0.67	4798	4883	1.76	4786	4710	-1.58	4770	4874	2.18
0	1200 SFPM 90° Tee Qb/Qc 0.6											
1	2874	2728	-5.07	2874	2825	-1.71	2883	3050	5.81	2883	2984	3.52
2	2915	2981	2.27	2915	2990	2.58	2904	3044	4.85	2904	3006	3.54
3	2859	2901	1.45	2859	2969	3.83	2873	2980	3.70	2873	3038	5.74
5	2831	2891	2.13	2831	2921	3.18	2872	2974	3.56	2872	2997	4.34
7.5	2932	3026	3.20	2932	3091	5.39	2866	3078	7.40	2866	3098	8.11

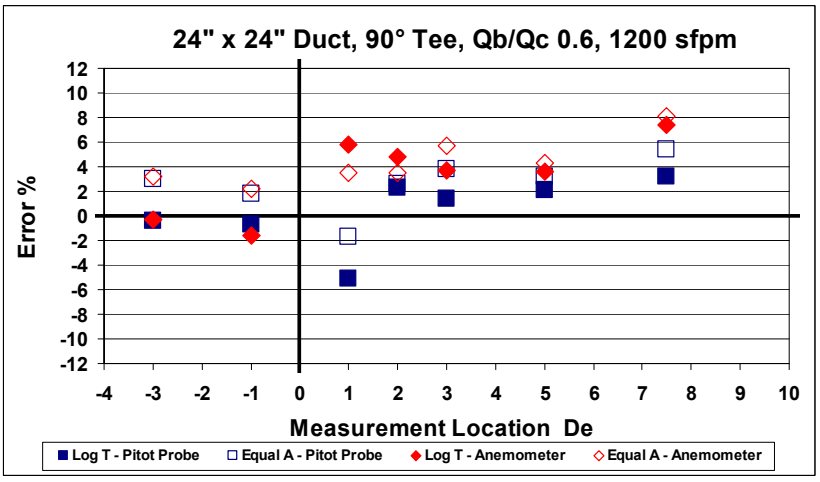

Figure 6.14 90° Tee, Qb/Qc = 0.6, 1200 SFPM Data Example

CHAPTER 7 - Conclusions

This paper described the setup of ASHRAE 1245-RP along with a discussion of the initial results. An experimental facility was setup to construct multiple duct configurations and test their influence on volumetric air flow rate measurements. The purpose was to use the results in developing guidelines for field technicians when making test and balance air flow measurements at various distances from a duct disturbance such as a diverging tee, elbow, or transition. Along with the influence of duct disturbance, comparisons of traverse algorithms and probe type were also performed.

A nozzle bank upstream of the duct configurations was used as the flow measurement standard for all tests along with a flow measurement station as a second standard for the tests using a diverging tee as the duct disturbance. It was necessary to conduct calibrations on all pressure transducers used for the nozzle bank pressure drop and flow measurement station. A calibration of the flow measurement station used for tee disturbances was also conducted to establish its flow coefficient. A leakage test was conducted to quantify the potential error from leakage through the duct and nozzle chamber which showed a leakage of 0.12% for disturbances other than the tee and up to 1.6% for the tee. The 1.6% is significant but believed to be an overestimate and applies to the worst case scenario when the branch to common flow ratio is 0.2. A straight section of duct was constructed to verify that the entire system was working properly and that a uniform fully developed flow could be produced with minimal error. An uncertainty analysis was done for the nozzle bank flow calculation with initial estimates of 0.75% to 1.75% depending on flow rate. This is still being investigated to determine the appropriate uncertainty in the nozzle discharge coefficient. An uncertainty estimate of 1.6% was determined for the traverse in a 24” x 24” duct.

Two traverse algorithms, log-Tchebycheff and equal area, were used to traverse the duct, measure the velocity profile, and determine the average flow rate. A pitot-static probe and hot wire anemometer were used to collect local velocity measurements in the duct using the two traverse algorithms. To make comparisons between the duct configurations, traverse location,

traverse algorithm, and probe type an error or difference between the traverse and flow standard was calculated.

Measurements of velocity profiles were taken for a 24" x 24" duct with a 90^o diverging tee, 90^o Elbow, 60^o and 90^o transitions, and with no disturbance. A flow rate was determined from the traverses and compared to the flow standard. No conclusive difference in error was observed due to probe type for the duct configurations mentioned above. It was noticed that there was a consistent bias of 3 to 4% high when the equal area method was used as the traverse algorithm versus log-Tchebycheff. This could be partially due to the fact that the equal area traverse requires fewer local velocity measurements points than log-Tchebycheff for the duct sizes tested. More likely this is more significantly due to the fact that the log-Tchebycheff method includes points closer to the duct wall than equal area. For the single flow path measurements there was no conclusive difference in observed error due to measurement location. For the diverging tee measurements; however, large anomalous errors were observed especially at locations downstream of the disturbance and close to the tee with low branch to common line flow ratios. Measurements upstream of the disturbance did seem to still produce the bias of 3 to 4% high when equal area is used. Also for upstream measurements, the probes seemed to give consistent readings with respect to each other.

Tests conducted up to the submittal of this thesis were comprised of all the 24" x 24" duct disturbances included the diverging tee. The remaining data will be collected and analyzed by other researchers.

References

1. ANSI/ASHRAE Standard 120-1999. Method of Testing to Determine Flow Resistance of HVAC Ducts and Fittings. American Society of Heating, Refrigeration, and Air-Conditioning Engineers, Inc.
2. ANSI/AMCA Standard 210-1985. Laboratory Methods of Testing Fans for Rating. Air movement and Control Association, Inc.
3. ASHRAE Standard 111-1988. Practices for Measurement, Testing, Adjusting, and Balancing of Building Heating, Ventilation, Air-Conditioning, and Refrigeration Systems. American Society of Heating, Refrigeration, and Air-Conditioning Engineers, Inc.
4. ASHRAE (2001). Handbook: Fundamentals. American Society of Heating, Refrigeration, and Air-Conditioning Engineers, Inc.
5. ASME MFC 3M-1989. Measurements of Fluid Flow in Pipes Using Orifice, Nozzle, and Venturi. American Society of Mechanical Engineers
6. Bardot, Dawn (2000). Determining the Influence of Turbulence Intensity on the Performance of Rotating Vane Anemometers (Thesis, Kansas State University, 2000).
7. Heber, A.J., Cole S.E., & Murphy J.P. (1991). Facility for Testing Exhaust Ventilation Fans. Applied Engineering in Agriculture, 7(5), 599-605.
8. Kaiser, K. J. (1993). Experimental, Analytical, and Numerical Evaluations of Commercial Ceiling and Wall Ventilation Inlets (Thesis, Kansas State University, 1993).
9. ISO 3966-1977. Measurement of fluid flow in closed conduits – Velocity area method using pitot static tubes. International Organization of Standardization
10. ISO 5168-1978. Measurement of Fluid Flow: Estimation of Uncertainty of a flow-rate measurement. International Organization of Standardization
11. ANSI/ASHRAE Standard 41.2-1987 (RA 92). Standard Methods for Laboratory Airflow Measurement. American Society of Heating, Refrigeration, and Air-Conditioning Engineers, Inc.

12. ANSI/ASHRAE Standard 41.6-1994 (RA 2006). Standard Method for Measurement of Moist Air Properties. American Society of Heating, Refrigeration, and Air-Conditioning Engineers, Inc.
13. Foltz, D. F. (1984). The Systematic and Random Errors of Portable Air Flow Balancing Instrumentation with Various Ventilation System Fittings. ASHRAE Transactions, 90(2B), 627-644.
14. George, R., Finaish, F., Sauer, H., and Howell, R. (1994). Predicting the Temperature, Humidity, Pressure, and/or Density Effects on Velocity Instrumentation. ASHRAE Transations, 100(1), 274-291.
15. Howell, R., Sauer, H., and Lahmon, R. (1984). Experimental K-factors for Finned Tube Coils Using a Rotary Vane Anemometer. ASHRAE Transactions, 90(2B), 611-626.
16. Howell, R., Sauer, H., and Lahmon, R. (1986). Influence of Upstream Disturbances on Correlation Coefficient for Vane Anemometers at Coil Faces. ASHRAE Transactions, 92(1A), 506-517.
17. Howell, R. and Sauer, H. (1987). Velocity Variation Effects on a Rotating Vane Anemometer at Coil Faces. ASHRAE Transactions, 93(2), 200-210.
18. Howell, R. and Sauer, H. (1989). Airflow Measurements at Coil Faces with Vane Anemometers-Experimental Results. ASHRAE Transactions, 95(2), 128-140.
19. Howell, R. and Sauer, H. (1990). Field Measurement of Air Velocity – Pitot Traverse of Vane Anemometer. ASHRAE Journal, March 1990, 32(3), 46-52.
20. Howell, R. and Sauer, H. (1990). Airflow Measurements at Coil Faces with Vane Anemometers-Statistical Correlation and Recommended Field Measurement Procedure. ASHRAE Transactions, 96(1), 502-511.
21. Suppo, M. (1984). Airflow Measurement at Air-System Coils Using the Rotating Vane Anemometer. ASHRAE Transactions, 90(2B), 605-610.
22. Beck, B., Hosni, M., and Morris, D. (2000). Determining Influence of Turbulence Intensity on the Performance of Rotating Vane Anemometers. Final Report, ASHRAE Research Project 986-RP.
23. Morris, D., Beck, B., and Hosni, M. (2001). Influence of Turbulence Intensity on the Performance of Rotating Vane Anemometers. ASHRAE Transactions, 107(1).

24. Beck, B., Morris, D., and Hosni, M., Uncertainty Analysis of the Experimental Results Investigating the Effects of Turbulence Intensity on the Performance of Rotating Vane Anemometers. Proceedings of the ASHRAE Summer Symposium, June 2002.
25. MacFerren, E. (1999). Equal Area vs. Log-Tchebycheff. HPAC Engineering, 71(12), 26-31.
26. SMACNA. (1995). HVAC Duct Construction Standards. 2nd Edition.
27. Beck, B. Terry, Payne, Greg, and Heitman, Trevor, The Aerodynamics of the Pitot-Static Tube and its Current Role in Non-Ideal Engineering Applications. Paper Number AC 2010-1803, Proceedings of the ASEE 2010 Annual Conference & Exposition, Louisville, Kentucky, June 20-23, 2010.

Appendix A - Seal Test

One Assumption in our measurements is that of minimal leakage in the duct or other parts of the system, in particular after the nozzle bank where the true flow rate is measured. Any leakage after the nozzle bank affects the apparent flow rate at the particular measurement location. The amount of leakage should be quantified to determine if it is significant. The seal test was performed early in the project and some issues with standard 120 compliance existed. Also, equations from (AMCA, 1985) were used because that is what the previous thesis using this nozzle chamber (Kaiser, 1993) used and standard 120 was not yet implemented. If, because of this, we assume a large uncertainty on the leakage measured it will still show minimal leakage. The following describes the test performed to determine the severity of leakage the system has.

A.1 Duct Sealing Procedure

Each situation will use sealant and the same seal procedure. This procedure includes using Kingco 11-376 super-seal water based duct sealant or equivalent duct sealant. The sealant is applied to all the S Lock and Drives at each seam. The transition from the nozzle chamber to the duct is sealed with weather stripping.

A.2 Seal Test Procedure

A seal test was conducted on the straight 24" x 24" duct with no disturbances. An end cap, shown in Figure A.1, was placed on the end of the duct to reduce the flow to a theoretical value of 0 SCFM. The flow actually measured gives us a representative measurement of the amount of leakage. The static pressure in the duct was brought to 1" water column. This is a higher pressure than the duct will see in all situations of this research except the tee. A second leakage test needed to performed for the tee and is discussed in section *A.4 Leakage Check for Tee*. At the maximum flow rate of 9600 SCFM the duct maximum duct pressure is approximately 0.75" based on experimental data. Therefore any leakages produced by this pressure will be larger than the actual leakage during the tests. This pressure was measured at 1

equivalent diameter upstream of the theoretical disturbance location. The maximum duct pressure mention previously comes from the total static pressure drop in the duct and would be located at the duct entrance. It was determined from an example of experimental data and calculated from the difference between (total static pressure at the nozzle inlet) and the (static pressure drop across the nozzles). Any pressure downstream of the nozzle chamber would be less than that. While maintaining this pressure the leakage rate was measured at the nozzle bank. All nozzles but the smallest were plugged. This was to give higher pressure drop across the nozzle bank and therefore greater accuracy from our pressure transducer.

Figure A.1 End Cap

A.3 Duct Leakage Measurement

The average leakage measured was 11.6 SCFM. This corresponds to the following percentages for each flow rate which can be seen in table A.1. The table is a little misleading in that it shows a possible leakage of close to 1% at the lowest flow rate. This is incorrect because the duct pressure was much higher than it would have been at that actual tested flow rate showing an unrealistic leakage that would not be present. In reality the duct pressure would be less than 0.1" and the leakage would be quite small. The higher flow rate cases are the ones with

meaning and even they are a maximum. The most realistic is the closest to the flow rate that would be obtained with 1" duct pressure which is 9600 SCFM. At that flow rate the leakage rate is 0.12%. ASHRAE Standard 120 specifies a maximum leakage of no more than 0.5%. Even with large uncertainty in our leakage measurement we are significantly below this. This is especially true due to the fact that the duct pressure was significantly larger than expected during the test. The fluctuations in the leakage rate are also shown in Figure A.2.

Table A.1 Nozzle Leakage Percentage

Nominal Flow Rate	Leagage	
SCFM	SCFM	%
9600	11.6	0.12%
7200	11.6	0.16%
6533	11.6	0.18%
4900	11.6	0.24%
4800	11.6	0.24%
3267	11.6	0.36%
2400	11.6	0.48%
1633	11.6	0.71%
1200	11.6	0.97%

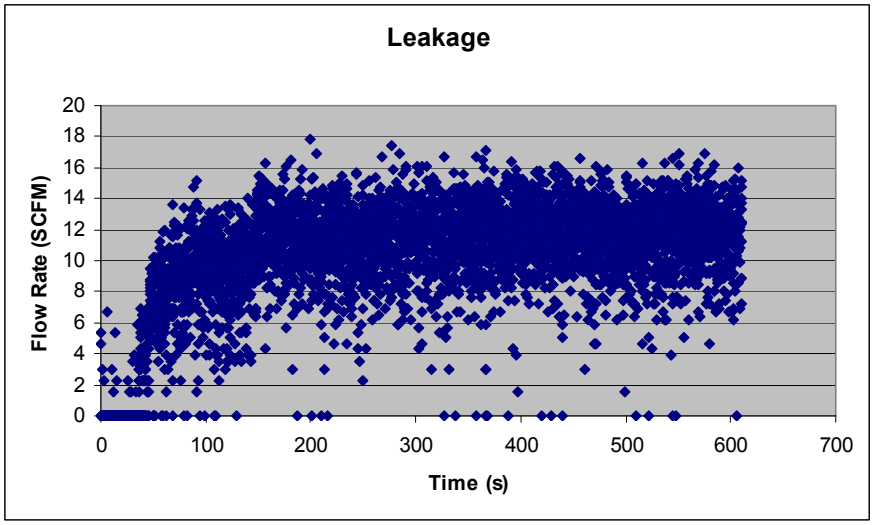

Figure A.2 Leakage Fluctuations

A.4 Leakage Check for Tee

When the tee was installed it was realized that much higher duct pressures would be encountered. It was necessary to quantify the leakage with the higher duct pressure especially with a branch to common flow ratio (Qb/Qc) of 0.2 and the highest flow rate. Duct pressure could reach over 5 inches of water column. The leakage was in fact higher and additional duct sealant and reinforcement was necessary. Wooden frames were placed around the duct seams to limit warping and sealant cracking. The following duct leakage was obtained after the reinforcements were in place shown in Figure A.3 below.

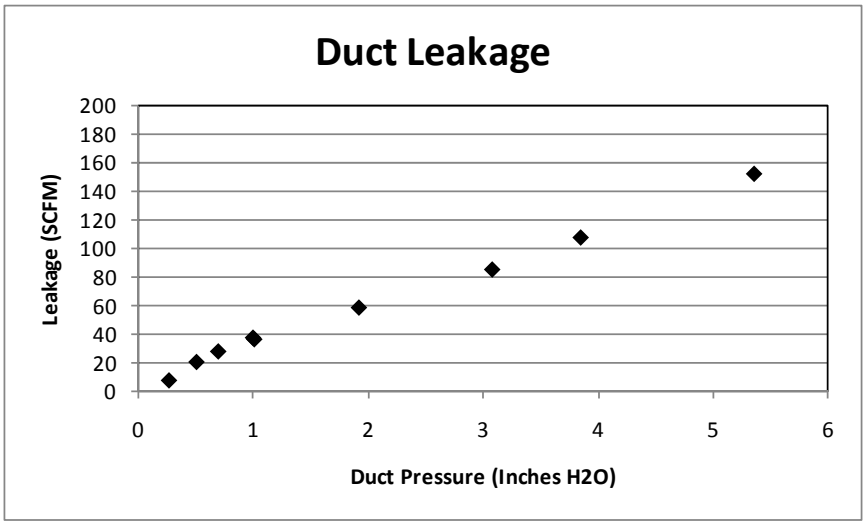

Figure A.3 Duct Leakage for Tee

At the highest flow rate of 9600 SCFM the duct leakage is approximately 150 SCFM or 1.6%. This is at the point greater than 5" H2O and represents the highest leakage expected with Qb/Qc = 0.2. Not all tee configurations and flow rates will have this high of leakage. This is more significant than the previous measurements without the tee but should be the worst case scenario considering for actual tests the 5" H2O is only at the duct inlet and decreases down the length of the duct.

A.5 Seal Test Conclusions

The seal tests described above were conducted and determined the leakage rate at 1" W.C. static pressure for all duct disturbances other than the tee and up to 5" W.C. for the tee.

The leakage without the tee was determined to be small, around 0.12% at the highest flow rate. This is the percentage from the flow rate where the duct pressure most closely represents values actually seen. This leakage is significantly smaller than the requirement of ASHRAE Standard 120; therefore, the duct seal procedure proves to be adequate for this research. The leakage at a duct pressure seen by the tee was higher caused by increased pressure drop especially when the branch to common flow ratio is small. The leakage could be as high as 1.6% although this is believed to be a worst-case estimate.

Appendix B - Data

B.1 Data (24” x 24” Upstream Duct Size, No Disturbance)

Measurement Location	Pitot Probe						Anemometer					
	Log-T			Equal Area			Log-T			Equal Area		
De	Q(Standard) SCFM	Traverse SCFM	Error %	Q(Standard) SCFM	Traverse SCFM	Error %	Q(Standard) SCFM	Traverse SCFM	Error %	Q(Standard) SCFM	Traverse SCFM	Error %
-3	2400	2421	0.90	2401	2518	4.85	2403	2430	1.16	2403	2542	5.76
-1	2400	2407	0.30	2399	2515	4.82	2399	2395	-0.17	2394	2514	5.01
0	600 SFPM Straight Duct											
1	2401	2424	0.99	2405	2532	5.28	2401	2409	0.33	2404	2521	4.85
2	2416	2408	-0.30	2420	2550	5.38	2418	2467	2.01	2417	2587	7.02
3	2396	2418	0.92	2394	2509	4.79	2398	2395	-0.13	2398	2488	3.73
5	2399	2436	1.52	2399	2547	6.14	2401	2426	1.04	2398	2518	5.00
7.5	2401	2384	-0.71	2400	2479	3.26	2396	2372	-1.03	2398	2482	3.49

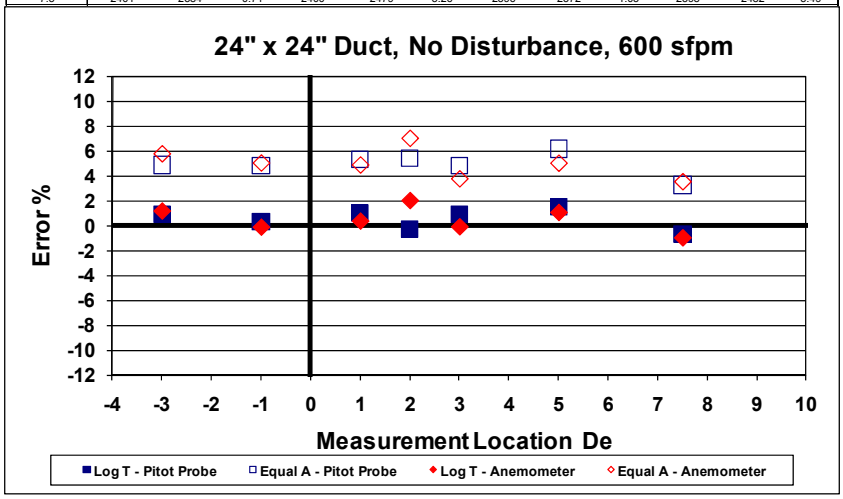

Figure B.1 Data - No Disturbance, 600 fpm

Measurement Location	Pitot Probe						Anemometer					
	Log-T			Equal Area			Log-T			Equal Area		
De	Q(Standard) SCFM	Traverse SCFM	Error %	Q(Standard) SCFM	Traverse SCFM	Error %	Q(Standard) SCFM	Traverse SCFM	Error %	Q(Standard) SCFM	Traverse SCFM	Error %
-3	4770	4817	0.97	4774	4974	4.19	4793	4750	-0.89	4788	4900	2.33
-1	4798	4808	0.21	4790	4977	3.89	4795	4786	-0.18	4791	4953	3.37
0	1200 SFPM Straight Duct											
1	4807	4839	0.68	4817	5035	4.54	4802	4777	-0.52	4802	5013	4.39
2	4796	4833	0.77	4795	4991	4.08	4806	4903	2.02	4810	5161	7.31
3	4798	4812	0.30	4795	4980	3.86	4795	4748	-0.99	4798	4928	2.70
5	4812	4899	1.81	4818	5093	5.69	4794	4810	0.34	4791	4991	4.18
7.5	4796	4742	-1.14	4784	4910	2.63	4797	4703	-1.97	4795	4914	2.48

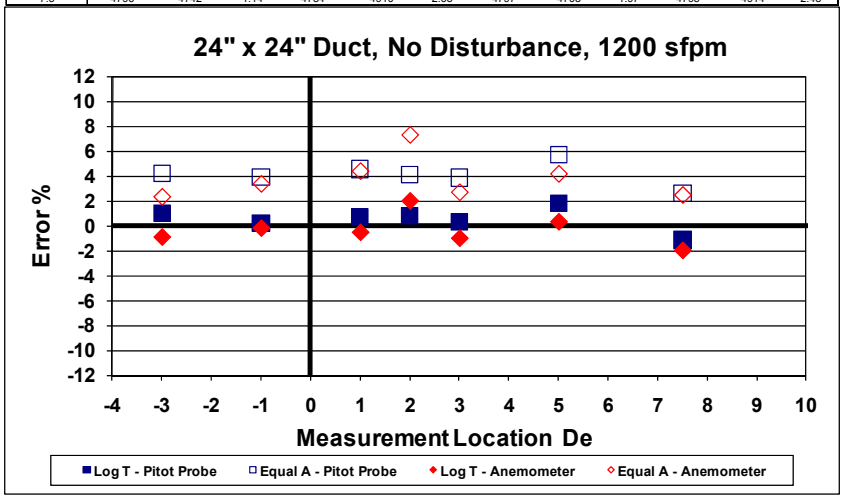

Figure B.2 Data - No Disturbance, 1200 fpm

Measurement Location	Pitot Probe						Anemometer					
	Log-T			Equal Area			Log-T			Equal Area		
De	Q(Standard) SCFM	Traverse SCFM	Error %	Q(Standard) SCFM	Traverse SCFM	Error %	Q(Standard) SCFM	Traverse SCFM	Error %	Q(Standard) SCFM	Traverse SCFM	Error %
-3	7207	7231	0.33	7201	7471	3.74	7202	7195	-0.09	7203	7449	3.42
-1	7221	7229	0.11	7241	7522	3.87	7207	7146	-0.83	7220	7453	3.22
0	1800 SFPM Straight Duct											
1	7198	7241	0.61	7192	7503	4.31	7165	7069	-1.34	7128	7330	2.84
2	7190	7215	0.35	7182	7476	4.10	7184	7151	-0.46	7161	7376	3.00
3	7175	7191	0.22	7164	7440	3.85	7198	7072	-1.75	7192	7318	1.74
5	7196	7336	1.95	7191	7606	5.77	7209	7114	-1.32	7208	7368	2.21
7.5	7193	7160	-0.46	7195	7388	2.68	7202	7008	-2.69	7205	7234	0.40

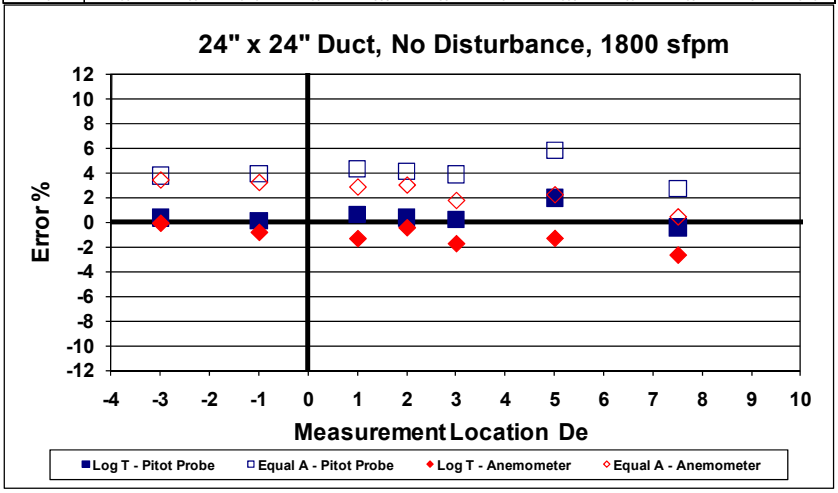

Figure B.3 Data - No Disturbance, 1800 fpm

Measurement Location	Pitot Probe						Anemometer					
	Log-T			Equal Area			Log-T			Equal Area		
De	Q(Standard) SCFM	Traverse SCFM	Error %	Q(Standard) SCFM	Traverse SCFM	Error %	Q(Standard) SCFM	Traverse SCFM	Error %	Q(Standard) SCFM	Traverse SCFM	Error %
-3	9583	9626	0.45	9572	9936	3.80	9592	9691	1.03	9588	10064	4.97
-1	9582	9648	0.69	9549	9929	3.98	9576	9450	-1.32	9548	9720	1.80
0	2400 SFPM Straight Duct											
1	9593	9682	0.92	9587	10041	4.73	9625	9514	-1.15	9631	9929	3.09
2	9588	9664	0.80	9579	10033	4.73	9582	9608	0.27	9577	9928	3.66
3	9589	9649	0.63	9579	9985	4.24	9599	9494	-1.08	9595	9758	1.70
5	9583	9804	2.31	9573	10116	5.67	9581	9620	0.40	9561	9844	2.95
7.5	9592	9607	0.16	9576	9829	2.64	9591	9408	-1.91	9571	9624	0.55

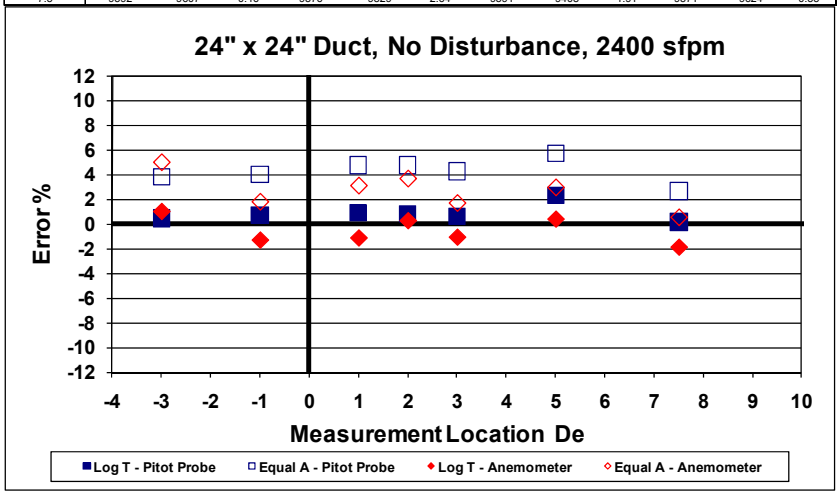

Figure B.4 Data - No Disturbance, 2400 fpm

B.2 Data (24” x 24” Upstream Duct Size, 60° Transition)

Measurement Location	Pitot Probe						Anemometer					
	Log-T			Equal Area			Log-T			Equal Area		
De	Q(Standard) SCFM	Traverse SCFM	Error %	Q(Standard) SCFM	Traverse SCFM	Error %	Q(Standard) SCFM	Traverse SCFM	Error %	Q(Standard) SCFM	Traverse SCFM	Error %
-3	1202	1216	1.21	1203	1263	5.01	1196	1178	-1.56	1196	1239	3.59
-1	1198	1188	-0.84	1203	1248	3.70	1201	1181	-1.62	1202	1234	2.68
0	600 SFPM 60° Transition											
1	1201	1199	-0.17	1200	1237	3.04	1200	1185	-1.23	1200	1247	3.94
2	1196	1203	0.56	1199	1252	4.44	1198	1201	0.23	1195	1228	2.80
3	1199	1180	-1.53	1198	1225	2.18	1199	1180	-1.58	1199	1232	2.78
5	1196	1205	0.72	1195	1252	4.78	1198	1223	2.02	1199	1277	6.50
7.5	1202	1231	2.45	1201	1280	6.56	1202	1240	3.15	1202	1297	7.92

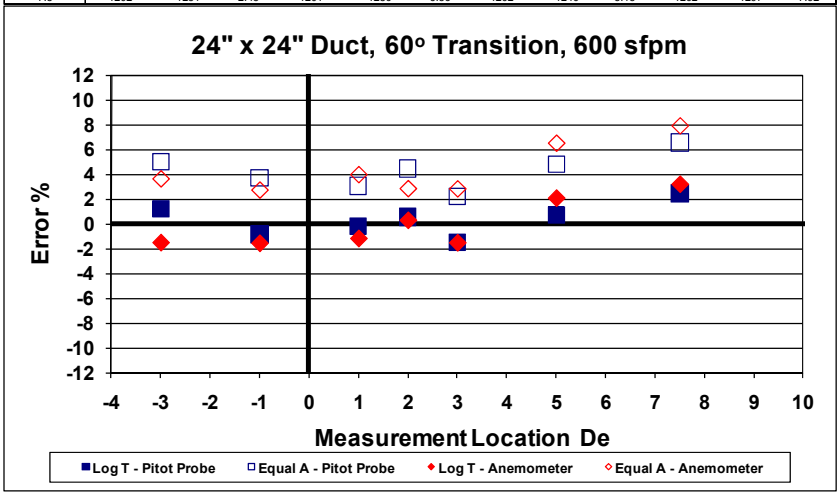

Figure B.5 Data - 60° Transition, 600 fpm

Measurement Postion	Pitot Probe						Anemometer					
	Log-T			Equal Area			Log-T			Equal Area		
De	Q(Standard) SCFM	Traverse SCFM	Error %	Q(Standard) SCFM	Traverse SCFM	Error %	Q(Standard) SCFM	Traverse SCFM	Error %	Q(Standard) SCFM	Traverse SCFM	Error %
-3	2403	2420	0.68	2410	2537	5.29	2396	2428	1.34	2395	2525	5.45
-1	2399	2382	-0.72	2397	2480	3.48	2401	2397	-0.18	2402	2491	3.69
0	1200 SFPM 60° Transition											
1	2406	2398	-0.32	2405	2505	4.13	2393	2345	-2.03	2399	2442	1.79
2	2406	2434	1.14	2407	2507	4.13	2406	2370	-1.51	2408	2432	1.00
3	2398	2364	-1.39	2397	2431	1.42	2402	2357	-1.90	2403	2440	1.54
5	2398	2422	0.99	2394	2488	3.92	2381	2399	0.76	2379	2475	4.04
7.5	2402	2465	2.62	2405	2567	6.71	2400	2449	2.05	2401	2569	6.99

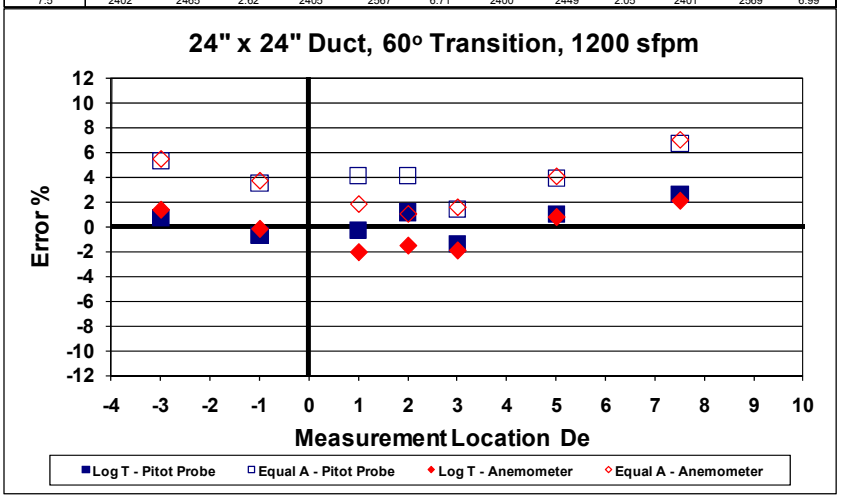

Figure B.6 Data - 60° Transition, 1200 fpm

Measurement Location	Pitot Probe						Anemometer					
	Log-T			Equal Area			Log-T			Equal Area		
De	Q(Standard) SCFM	Traverse SCFM	Error %	Q(Standard) SCFM	Traverse SCFM	Error %	Q(Standard) SCFM	Traverse SCFM	Error %	Q(Standard) SCFM	Traverse SCFM	Error %
-3	3595	3614	0.53	3606	3766	4.44	3611	3698	2.40	3611	3791	4.98
-1	3613	3619	0.17	3611	3756	3.99	3603	3603	0.01	3586	3661	2.09
0	1800 SFPM 60° Transition											
1	3604	3588	-0.45	3601	3730	3.59	3612	3562	-1.37	3618	3698	2.19
2	3610	3636	0.72	3618	3756	3.83	3611	3540	-1.96	3621	3685	1.77
3	3594	3506	-2.47	3598	3630	0.87	3598	3498	-2.77	3603	3633	0.84
5	3599	3642	1.20	3596	3748	4.21	3602	3617	0.42	3603	3767	4.55
7.5	3598	3676	2.18	3592	3801	5.82	3600	3667	1.86	3602	3833	6.44

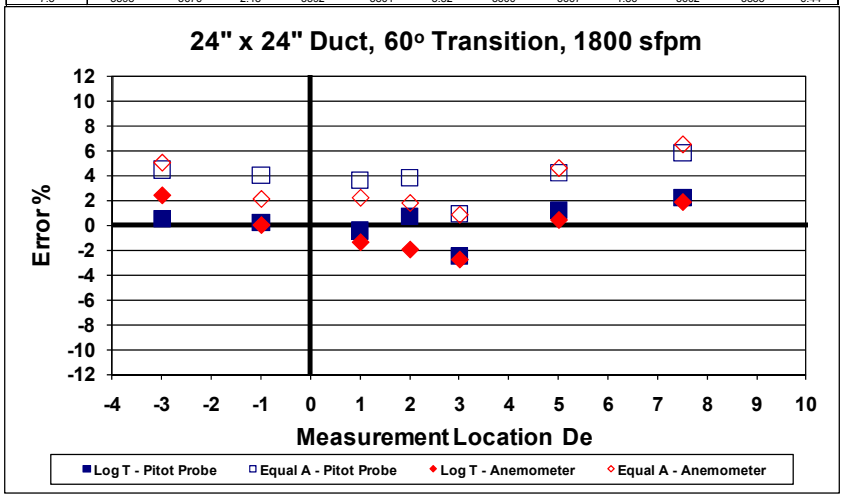

Figure B.7 Data - 60° Transition, 1800 fpm

Measurement Location	Pitot Probe						Anemometer					
	Log-T			Equal Area			Log-T			Equal Area		
De	Q(Standard) SCFM	Traverse SCFM	Error %	Q(Standard) SCFM	Traverse SCFM	Error %	Q(Standard) SCFM	Traverse SCFM	Error %	Q(Standard) SCFM	Traverse SCFM	Error %
-3	4802	4838	0.75	4804	5010	4.29	4811	4817	0.12	4812	5016	4.25
-1	4795	4771	-0.49	4785	4940	3.24	4799	4784	-0.32	4796	4908	2.32
0	2400 SFPM 60° Transition											
1	4820	4837	0.35	4802	4983	3.77	4815	4786	-0.60	4824	4923	2.06
2	4792	4807	0.31	4802	4960	3.27	4797	4711	-1.79	4812	5060	5.16
3	4805	4678	-2.64	4804	4828	0.51	4812	4704	-2.26	4817	4947	0.63
5	4789	4813	0.51	4775	4943	3.52	4827	4891	1.32	4831	5039	4.32
7.5	4798	4908	2.31	4796	5070	5.71	4805	4925	2.50	4805	5138	6.95

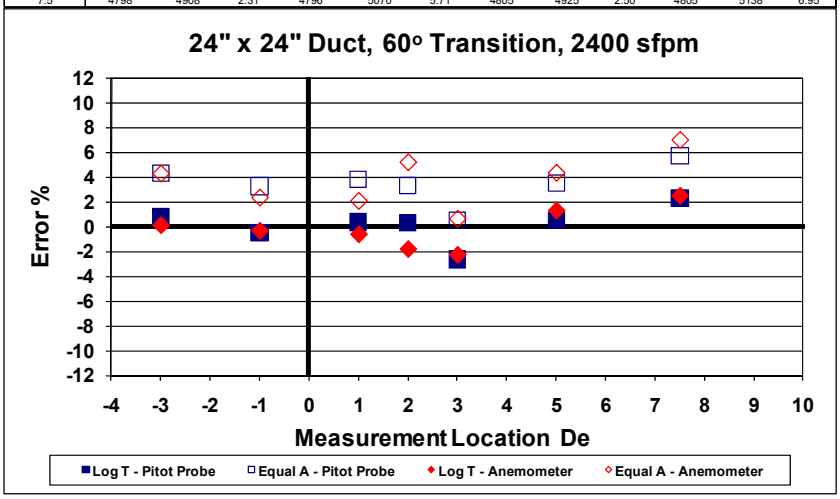

Figure B.8 Data - 60° Transition, 2400 fpm

B.3 Data (24” x 24” Upstream Duct Size, 90° Transition)

Measurement Location	Pitot Probe						Anemometer					
	Log-T			Equal Area			Log-T			Equal Area		
De	Q(Standard) SCFM	Traverse SCFM	Error %	Q(Standard) SCFM	Traverse SCFM	Error %	Q(Standard) SCFM	Traverse SCFM	Error %	Q(Standard) SCFM	Traverse SCFM	Error %
-3	1203	1220	1.40	1199	1243	3.67	1199	1180	-1.53	1198	1235	3.07
-1	1203	1185	-1.50	1208	1260	4.30	1204	1173	-2.60	1201	1221	1.66
0	600 SFPM 90° Transition											
1	1199	1206	0.59	1198	1264	5.43	1197	1199	0.16	1196	1250	4.45
2	1198	1204	0.45	1201	1252	4.26	1201	1201	-0.02	1203	1251	3.98
3	1198	1172	-2.22	1200	1229	2.41	1205	1177	-2.27	1206	1228	1.85
5	1210	1236	2.18	1212	1287	6.20	1212	1237	2.06	1209	1275	5.46
7.5	1204	1235	2.52	1205	1293	7.31	1201	1252	4.24	1201	1296	7.88

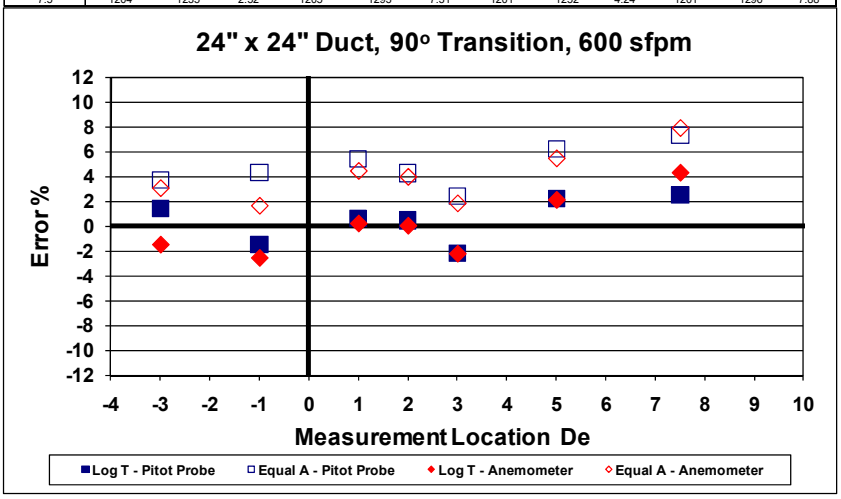

Figure B.9 Data - 90° Transition, 600 fpm

Measurement Location	Pitot Probe						Anemometer					
	Log-T			Equal Area			Log-T			Equal Area		
De	Q(Standard) SCFM	Traverse SCFM	Error %	Q(Standard) SCFM	Traverse SCFM	Error %	Q(Standard) SCFM	Traverse SCFM	Error %	Q(Standard) SCFM	Traverse SCFM	Error %
-3	2395	2421	1.06	2395	2522	5.33	2391	2407	0.71	2394	2526	5.51
-1	2408	2395	-0.54	2412	2522	4.56	2402	2404	0.06	2404	2504	4.15
0	1200 SFPM 90° Transition											
1	2403	2428	1.04	2405	2524	4.96	2406	2384	-0.91	2409	2473	2.67
2	2406	2431	1.06	2409	2507	4.09	2403	2365	-1.58	2402	2452	2.05
3	2413	2383	-1.22	2409	2440	1.25	2406	2348	-2.40	2413	2442	1.19
5	2400	2448	1.99	2396	2521	5.19	2395	2446	2.14	2390	2525	5.64
7.5	2400	2458	2.42	2400	2567	6.94	2393	2430	1.55	2387	2526	5.80

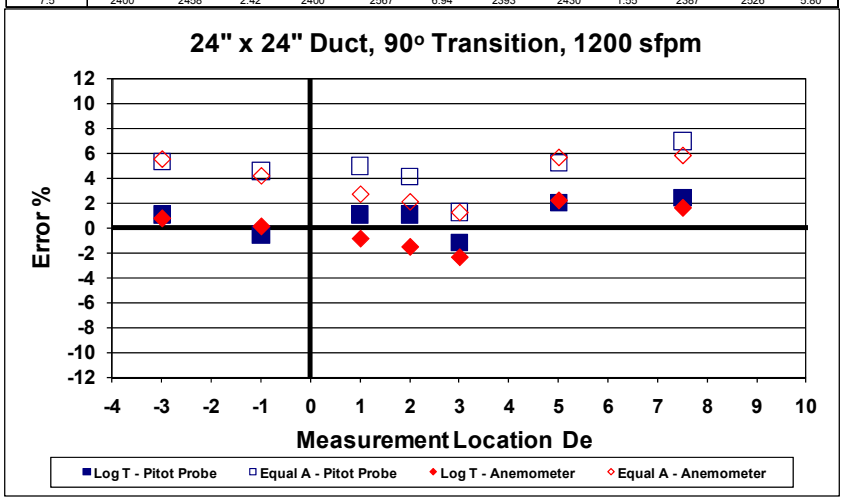

Figure B.10 Data - 90° Transition, 1200 fpm

Measurement Location	Pitot Probe						Anemometer					
	Log-T			Equal Area			Log-T			Equal Area		
De	Q(Standard) SCFM	Traverse SCFM	Error %	Q(Standard) SCFM	Traverse SCFM	Error %	Q(Standard) SCFM	Traverse SCFM	Error %	Q(Standard) SCFM	Traverse SCFM	Error %
-3	3594	3587	-0.21	3592	3728	3.78	3607	3643	0.99	3613	3778	4.57
-1	3618	3613	-0.15	3618	3779	4.45	3590	3551	-1.09	3579	3677	2.72
0	1800 SFPM 90° Transition											
1	3589	3585	-0.11	3587	3730	4.00	3611	3606	-0.13	3613	3773	4.44
2	3599	3611	0.35	3607	3737	3.61	3612	3593	-0.51	3621	3713	2.53
3	3611	3544	-1.84	3613	3661	1.32	3603	3508	-2.64	3604	3610	0.17
5	3588	3632	1.22	3577	3710	3.71	3613	3694	2.25	3620	3818	5.45
7.5	3605	3720	3.20	3612	3846	6.50	3610	3718	2.98	3610	3871	7.21

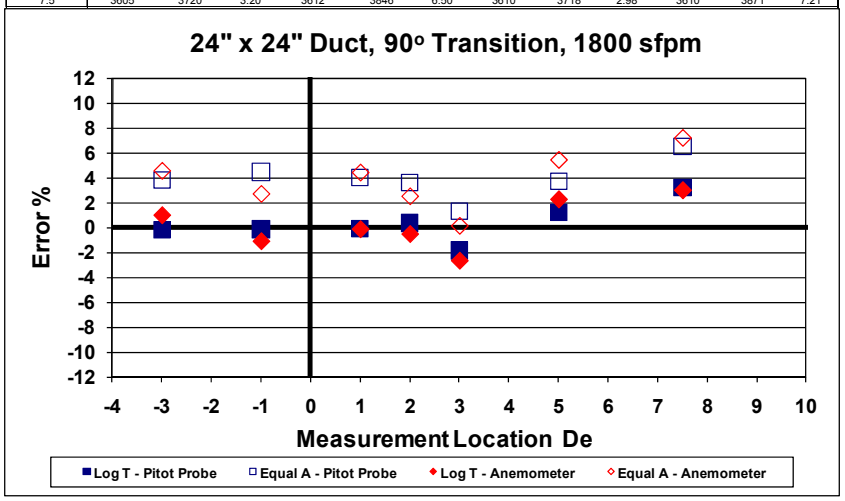

Figure B.11 Data - 90° Transition, 1800 fpm

Measurement Location	Pitot Probe						Anemometer					
	Log-T			Equal Area			Log-T			Equal Area		
De	Q(Standard) SCFM	Traverse SCFM	Error %	Q(Standard) SCFM	Traverse SCFM	Error %	Q(Standard) SCFM	Traverse SCFM	Error %	Q(Standard) SCFM	Traverse SCFM	Error %
-3	4810	4841	0.64	4815	5049	4.86	4806	4867	1.26	4805	4995	3.95
-1	4796	4752	-0.92	4793	4954	3.37	4790	4780	-0.22	4782	5003	4.61
0	2400 SFPM 90° Transition											
1	4802	4805	0.06	4788	4977	3.95	4795	4727	-1.43	4797	4910	2.36
2	4792	4803	0.22	4792	4943	3.15	4804	4735	-1.45	4804	4885	1.69
3	4797	4668	-2.69	4795	4790	-0.11	4798	4691	-2.23	4798	4834	0.73
5	4824	4914	1.86	4830	5054	4.63	4805	4878	1.54	4818	5051	4.84
7.5	4805	4936	2.72	4802	5096	6.12	4805	4959	3.19	4796	5142	7.20

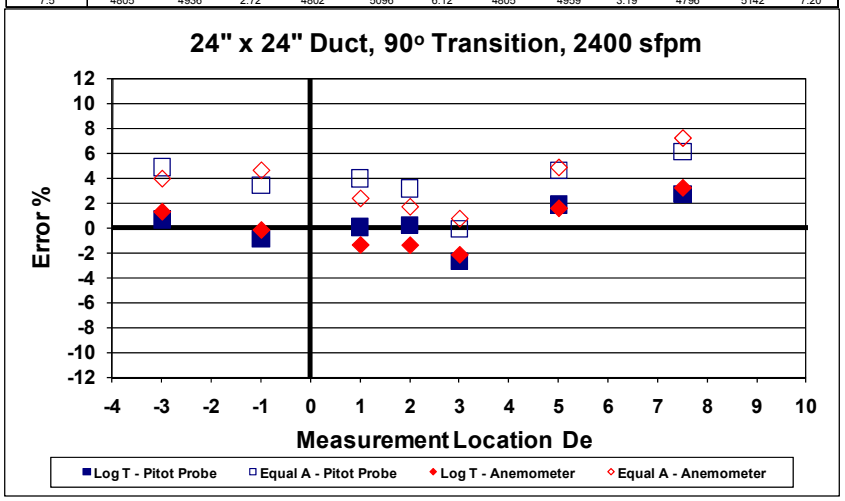

Figure B.12 Data - 90° Transition, 2400 fpm

B.4 Data (24” x 24” Upstream Duct Size, 90° Elbow)

Measurement Location	Pitot Probe						Anemometer					
	Log-T			Equal Area			Log-T			Equal Area		
De	Q(Standard) SCFM	Traverse SCFM	Error %	Q(Standard) SCFM	Traverse SCFM	Error %	Q(Standard) SCFM	Traverse SCFM	Error %	Q(Standard) SCFM	Traverse SCFM	Error %
-3	2400	2426	1.10	2399	2518	4.96	2402	2448	1.92	2401	2548	6.11
-1	2395	2410	0.64	2387	2495	4.53	2400	2404	0.17	2404	2516	4.63
0	600 SFPM 90° Elbow											
1	2404	2381	-0.98	2400	2480	3.31	2400	2377	-0.99	2401	2486	3.50
2	2398	2415	0.68	2393	2484	3.81	2398	2455	2.37	2399	2530	5.45
3	2392	2404	0.50	2381	2480	4.15	2405	2419	0.57	2400	2493	3.87
5	2399	2470	2.96	2394	2548	6.43	2409	2437	1.15	2405	2511	4.40
7.5	2397	2394	-0.09	2397	2494	4.07	2397	2397	-0.02	2394	2506	4.66

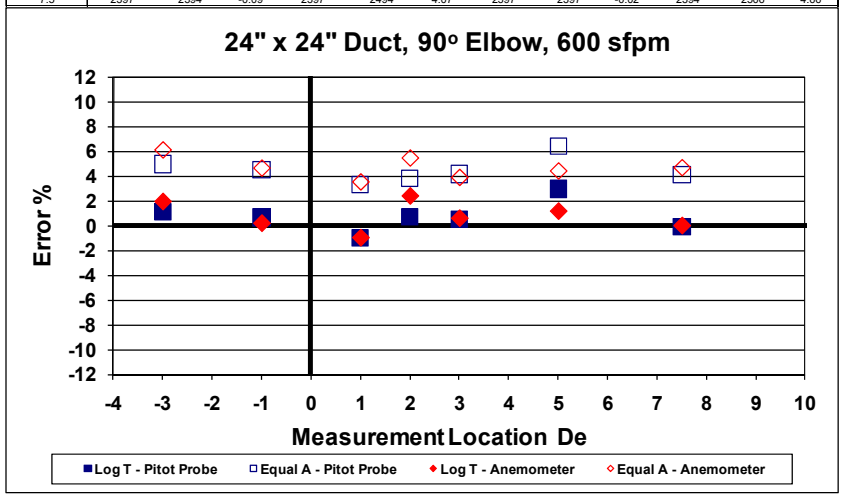

Figure B.13 Data - 90° Elbow, 600 fpm

Measurement Location	Pitot Probe						Anemometer					
	Log-T			Equal Area			Log-T			Equal Area		
De	Q(Standard) SCFM	Traverse SCFM	Error %	Q(Standard) SCFM	Traverse SCFM	Error %	Q(Standard) SCFM	Traverse SCFM	Error %	Q(Standard) SCFM	Traverse SCFM	Error %
-3	4794	4855	1.28	4788	5012	4.68	4794	4883	1.85	4793	5023	4.80
-1	4790	4785	-0.11	4791	4942	3.15	4802	4748	-1.12	4807	4910	2.14
0	1200 SFPM 90° Elbow											
1	4789	4718	-1.47	4779	4925	3.06	4785	4645	-2.93	4758	4800	0.87
2	4789	4824	0.74	4779	4952	3.62	4807	4880	1.51	4813	5019	4.28
3	4787	4770	-0.35	4764	4930	3.47	4797	4787	-0.21	4789	4943	3.20
5	4812	4933	2.51	4807	5099	6.07	4804	4828	0.49	4802	4920	2.46
7.5	4796	4759	-0.79	4796	4948	3.15	4794	4712	-1.70	4790	4900	2.30

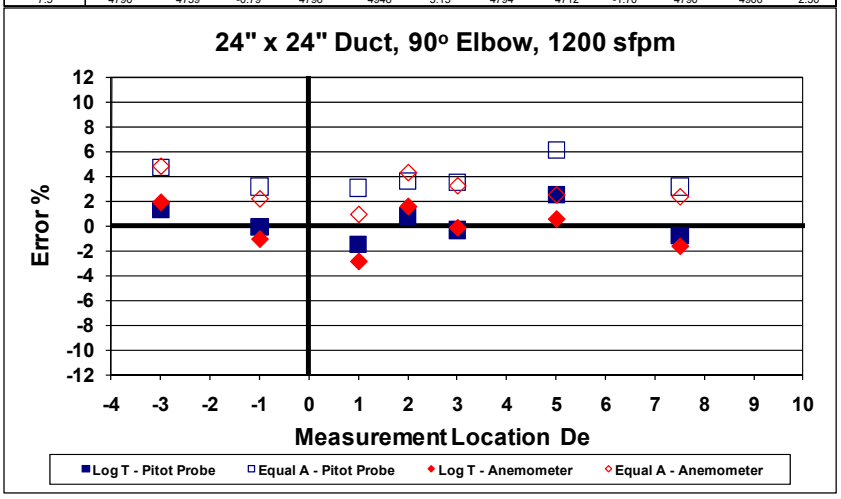

Figure B.14 Data - 90° Elbow, 1200 fpm

Measurement Location	Pitot Probe						Anemometer					
	Log-T			Equal Area			Log-T			Equal Area		
De	Q(Standard) SCFM	Traverse SCFM	Error %	Q(Standard) SCFM	Traverse SCFM	Error %	Q(Standard) SCFM	Traverse SCFM	Error %	Q(Standard) SCFM	Traverse SCFM	Error %
-3	7206	7210	0.07	7192	7494	4.21	7196	7250	0.76	7186	7495	4.29
-1	7182	7163	-0.27	7161	7382	3.09	7202	7064	-1.91	7200	7324	1.71
0	1800 SFPM 90° Elbow											
1	7198	7116	-1.14	7191	7407	3.00	7206	6986	-3.04	7208	7210	0.03
2	7202	7248	0.65	7196	7437	3.36	7200	7183	-0.23	7193	7589	5.50
3	7210	7222	0.17	7219	7477	3.57	7182	7073	-1.52	7162	7286	1.73
5	7195	7319	1.72	7177	7557	5.29	7194	7153	-0.57	7197	7390	2.68
7.5	7199	7144	-0.77	7211	7382	2.37	7208	7110	-1.36	7211	7364	2.12

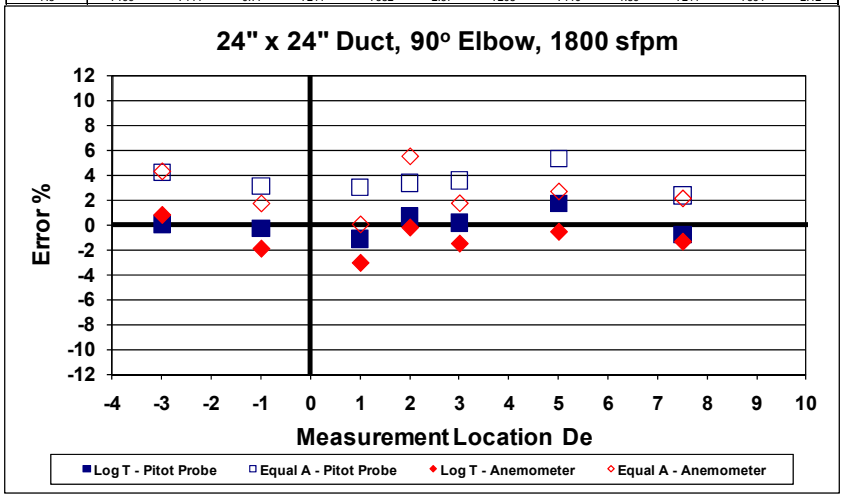

Figure B.15 Data - 90° Elbow, 1800 fpm

Measurement Location	Pitot Probe						Anemometer					
	Log-T			Equal Area			Log-T			Equal Area		
De	Q(Standard) SCFM	Traverse SCFM	Error %	Q(Standard) SCFM	Traverse SCFM	Error %	Q(Standard) SCFM	Traverse SCFM	Error %	Q(Standard) SCFM	Traverse SCFM	Error %
-3	9586	9709	1.28	9575	10040	4.85	9615	9815	2.08	9607	10028	4.38
-1	9572	9605	0.35	9538	9882	3.60	9607	9499	-1.12	9624	9819	2.02
0						2400 SFPM 90° Elbow						
1	9600	9534	-0.69	9594	9920	3.40	9610	9781	1.78	9608	9712	1.08
2	9608	9735	1.32	9604	9989	4.00	9586	9582	-0.04	9573	9928	3.70
3	9614	9702	0.92	9627	9992	3.79	9593	9442	-1.58	9598	9776	1.85
5	9598	9871	2.84	9595	10180	6.10	9611	9582	-0.30	9614	9874	2.70
7.5	9589	9602	0.14	9570	9847	2.89	9607	9478	-1.34	9609	9803	2.01

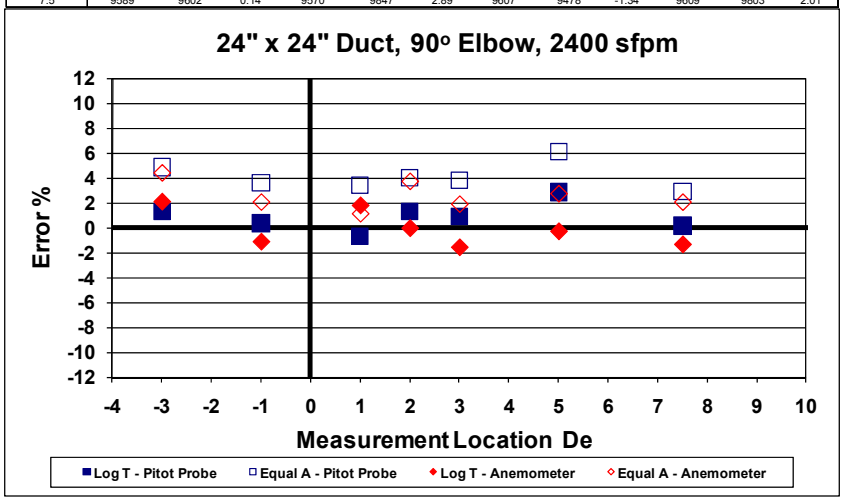

Figure B.16 Data - 90° Elbow, 2400 fpm

B.5 Data (24” x 24” Upstream Duct Size, 90° Tee)

An error in the humidity measurement was discovered in some of the tee data after the deconstruction of the duct configuration. There appears to have been a malfunction in the humidity sensor. Negative humidity was recorded for the corrected data indicated in Table B.1 below. The original data in the table had a positive humidity value and was not affected by a humidity sensor malfunction. It is believed that the malfunction was tied to a drop out of the humidity sensor excitation voltage. This inaccurate humidity measurement affects the nozzle bank and FMS flow rates but does not affect the traverse measurements. The affect results in a small error in density calculation. It can be seen from Table 3.3 that it takes a large change in humidity to have a significant impact on density. The data was corrected by recalculating the flow rates at 50% relative humidity resulting in a decreased density and increased flow rate. The correction is on the order of 0.3% to 0.4% increased flow rate. Figures B.17 and B.18 show an example of the change in the data. The change is small and not noticeable on the charts. The rest of the data presented below is corrected when appropriate based on Table B.1. The corrected data now has an absolute uncertainty in relative humidity of +/-50% relative humidity.

Table B.1 Corrected Data Summary

Measurement	2400 SCFM						4800 SCFM					
	Qb / Qc = 0.2		Qb / Qc = 0.4		Qb / Qc = 0.6		Qb / Qc = 0.2		Qb / Qc = 0.4		Qb / Qc = 0.6	
Location	pitot	anem	pitot	anem	pitot	anem	pitot	anem	pitot	anem	pitot	anem
-3	Original	Original	Original	Original	Original	Original	Original	Original	Original	Original	Original	Original
-1	Original	Original	Original	Corrected	Original	Original	Corrected	Original	Corrected	Original	Original	Original
0												
1	Corrected	Original	Corrected	Original	Corrected	Original	Corrected	Corrected	Corrected	Corrected	Corrected	Corrected
2	Corrected	Original	Corrected	Original	Corrected	Original	Corrected	Original	Corrected	Original	Corrected	Original
3	Corrected	Corrected	Corrected	Corrected	Corrected	Corrected	Corrected	Corrected	Corrected	Corrected	Corrected	Corrected
5	Corrected	Corrected	Corrected	Corrected	Corrected	Corrected	Corrected	Corrected	Corrected	Corrected	Corrected	Corrected
7.5	Corrected	Corrected	Corrected	Corrected	Corrected	Corrected	Corrected	Corrected	Corrected	Corrected	Corrected	Corrected
Measurement	7200 SCFM						9600 SCFM					
	Qb / Qc = 0.2		Qb / Qc = 0.4		Qb / Qc = 0.6		Qb / Qc = 0.2		Qb / Qc = 0.4		Qb / Qc = 0.6	
Location	pitot	anem	pitot	anem	pitot	anem	pitot	anem	pitot	anem	pitot	anem
-3	Original	Original	Original	Original	Original	Original	Original	Original	Original	Original	Original	Original
-1	Original	Original	Original	Original	Original	Corrected	Original	Original	Original	Original	Original	Original
0												
1	Corrected	Original	Corrected	Original	Corrected	Original	Corrected	Original	Corrected	Original	Corrected	Original
2	Corrected	Original	Corrected	Corrected	Corrected	Corrected	Corrected	Corrected	Corrected	Corrected	Corrected	Corrected
3	Corrected	Corrected	Corrected	Corrected	Corrected	Corrected	Corrected	Corrected	Corrected	Corrected	Corrected	Corrected
5	Corrected	Corrected	Corrected	Corrected	Corrected	Corrected	Corrected	Corrected	Corrected	Corrected	Corrected	Corrected
7.5	Corrected	Corrected	Corrected	Corrected	Corrected	Corrected	Corrected	Corrected	Corrected	Corrected	Corrected	Corrected

Original Data - Uncorrected												
Measurement Location	Pitot Probe						Anemometer					
	Log-T			Equal Area			Log-T			Equal Area		
De	Q(Standard) SCFM	Traverse SCFM	Error %	Q(Standard) SCFM	Traverse SCFM	Error %	Q(Standard) SCFM	Traverse SCFM	Error %	Q(Standard) SCFM	Traverse SCFM	Error %
-3	2393	2372	-0.90	2388	2474	3.60	2393	2429	1.51	2381	2507	5.29
-1	2396	2352	-1.86	2393	2441	2.00	2398	2380	-0.77	2397	2480	3.45
0	600 SFPM 90° Tee Qb/Qc 0.2											
1	477	385	-19.14	477	386	-18.96	474	725	52.90	474	637	34.35
2	497	495	-0.40	497	415	-16.50	485	546	12.71	484	505	4.30
3	491	543	10.59	491	522	6.31	495	533	7.68	495	500	1.01
5	493	506	2.76	493	512	3.82	491	510	3.79	491	505	2.73
7.5	492	504	2.43	492	517	4.92	492	529	7.51	492	497	1.11
Corrected Data												
Measurement Location	Pitot Probe						Anemometer					
	Log-T			Equal Area			Log-T			Equal Area		
De	Q(Standard) SCFM	Traverse SCFM	Error %	Q(Standard) SCFM	Traverse SCFM	Error %	Q(Standard) SCFM	Traverse SCFM	Error %	Q(Standard) SCFM	Traverse SCFM	Error %
-3	2393	2372	-0.90	2388	2474	3.60	2393	2429	1.51	2381	2507	5.29
-1	2396	2352	-1.86	2393	2441	2.00	2398	2380	-0.77	2397	2480	3.45
0	600 SFPM 90° Tee Qb/Qc 0.2											
1	478	385	-19.35	478	386	-19.16	474	725	52.90	474	637	34.35
2	499	495	-0.78	499	415	-16.82	485	546	12.71	484	505	4.30
3	492	543	10.42	492	522	6.15	496	533	7.46	496	500	0.80
5	494	506	2.49	494	512	3.54	492	510	3.56	492	505	2.50
7.5	494	504	2.14	494	517	4.63	494	529	7.14	494	497	0.77

Figure B.17 Data Correction Comparison (Data)

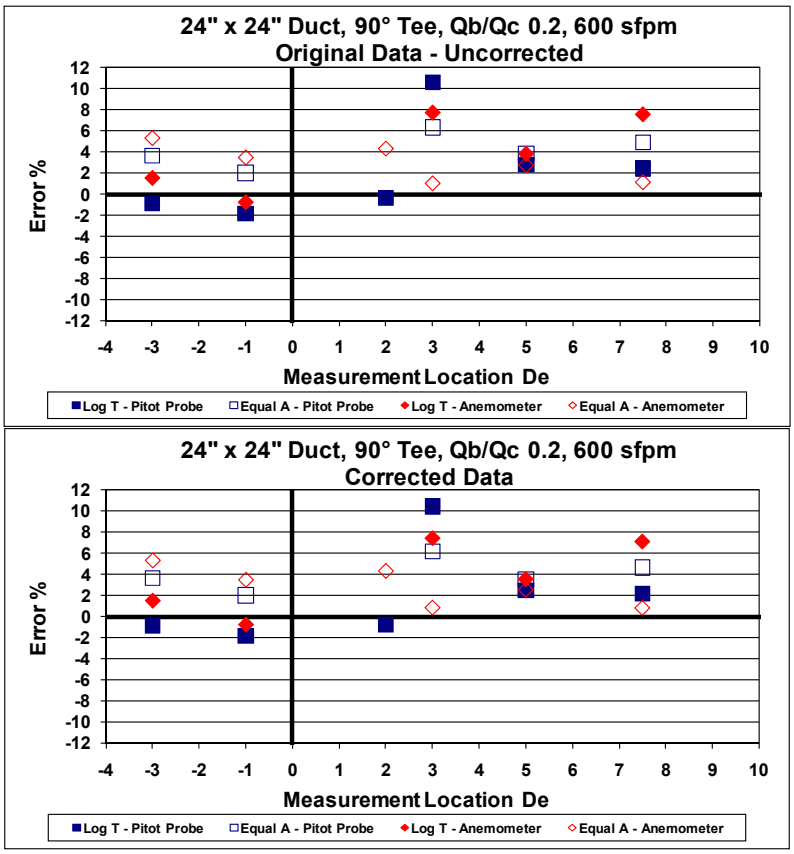

Figure B.18 Data Correction Comparison (Charts)

Measurement Location	Pitot Probe						Anemometer					
	Log-T			Equal Area			Log-T			Equal Area		
De	Q(Standard) SCFM	Traverse SCFM	Error %	Q(Standard) SCFM	Traverse SCFM	Error %	Q(Standard) SCFM	Traverse SCFM	Error %	Q(Standard) SCFM	Traverse SCFM	Error %
-3	2393	2372	-0.90	2388	2474	3.60	2393	2429	1.51	2381	2507	5.29
-1	2396	2352	-1.86	2393	2441	2.00	2398	2380	-0.77	2397	2480	3.45
0	600 SFPM 90° Tee Qb/Qc 0.2											
1	478	385	-19.35	478	386	-19.16	474	725	52.90	474	637	34.35
2	499	495	-0.78	499	415	-16.82	485	546	12.71	484	505	4.30
3	492	543	10.42	492	522	6.15	496	533	7.46	496	500	0.80
5	494	506	2.49	494	512	3.54	492	510	3.56	492	505	2.50
7.5	494	504	2.14	494	517	4.63	494	529	7.14	494	497	0.77

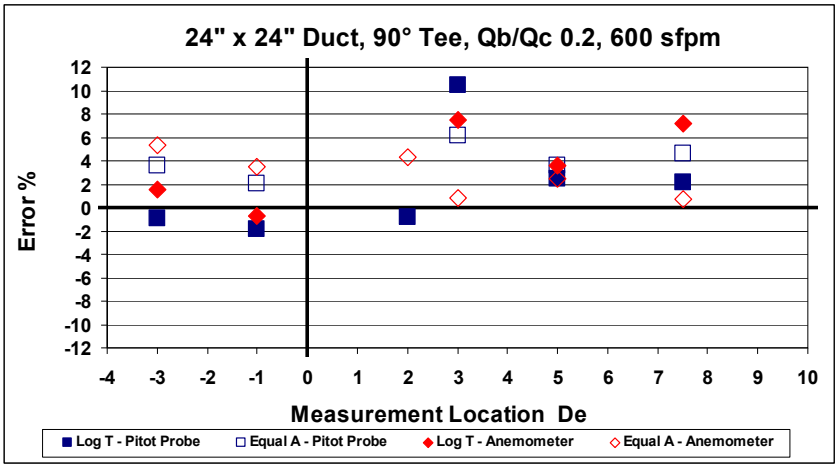

Figure B.19 Data - 90° Tee, Qb/Qc = 0.2, 600 fpm

Measurement Location	Pitot Probe						Anemometer					
	Log-T			Equal Area			Log-T			Equal Area		
De	Q(Standard) SCFM	Traverse SCFM	Error %	Q(Standard) SCFM	Traverse SCFM	Error %	Q(Standard) SCFM	Traverse SCFM	Error %	Q(Standard) SCFM	Traverse SCFM	Error %
-3	4781	4697	-1.77	4765	4862	2.04	4778	4789	0.23	4796	5144	7.24
-1	4806	4695	-2.31	4788	4840	1.08	4774	4685	-1.87	4789	4894	2.19
0	1200 SFPM 90° Tee Qb/Qc 0.2											
1	949	747	-21.26	949	577	-39.22	971	1436	47.80	971	1340	37.93
2	955	910	-4.74	955	793	-17.04	988	1088	10.05	988	990	0.18
3	929	960	3.35	929	961	3.37	993	1062	6.96	993	999	0.61
5	983	984	0.03	983	1011	2.77	992	1024	3.24	992	999	0.77
7.5	960	944	-1.71	960	977	1.73	979	1061	8.28	979	984	0.46

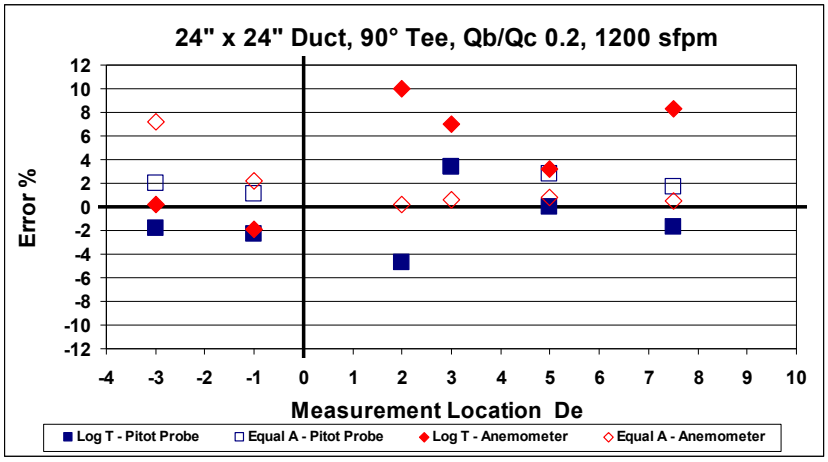

Figure B.20 Data - 90° Tee, Qb/Qc = 0.2, 1200 fpm

Measurement Location	Pitot Probe						Anemometer					
	Log-T			Equal Area			Log-T			Equal Area		
De	Q(Standard) SCFM	Traverse SCFM	Error %	Q(Standard) SCFM	Traverse SCFM	Error %	Q(Standard) SCFM	Traverse SCFM	Error %	Q(Standard) SCFM	Traverse SCFM	Error %
-3	7196	6966	-3.19	7179	6760	-5.84	7195	7098	-1.35	7182	7410	3.17
-1	7212	7028	-2.55	7211	7257	0.63	7210	6970	-3.32	7205	7411	2.86
0	1800 SFPM 90° Tee Qb/Qc 0.2											
1	1500	1419	-5.41	1500	1477	-1.54	1410	2192	55.41	1410	2020	43.21
2	1423	1176	-17.40	1423	1065	-25.16	1460	1450	-0.74	1460	1426	-2.39
3	1480	1496	1.08	1480	1480	0.00	1475	1464	-0.73	1475	1370	-7.12
5	1484	1461	-1.53	1484	1458	-1.79	1442	1402	-2.77	1442	1375	-4.68
7.5	1472	1361	-7.49	1472	1415	-3.86	1460	1499	2.67	1460	1395	-4.45

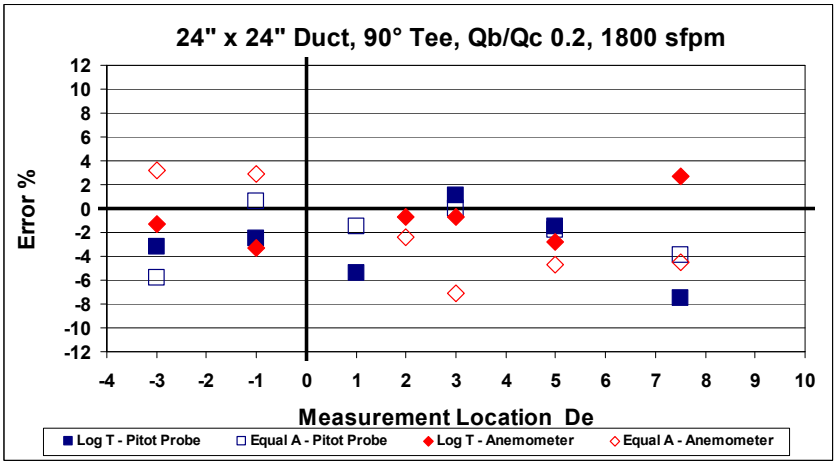

Figure B.21 Data - 90° Tee, Qb/Qc = 0.2, 1800 fpm

Measurement Location	Pitot Probe						Anemometer					
	Log-T			Equal Area			Log-T			Equal Area		
De	Q(Standard) SCFM	Traverse SCFM	Error %	Q(Standard) SCFM	Traverse SCFM	Error %	Q(Standard) SCFM	Traverse SCFM	Error %	Q(Standard) SCFM	Traverse SCFM	Error %
-3	8392	8115	-3.30	8388	8377	-0.13	8405	8210	-2.31	8396	8786	4.65
-1	8399	8153	-2.93	8383	8357	-0.31	8406	8248	-1.88	8434	8463	0.34
0	2100 SFPM 90° Tee Qb/Qc 0.2											
1	1779	1694	-4.78	1779	1786	0.39	1700	2678	57.48	1705	2416	41.70
2	1717	1348	-21.48	1717	1227	-28.53	1749	2072	18.43	1749	1717	-1.86
3	1717	1720	0.20	1717	1634	-4.85	1682	1694	0.70	1682	1590	-5.52
5	1706	1575	-7.68	1706	1671	-2.07	1672	1584	-5.24	1672	1608	-3.81
7.5	1750	1640	-6.29	1750	1684	-3.78	1820	2159	18.67	1820	1737	-4.54

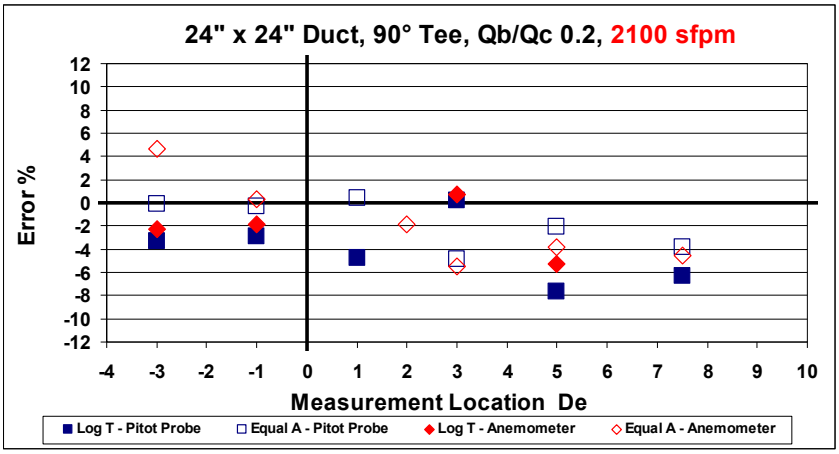

Figure B.22 Data - 90° Tee, Qb/Qc = 0.2, 2100 fpm

Measurement Location	Pitot Probe						Anemometer					
	Log-T			Equal Area			Log-T			Equal Area		
De	Q(Standard) SCFM	Traverse SCFM	Error %	Q(Standard) SCFM	Traverse SCFM	Error %	Q(Standard) SCFM	Traverse SCFM	Error %	Q(Standard) SCFM	Traverse SCFM	Error %
-3	2398	2407	0.39	2387	2498	4.66	2399	2413	0.61	2386	2510	5.20
-1	2393	2357	-1.49	2385	2455	2.93	2407	2395	-0.49	2409	2490	3.35
0	600 SFPM 90° Tee Qb/Qc 0.4											
1	964	942	-2.37	964	941	-2.45	956	1021	6.87	955	973	1.87
2	979	1029	5.12	979	993	1.44	963	979	1.66	963	969	0.68
3	950	1000	5.25	950	1016	6.91	975	1032	5.79	975	1025	5.15
5	971	1002	3.23	971	1002	3.15	959	1005	4.74	959	999	4.12
7.5	981	1016	3.56	981	1040	5.96	974	1072	10.09	974	1025	5.30

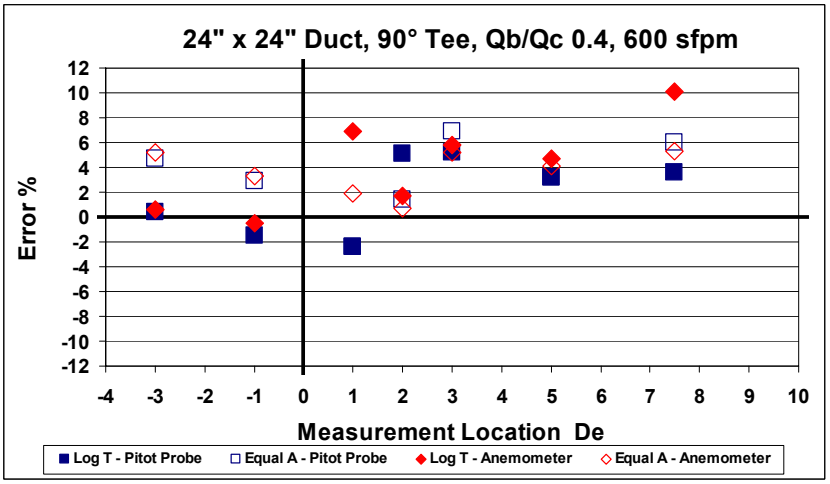

Figure B.23 Data - 90° Tee, Qb/Qc = 0.4, 600 fpm

Measurement Location	Pitot Probe						Anemometer					
	Log-T			Equal Area			Log-T			Equal Area		
De	Q(Standard) SCFM	Traverse SCFM	Error %	Q(Standard) SCFM	Traverse SCFM	Error %	Q(Standard) SCFM	Traverse SCFM	Error %	Q(Standard) SCFM	Traverse SCFM	Error %
-3	4785	4730	-1.16	4795	4908	2.35	4792	6650	38.78	4782	5044	5.48
-1	4804	4742	-1.29	4785	4873	1.84	4803	4766	-0.76	4792	4879	1.81
0	1200 SFPM 90° Tee Qb/Qc 0.4											
1	1920	1857	-3.29	1920	1935	0.79	1901	2043	7.49	1901	1994	4.91
2	1920	1997	4.01	1920	1953	1.70	1939	1966	1.38	1939	1890	-2.52
3	1918	2001	4.34	1918	2023	5.44	1917	2062	7.59	1917	2069	7.96
5	1916	1971	2.87	1916	1973	2.99	1916	2030	5.95	1916	2007	4.76
7.5	1945	2004	3.05	1945	2036	4.71	1916	2108	9.98	1916	2026	5.69

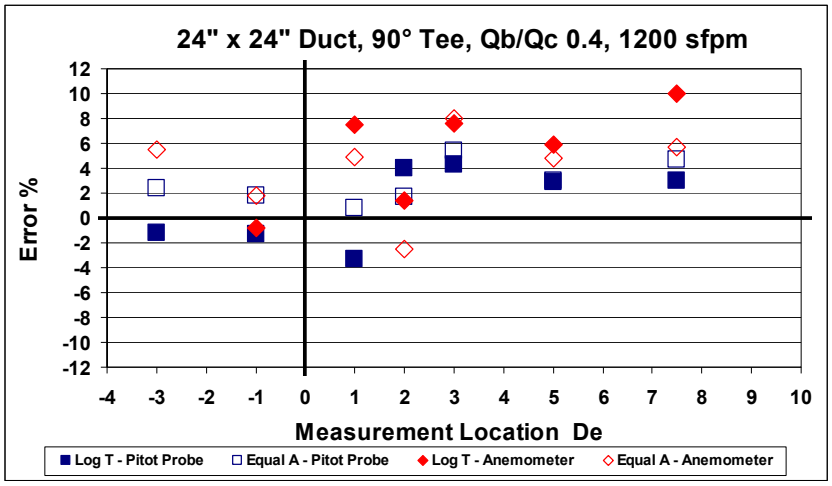

Figure B.24 Data - 90° Tee, Qb/Qc = 0.4, 1200 fpm

Measurement Location	Pitot Probe						Anemometer					
	Log-T			Equal Area			Log-T			Equal Area		
De	Q(Standard) SCFM	Traverse SCFM	Error %	Q(Standard) SCFM	Traverse SCFM	Error %	Q(Standard) SCFM	Traverse SCFM	Error %	Q(Standard) SCFM	Traverse SCFM	Error %
-3	7198	7064	-1.87	7205	7325	1.66	7167	6870	-4.15	7133	7361	3.19
-1	7196	7050	-2.03	7200	7263	0.88	7199	7006	-2.67	7201	7193	-0.12
0	1800 SFPM 90° Tee Qb/Qc 0.4											
1	2899	2765	-4.64	2899	2797	-3.53	2862	3066	7.12	2862	3024	5.64
2	2842	2830	-0.43	2842	2762	-2.83	2930	2973	1.46	2930	2857	-2.51
3	2947	2969	0.74	2947	3012	2.20	2912	2990	2.67	2912	2968	1.94
5	2858	2856	-0.07	2858	2884	0.90	2941	3004	2.17	2941	2978	1.28
7.5	2914	2817	-3.36	2914	2937	0.77	2922	3088	5.68	2922	2986	2.18

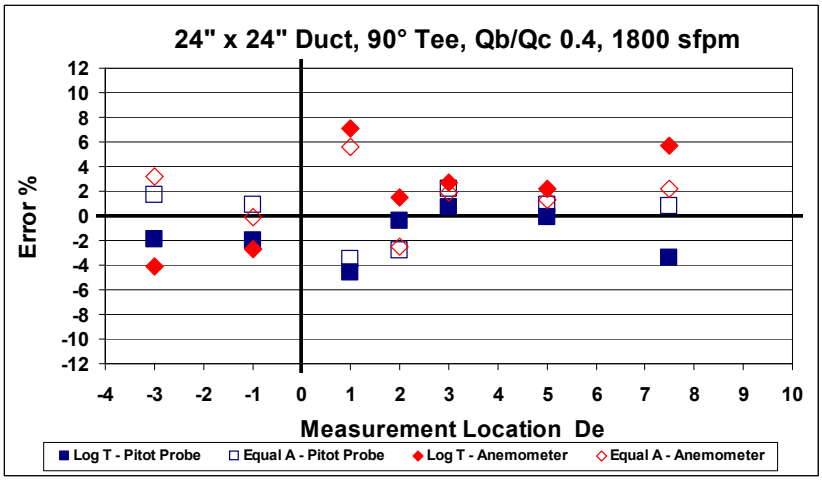

Figure B.25 Data - 90° Tee, Qb/Qc = 0.4, 1800 fpm

Measurement Location	Pitot Probe						Anemometer					
	Log-T			Equal Area			Log-T			Equal Area		
De	Q(Standard) SCFM	Traverse SCFM	Error %	Q(Standard) SCFM	Traverse SCFM	Error %	Q(Standard) SCFM	Traverse SCFM	Error %	Q(Standard) SCFM	Traverse SCFM	Error %
-3	9574	9370	-2.13	9530	9604	0.77	9204	8998	-2.25	9192	9221	0.31
-1	9591	9353	-2.49	9579	9620	0.43	9566	9817	2.62	9479	9936	4.83
0	2400 SFPM 90° Tee Qb/Qc 0.4											
1	3914	3681	-5.96	3914	3694	-5.64	3900	4134	6.00	3906	3956	1.27
2	3911	3824	-2.22	3911	3710	-5.15	3936	4001	1.65	3936	3763	-4.39
3	3932	3925	-0.17	3932	3929	-0.09	3904	4068	4.20	3904	3966	1.58
5	3766	3735	-0.83	3766	3716	-1.34	3790	3912	3.20	3790	3881	2.39
7.5	3844	3780	-1.67	3844	3856	0.30	3788	4068	7.39	3788	3821	0.87

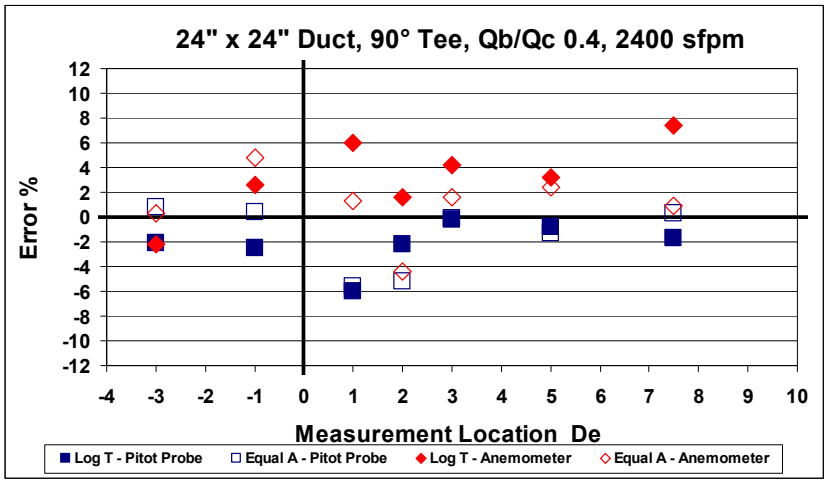

Figure B.26 Data - 90° Tee, Qb/Qc = 0.4, 2400 fpm

Measurement Location	Pitot Probe						Anemometer					
	Log-T			Equal Area			Log-T			Equal Area		
De	Q(Standard) SCFM	Traverse SCFM	Error %	Q(Standard) SCFM	Traverse SCFM	Error %	Q(Standard) SCFM	Traverse SCFM	Error %	Q(Standard) SCFM	Traverse SCFM	Error %
-3	2396	2398	0.08	2393	2489	4.00	2397	2437	1.67	2387	2498	4.63
-1	2402	2374	-1.17	2404	2486	3.40	2399	2396	-0.14	2393	2493	4.15
0	600 SFPM 90° Tee Qb/Qc 0.6											
1	1445	1366	-5.52	1445	1434	-0.81	1454	1525	4.93	1454	1538	5.79
2	1444	1496	3.59	1444	1504	4.17	1468	1502	2.38	1468	1487	1.32
3	1465	1500	2.42	1465	1548	5.67	1436	1495	4.05	1436	1515	5.46
5	1457	1508	3.52	1457	1522	4.44	1438	1503	4.52	1438	1520	5.67
7.5	1438	1494	3.89	1438	1536	6.75	1447	1537	6.25	1447	1539	6.40

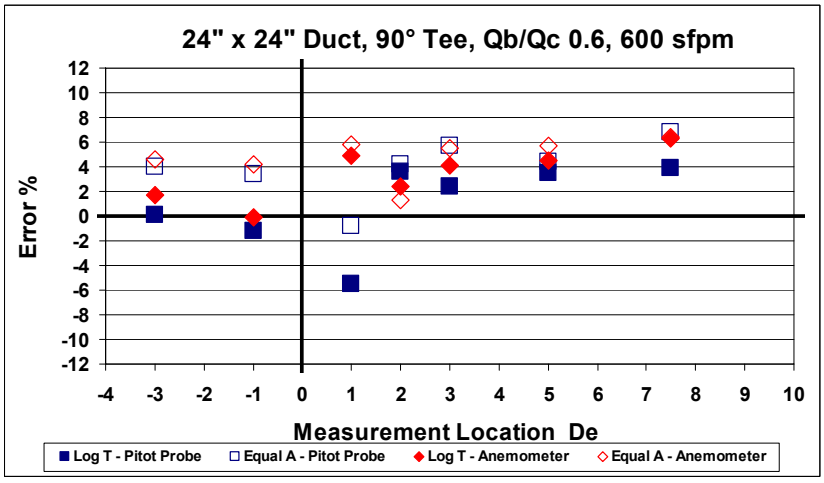

Figure B.27 Data - 90° Tee, Qb/Qc = 0.6, 600 fpm

Measurement Location	Pitot Probe						Anemometer					
	Log-T			Equal Area			Log-T			Equal Area		
De	Q(Standard) SCFM	Traverse SCFM	Error %	Q(Standard) SCFM	Traverse SCFM	Error %	Q(Standard) SCFM	Traverse SCFM	Error %	Q(Standard) SCFM	Traverse SCFM	Error %
-3	4788	4769	-0.41	4792	4937	3.01	4795	4780	-0.31	4771	4924	3.21
-1	4794	4762	-0.67	4798	4883	1.76	4786	4710	-1.58	4770	4874	2.18
0	1200 SFPM 90° Tee Qb/Qc 0.6											
1	2874	2728	-5.07	2874	2825	-1.71	2883	3050	5.81	2883	2984	3.52
2	2915	2981	2.27	2915	2990	2.58	2904	3044	4.85	2904	3006	3.54
3	2859	2901	1.45	2859	2969	3.83	2873	2980	3.70	2873	3038	5.74
5	2831	2891	2.13	2831	2921	3.18	2872	2974	3.56	2872	2997	4.34
7.5	2932	3026	3.20	2932	3091	5.39	2866	3078	7.40	2866	3098	8.11

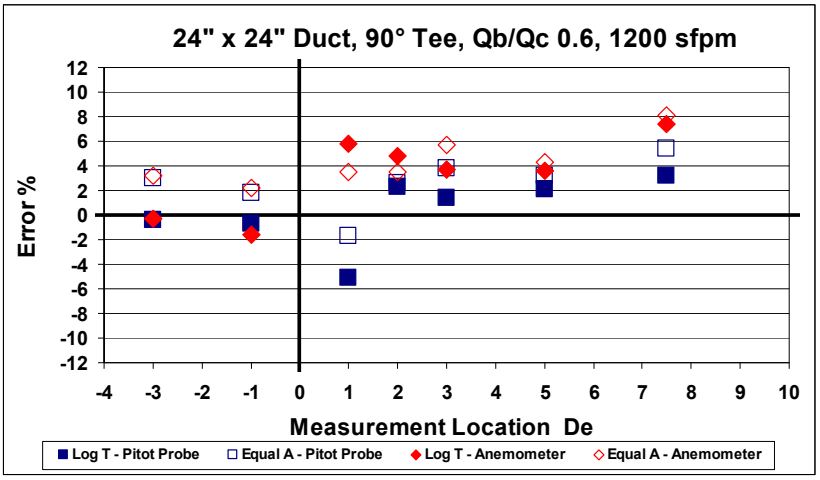

Figure B.28 Data - 90° Tee, Qb/Qc = 0.6, 1200 fpm

Measurement Location	Pitot Probe						Anemometer					
	Log-T			Equal Area			Log-T			Equal Area		
De	Q(Standard) SCFM	Traverse SCFM	Error %	Q(Standard) SCFM	Traverse SCFM	Error %	Q(Standard) SCFM	Traverse SCFM	Error %	Q(Standard) SCFM	Traverse SCFM	Error %
-3	7160	7093	-0.94	7118	7291	2.43	7224	7260	0.50	7238	7425	2.58
-1	7192	7063	-1.79	7199	7327	1.78	7238	6990	-3.44	7238	7254	0.21
0	1800 SFPM 90° Tee Qb/Qc 0.6											
1	4321	4148	-4.01	4321	4279	-0.97	4277	4722	10.40	4275	4664	9.10
2	4301	4416	2.68	4301	4368	1.54	4345	4505	3.68	4345	4453	2.49
3	4370	4454	1.94	4370	4526	3.57	4329	4671	7.91	4329	4596	6.17
5	4272	4378	2.49	4272	4421	3.49	4299	4517	5.06	4299	4581	6.55
7.5	4323	4435	2.59	4323	4516	4.47	4360	4435	1.72	4360	4657	6.80

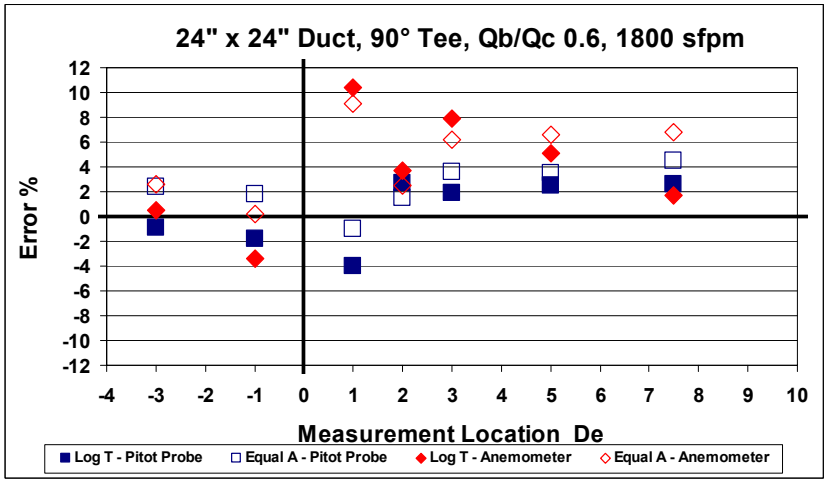

Figure B.29 Data - 90° Tee, Qb/Qc = 0.6, 1800 fpm

Measurement Location	Pitot Probe						Anemometer					
	Log-T			Equal Area			Log-T			Equal Area		
De	Q(Standard) SCFM	Traverse SCFM	Error %	Q(Standard) SCFM	Traverse SCFM	Error %	Q(Standard) SCFM	Traverse SCFM	Error %	Q(Standard) SCFM	Traverse SCFM	Error %
-3	9582	9454	-1.33	9569	9767	2.07	9586	9470	-1.21	9588	9666	0.81
-1	9600	9457	-1.49	9580	9652	0.75	9600	13394	39.52	9565	9925	3.77
0	2400 SFPM 90° Tee Qb/Qc 0.6											
1	5712	5338	-6.55	5712	5691	-0.37	5732	9475	65.31	5737	6095	6.23
2	5716	5974	4.51	5716	5342	-6.54	5796	6111	5.43	5796	6164	6.35
3	5785	5834	0.85	5785	5926	2.44	5777	6207	7.43	5777	6114	5.83
5	5687	5788	1.78	5687	5841	2.71	5719	6624	15.83	5719	6104	6.74
7.5	5695	5807	1.96	5695	5875	3.16	5796	6093	5.12	5796	6195	6.88

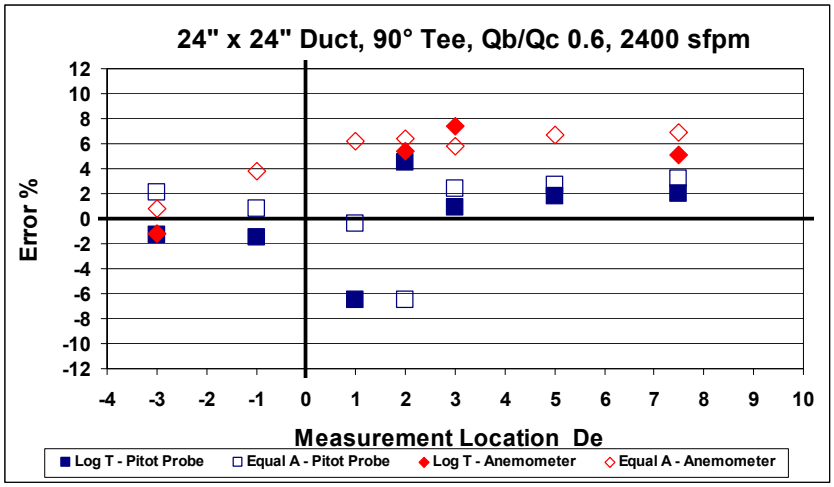

Figure B.30 Data - 90° Tee, Qb/Qc = 0.6, 2400 fpm

Appendix C - Calibrations

C.1 Pressure Transducer Calibrations

Calibrations of the pressure transducers used in 1245-RP were performed with a water micromanometer, digital multi-meter (DMM), and calibrator typically used in calibration of hot wire anemometers. The pressure source for the calibration was created with an air compressor in conjunction with the calibrator. The calibrator uses air flow from the air compressor to create a pressure difference across a nozzle. The calibrator had an air chamber to deliver consistent air flow in an attempt to limit fluctuations for the compressor. The pressure difference was measured with the micromanometer while hooked up in parallel with the pressure transducer. A voltage reading is taken from the pressure transducer with the DMM. Transducers required to be calibrated were used to measure pressures at the nozzle bank and the FMS. These transducers were discussed in sections *3.2.3 Static Pressure* and *3.3 Air Flow Measurement Station*. Data and plots of the calibration curves obtained are shown below.

C.1.1 Nozzle Chamber Pressure Transducers

Manometer "W.C.	DMM Voltage
9.956	5.064
8.953	4.653
8.469	4.455
7.995	4.260
7.471	4.049
6.966	3.846
6.475	3.645
5.974	3.443
5.283	3.176
4.993	3.049
4.497	2.848
3.982	2.640
3.427	2.428
2.967	2.233
2.458	2.039
1.977	1.836
1.450	1.625
0.973	1.427
0.712	1.325
0.479	1.228
0.359	1.181
0.000	1.035

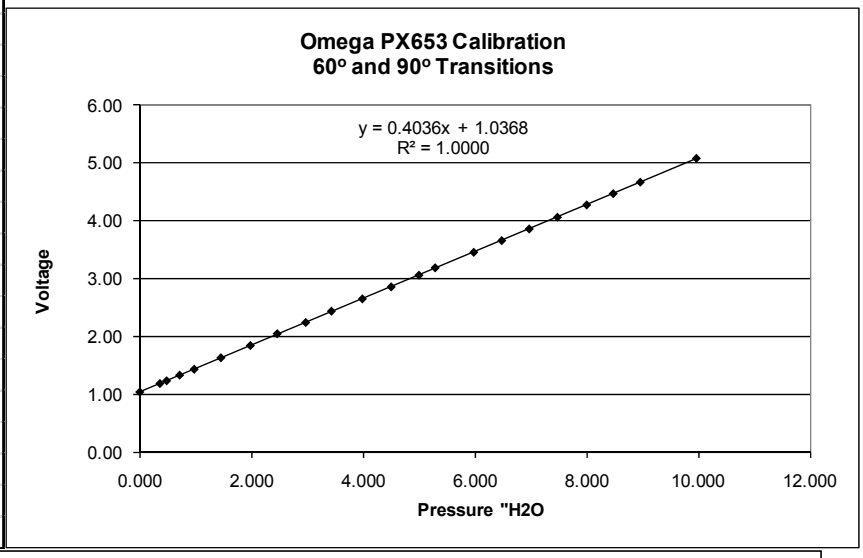

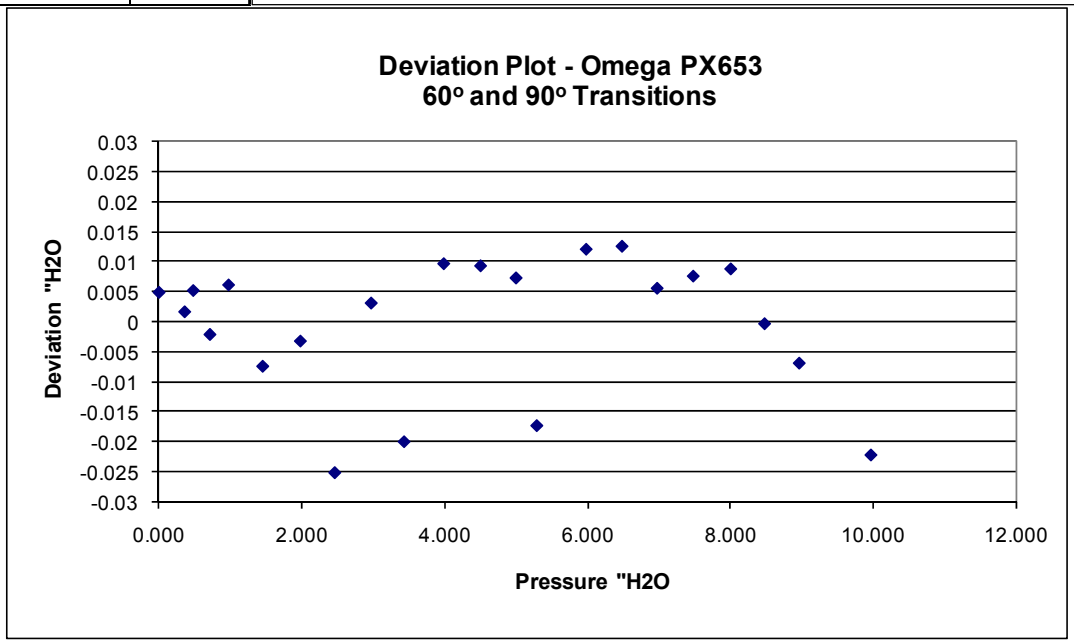

Figure C.1 Omega PX653 10" Pressure Transducer Calibration 1

Manometer "W.C.	DMM Voltage
0.000	1.036
0.992	1.440
1.993	1.845
2.992	2.252
3.989	2.659
4.996	3.063
5.980	3.462
6.984	3.868
7.983	4.276
8.977	4.677
9.977	5.088
8.977	4.682
7.986	4.279
6.983	3.871
5.995	3.467
4.993	3.064
3.999	2.658
2.991	2.252
2.001	1.849
1.001	1.444
0.000	1.036

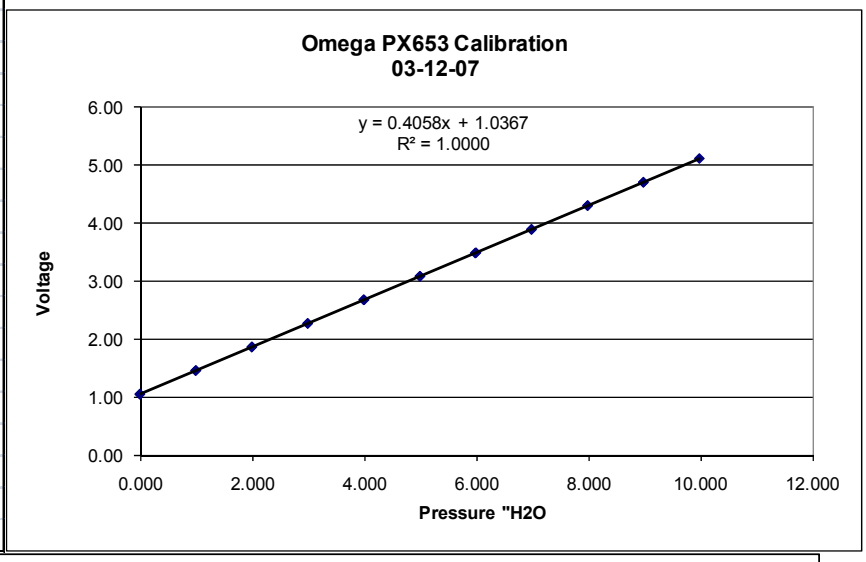

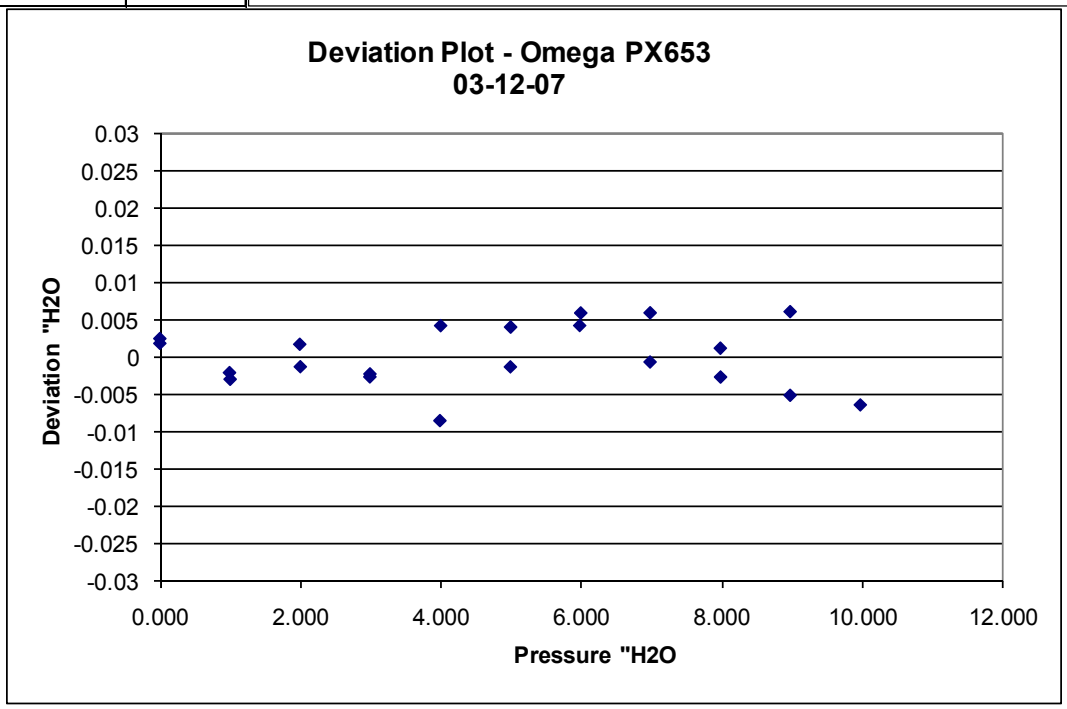

Figure C.2 Omega PX653 10" Pressure Transducer Calibration 2

Manometer "W.C.	DMM Voltage
0.000	0.037
0.992	0.530
1.993	1.032
2.992	1.534
3.989	2.038
4.996	2.542
5.980	3.038
6.984	3.542
7.983	4.045
8.977	4.544
9.977	5.045
8.977	4.547
7.986	4.050
6.983	3.544
5.995	3.045
4.993	2.541
3.999	2.041
2.991	1.534
2.001	1.036
1.001	0.536
0.000	0.037

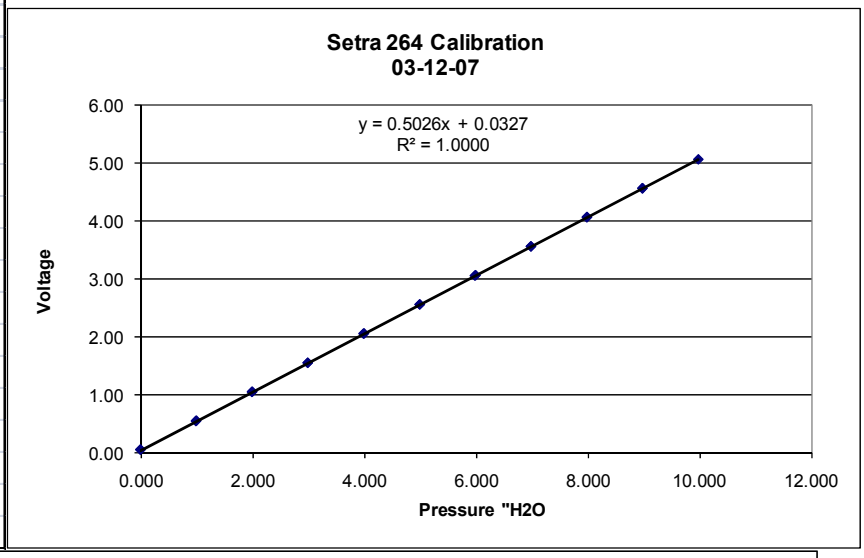

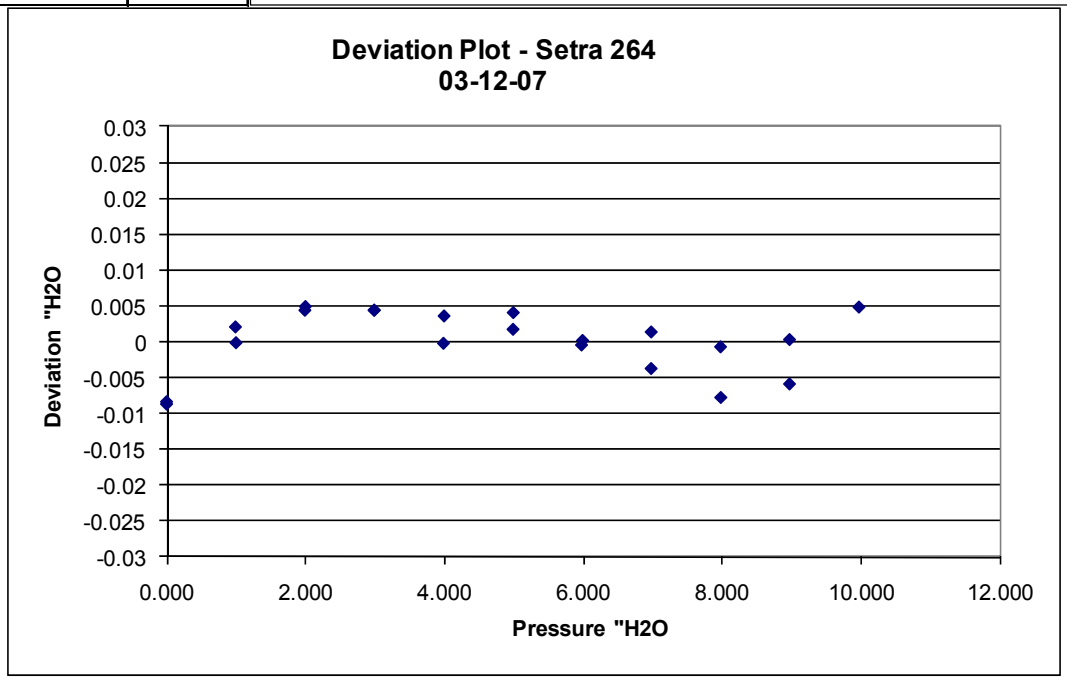

Figure C.3 Setra 264 10" Pressure Transducer Calibration

C.1.2 FMS Pressure Transducers

Manometer "W.C.	DMM Voltage
0.000	1.015
0.482	1.388
0.981	1.757
1.484	2.136
1.978	2.522
2.476	2.901
2.972	3.304
3.467	3.705
3.972	4.127
4.468	4.506
4.973	4.935
0.000	1.016

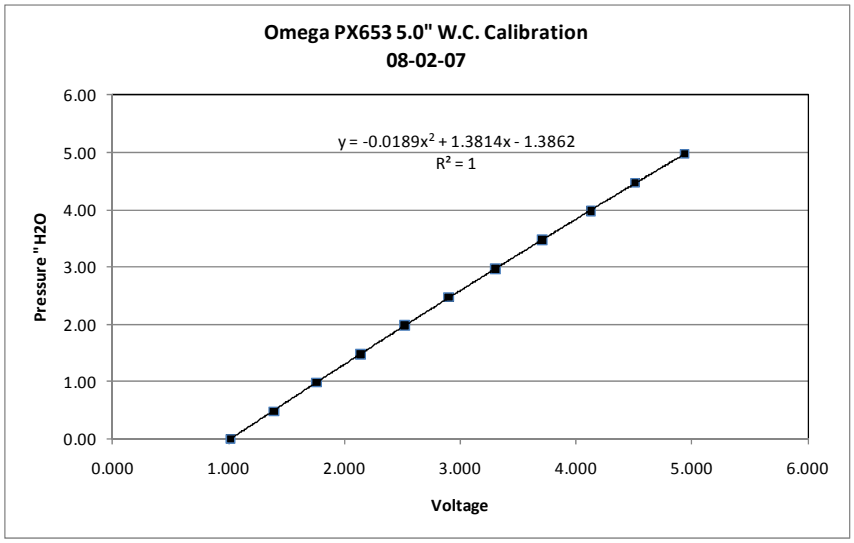

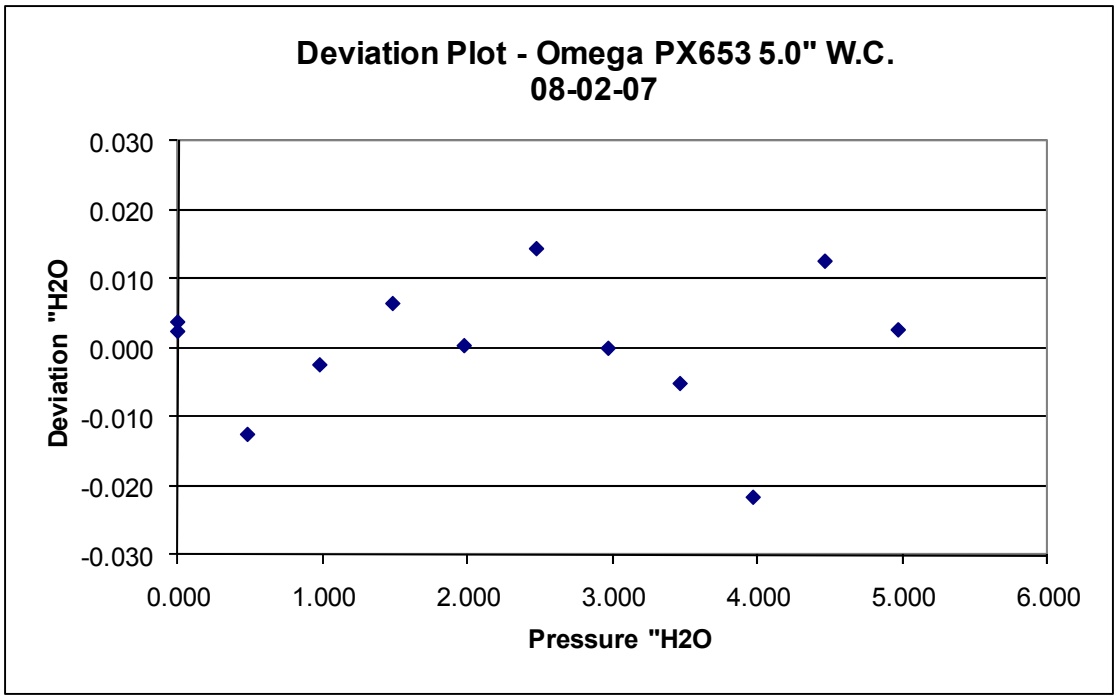

Figure C.4 Omega PX653 5" Pressure Transducer Calibration

Manometer "W.C.	DMM Voltage
0.000	0.115
0.461	4.850
0.410	4.248
0.360	3.784
0.310	3.202
0.260	2.745
0.210	2.251
0.161	1.722
0.111	1.206
0.061	0.727
0.004	0.166
0.000	0.110

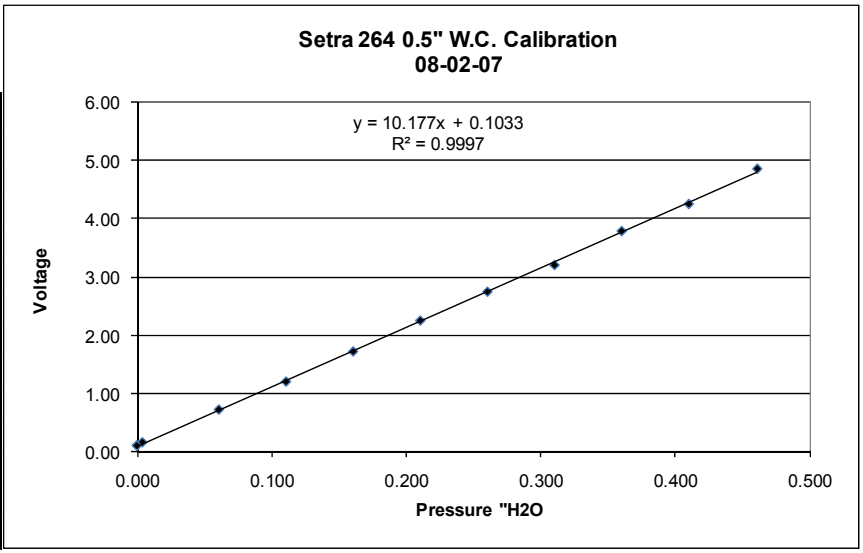

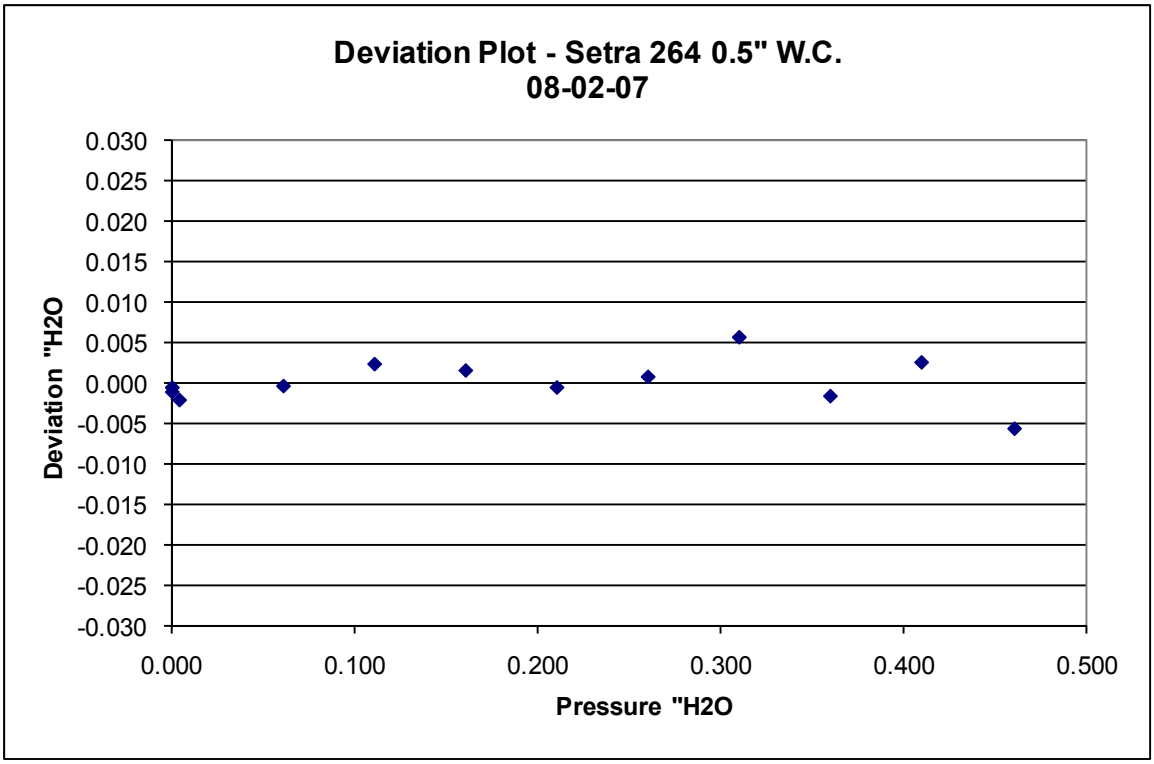

Figure C.5 Setra 264 0.5" Pressure Transducer Calibration

C.2 FMS Calibration

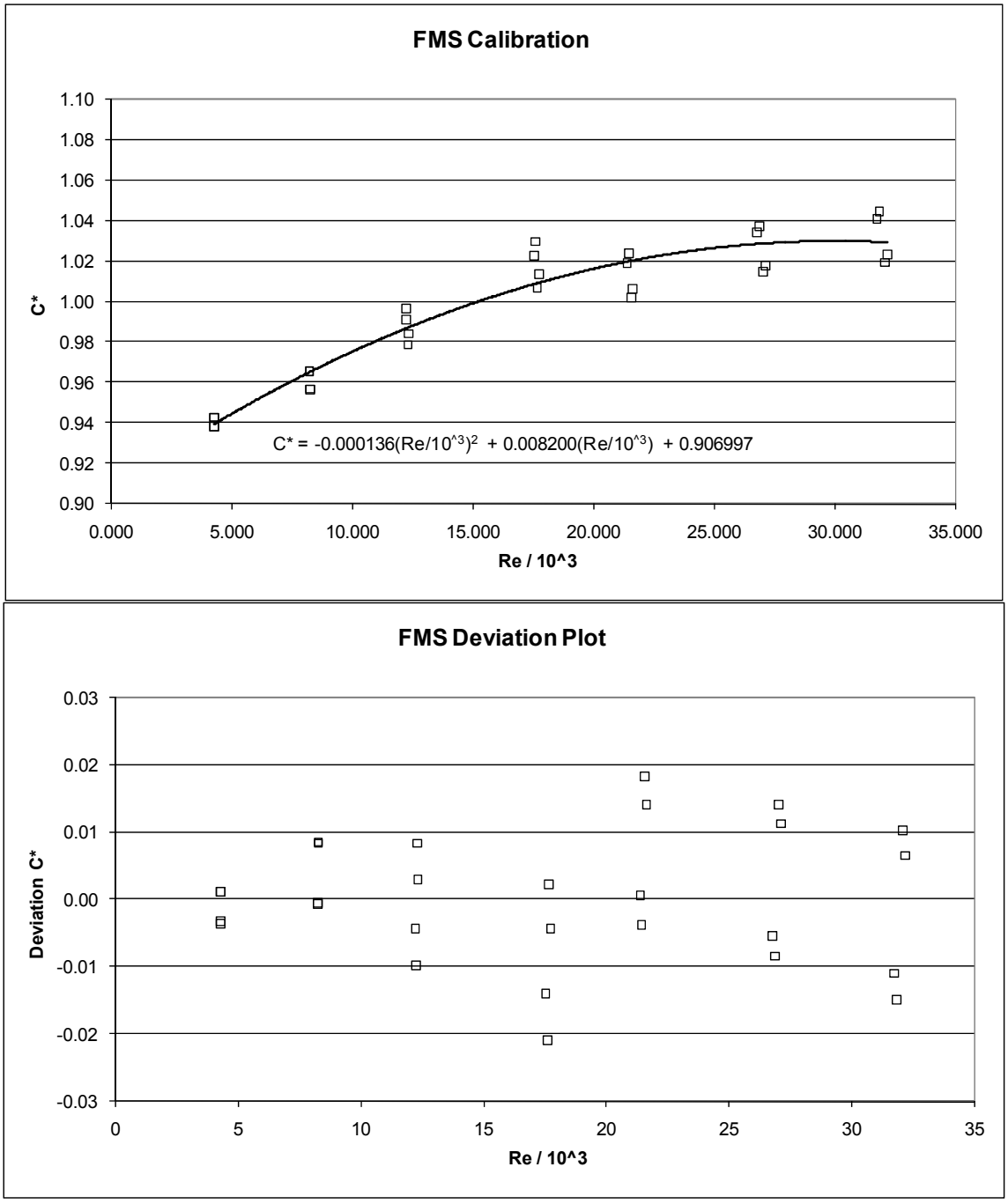

Figure C.6 FMS Calibration

C.3 Humidity Sensor Calibration

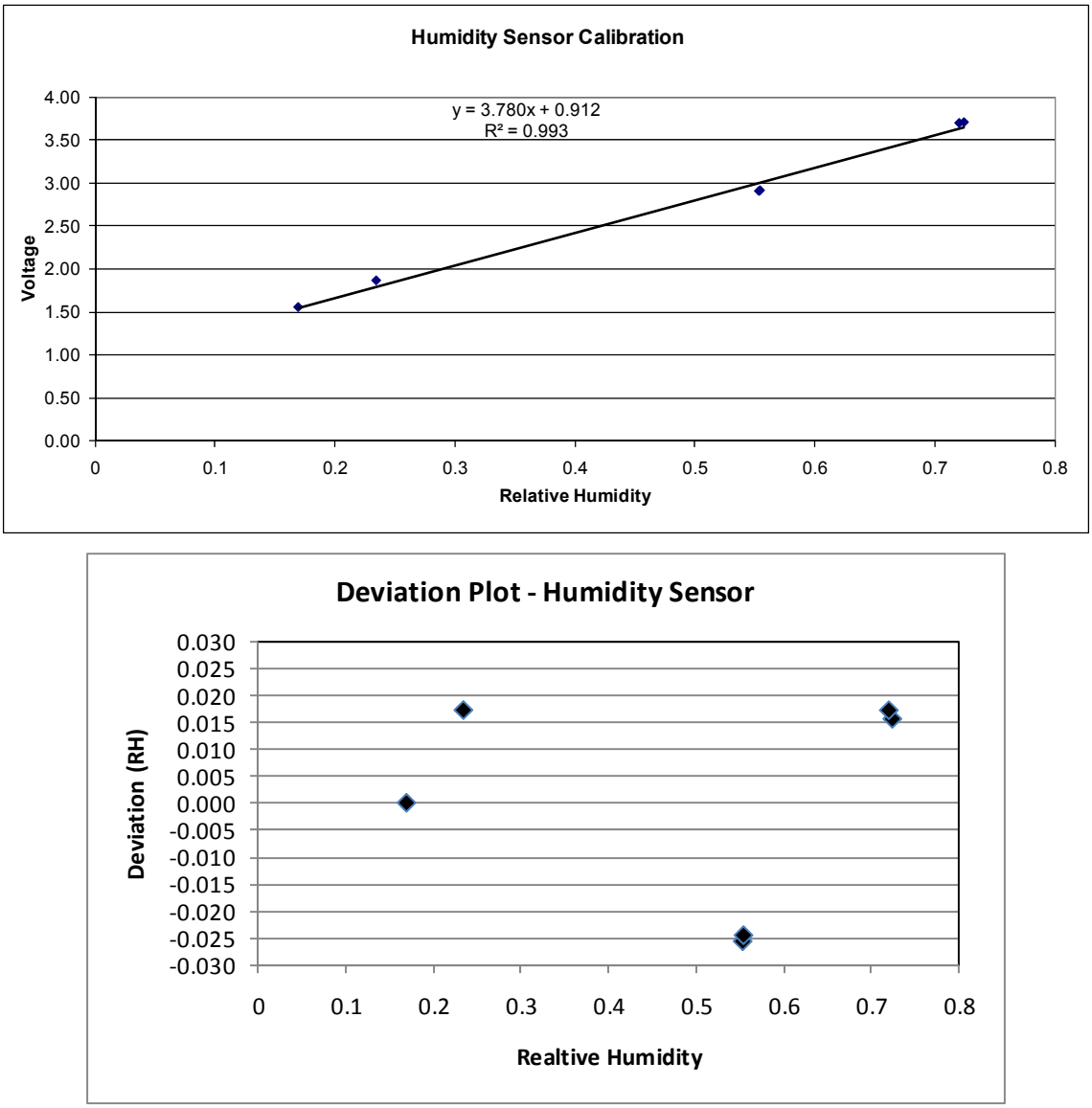

Figure C.7 Humidity Sensor Calibration

Appendix D - Instrument Specifications

Alnor EBT 720 Electronic Balancing Tool

Velocity: +/- 3.0% of reading

TSI VelociCalc Model 8347 Air Velocity Meter

Velocity: +/- 3.0% of reading

Temperature: +/- 0.3 ^{o}C + 0.03 ^{o}C/ ^{o}C for change in instrument temperature from 25 ^{o}C

Relative Humidity: +/-3%

Omega PX653 Pressure Transducers

Pressure: 0.25% full scale output (FSO) based on best fit line (BFL)

Setra 264 Pressure Transducers

Pressure: 0.25% full scale output (FSO) based on best fit line (BFL)

Paragon Controls FE-1500 Air Flow Measurement Station

Air Flow Rate: +/-2%

HyCal Model IH-3602 Humidity Sensor

Instrument specification

Relative Humidity: +/-2% at 25^{o}C and 5 Vdc excitation voltage

Project Calibration

Relative Humidity: +/-3%

Omega 44000 series 5,000 ohm thermistor

Interchangeability: +/-0.2^{o}C

Barometer

Scale Readability: 0.01” hg

Meriam Micromanometer Model 34FB2

Range 0 – 10” H2O

Uncertainty +/-0.003” H2O

Appendix E - Example Calculations

This appendix contains an example of the calculations used for this research. Two examples are shown. The first example is for data collected at 3 De upstream of the 90° Tee, the pitot-static probe, and log-Tchebycheff traverse at 7200 SCFM and Qb/Qc = 0.4. The second example is for 7.5 De downstream of the 90° Tee, the thermal anemometer, and equal area traverse at 7200 SCFM and Qb/Qc = 0.4. Example 1 includes calculations for air properties, the nozzle bank and the upstream log-Tchebycheff traverse. Example 2 includes calculations for the FMS and the downstream equal area traverse.

E.1 Example Data

E.1.1 Example 1 Data

The traverse data for example 1 is presented in Figure E.1 below. Multiple points were recorded with the LabView VI and averaged. The example uses one of those points where the following data point was recorded:

- Temperature inside Nozzle Chamber (t) 27.03° C
- Barometric Pressure (P) 98.70 kPa
- Relative Humidity Sensor Voltage for (ϕ) 2.254 Volts
- Omega Pressure Transducer Voltage for ($\Delta P_{s,\,1-2}$) 2.134 Volts
- Setra Pressure Transducer Voltage for (p_1) 2.547 Volts

These values are used with the instrument's calibration curves to achieve the pressure and humidity values.

$$\phi = \frac{\text{Voltage - } 0.912}{3.780} \tag{E.1}$$

$$\Delta P_{s,\,1-2} = \frac{\text{Voltage - } 1.0367}{0.4058} \tag{E.2}$$

$$P_1 = \frac{\text{Voltage - } 0.0327}{0.5025} \tag{E.3}$$

Relative Humidity: $\phi = 0.355$

Nozzle Pressure Drop: $\Delta P_{s,\,1-2} = 2.704$" H2O = 673.5 Pa

Nozzle Inlet Pressure: $P_1 = 5.004$" H2O = 1246.4 Pa

Initial Conditions				
Barometric Pressure "hg	29.28	Qb / Qc	0.4	
Barometer Temperature °C	77.60	Frequency hz	45.53	
Barometric Pressure kPa	98.70	Nozzles Plugged	none	
		Log-Tchebycheff		
1633	1728	1772	1779	1638
1746	2016	2046	2037	1758
1638	1932	2008	1991	1740
1607	1898	1820	1886	1718
1427	1669	1495	1606	1559

Figure E.1 Traverse Data - 90° Tee, 3 De Upstream, Pitot Probe, 1800 fpm

E.1.2 Example 2 Data

Traverse data for example 2 is presented in Figure E.2 below. Air property and nozzle bank calculations won't be repeated for example 2. The procedure for those is the same as example 1 described in E.2 and E.3 below. The following are the results of these calculations as well as other measured data required for the example. Multiple points were recorded with the LabView VI and averaged. The example uses the average of those points where the following data was recorded:

- Temperature inside Nozzle Chamber (t) 18.32° C
- Barometric Pressure (P) 97.64 kPa
- Air Viscosity (μ_o) 1.811e-5 $Pa \cdot s$
- Air Density (ρ_o) 1.1623 kg/m^3
- Nozzle Bank Flow Rate (Q_{SCFM}(Nozzle Bank)) 7218.3 SCFM
- Omega 5.0" Pressure Transducer Voltage for (P_v) 2.118 Volts

The value of the pressure transducer output is used with the instrument's calibration curve to achieve the dynamic pressure. In this case a quadratic equation was used because it produced lower deviations than a linear curve.

$$P_v = -0.0189\text{Voltage}^2 + 1.3814\text{Voltage} - 1.3862 \quad \textbf{(E.4)}$$

$P_V = 1.455$" H2O = 362.4 Pa

Initial Conditions			
Barometric Pressure "hg	28.92	Qb / Qc	0.4
Barometer Temperature °F	62.00	Frequency hz	44.60
Barometric Pressure kPa	97.64	Nozzles Plugged	None
		Equal Area	
1155	1220	1410	1825
1230	1290	1540	1860
1255	1445	1745	1940

Figure E.2 Traverse Data - 90° Tee, 7.5 De Downstream, Anemometer, 1800 fpm

E.2 Example Air Property Calculations

This air property example is based on data for example 1 presented in E.1.1 above. The viscosity and density are calculated below.

E.2.1 Example Air Viscosity Calculation

The air viscosity at the nozzle inlet is a function of temperature and can be calculated from ASHRAE Standard 120 section 9 Equation 5. The viscosity at the nozzle inlet is calculated; however, later equations require the viscosity at the nozzle outlet. The viscosity at the inlet can be used because the temperature doesn't drastically change across the nozzle. Also standard l20 allows for the viscosity to be assumed constant over the range of 4°C to 32°C.

$$\mu_o = (17.23 + 0.048t)10^{-6} \quad \textbf{(E.5)}$$

$\mu_o = 1.853\text{e-}5 \ \text{Pa} \cdot \text{s}$

E.2.2 Example Air Density Calculation

The equations for calculating air density come from ASHRAE Fundamentals chapter 6. The method is as follows:

Step 1: *Calculation of Saturation Pressure*

The saturation pressure $P_{ws}(T)$ is calculated using Equation 6 of chapter 6 as follows:

$$\ln(P_{ws}(T)) = \frac{C_8}{T} + C_9 + C_{10}T + C_{11}T^2 + C_{12}T^3 + C_{13}\ln(T) \qquad \textbf{(E.6)}$$

Where T = t + 273.15

And the constants in Equation (E.6) are given in Table E.1.

P_{ws} = 3573.6 Pa = 3.5736 kPa

Table E.1 Saturation Pressure Equation Constants

Constants	
C8	-5.8002206E+03
C9	1.3914993E+00
C10	-4.8640239E-02
C11	4.1764768E-05
C12	-1.4452093E-08
C13	6.5459673E+00

Step 2: *Calculation of Partial Vapor Pressure*

The partial vapor pressure P_w is calculated using the saturation pressure and the relative humidity.

$$P_w = \phi P_{ws}(T) \qquad \textbf{(E.7)}$$

P_w = 1.2686 kPa

Step 3: *Calculation of Humidity Ratio*

The humidity ratio ω is calculated from the partial vapor pressure and barometric pressure.

$$\omega = 0.62198 * \frac{P_w}{P - P_w} \qquad \textbf{(E.8)}$$

ω = 0.00810

Step 4: *Calculation of Specific Volume per mass of dry air*

The specific volume per mass of dry air ν is calculated from the humidity ratio, dry bulb temperature, and barometric pressure P.

$$\nu = R_{da} * T * \frac{(1 + 1.6078 * \omega)}{P} \quad \textbf{(E.9)}$$

$\nu = 0.8844$ m^3/kg

Step 5: Calculation of Air Density

The air density ρ_o is calculated from the specific volume and the humidity ratio.

$$\rho_o = \frac{1 + \omega}{\nu} \quad \textbf{(E.10)}$$

$\rho_o = 1.1399$ kg/m^3

Step 6: Correction to Air Density

There is a correction to the air density for temperature and pressure since these could be different in the nozzle chamber than the general test site. The temperature was measured in the nozzle chamber so no correction is required for it. The pressure correction is made with Equation 4 of ASHRAE Standard 120 section 9.

$$\rho_1 = \rho_o \frac{P_1 + 1000P}{1000P} \quad \textbf{(E.11)}$$

$\rho_1 = 1.1543$ kg/m^3

E.3 Example Nozzle Bank Flow Rate Calculations

This nozzle bank flow rate calculation example is based on data for example 1 presented in E.1.1 above. The volumetric flow rate through the nozzle chamber is determined with procedure and equations in Chapter 3.

E.3.1 Example Alpha Ratio Calculation

$$\alpha = 1 - \frac{\Delta P_{s,\ 1\text{ - }2}}{P_1 + 1000P} \quad \textbf{(E.12)}$$

$\alpha = 0.99326$

E.3.2 Example Beta Ratio Calculation

The beta ratio β is the ratio of nozzle throat diameter to the approach duct diameter. For the chamber the beta ratio can be assumed to be zero.

$$\beta = d / D \qquad \textbf{(E.13)}$$

$\beta \cong 0.00$

E.3.3 Example Nozzle Expansion Factor Calculation

The nozzle expansion factor Y_n is a function of alpha ratio, beta ratio, and the specific heat ratio. In this case it is the same for all nozzles. The specific heat ratio γ may be taken as 1.402 according to ASHRAE Standard 120.

$$Y_n = \left(\frac{\gamma}{\gamma - 1} (\alpha^{2/\gamma}) \frac{1 - \alpha^{(\gamma-1)/\gamma}}{1 - \alpha} \frac{1 - \beta^4}{1 - \beta^4 \alpha^{2/\gamma}} \right)^{\frac{1}{2}} \qquad \textbf{(E.14)}$$

$Y_n = 0.99639$

E.3.4 Example Nozzle Discharge Coefficient Calculation

A discharge coefficient must be computed for each nozzle; however, some nozzles are the same and will have the same discharge coefficient. The subscript (n) represents the nozzle number 1 through 9. This example will show the procedure for nozzle 1 and report the result for other nozzles. In this case for 7200 SCFM, all nozzles are used and none are plugged. An initial estimate of Re must first be computed. The equation for this estimate is similar to the actual version of the equation with some assumptions made.

$$Re_{d_n} = 70,900 d_n \sqrt{\rho_1 \Delta P_{s,\,1-2}} \qquad \textbf{(E.15)}$$

Re_{d_1} (Initial Guess) = 250156.4

With an initial estimate of Re the iterative process with the equation below can be performed to obtain the discharge coefficient for each nozzle (C_n). The nozzle diameters (d_n) are available in Table 2.1. It was shown in Chapter 3 that one iteration is sufficient.

$$C_n = 0.9965 - 0.00653 \sqrt{\frac{10^6}{Re_{d_n}}} \qquad \textbf{(E.16)}$$

C_1 (Initial Guess) = 0.98344

$$Re_{d_n} = \frac{1.414 C_n d_n Y_n}{\mu_o} \sqrt{\rho_1 \Delta P_{s,\,1-2}} \qquad \textbf{(E.17)}$$

Re_{d_1} (1st Iteration) = 264819.0

C_1 (1st Iteration) = 0.98381

C_2 (1st Iteration) = 0.98492

C_3 (1st Iteration) = 0.98440

C_4 (1st Iteration) = 0.98230

C_5 (1st Iteration) = 0.97395

C_6 (1st Iteration) = 0.97851

C_7 (1st Iteration) = 0.98381

C_8 (1st Iteration) = 0.98492

C_9 (1st Iteration) = 0.98440

E.3.5 Example Volumetric Air Flow Rate Calculation

The volumetric flow rate is determined from Equation 4 of Chapter 3 and the nozzle areas were presented in Table 2.1.

$$Q = 1414 Y_n \sqrt{\frac{\Delta P_{s,\,1-2}}{\rho_1}} \Sigma(C_n A_n) \qquad \textbf{(E.18)}$$

Q = 3517.7 L/s = 7453.6 ACFM

A correction must be made to standard density with Equation 14 of Chapter 3.

$$Q_{SCFM} = Q_{ACFM} \left(\frac{P}{T}\right)\left(\frac{21.1 + 273.15}{101.325}\right) \qquad \textbf{(E.19)}$$

Q_{SCFM} (Nozzle Bank) = 7207.2 SCFM

E.4 Example 1 Traverse Flow Rate and Error Calculations

E.4.1 Example 1 Traverse Flow Rate Calculation

The traverse flow rate is simply calculated from the average of the velocity measurements in the traverse and the duct area which is 4 ft^2 in this case. The EBT 720 has already converted the velocity measurements to standard density. The average velocity of the traverse points in Figure E.1 is the following:

V_{AVG} = 1765.9 SFPM

$$Q_{Traverse} = V_{AVG} A_{duct} \qquad \textbf{(E.20)}$$

$Q_{Traverse}$ = 7063.6 SCFM

E.4.2 Example 1 Traverse Error Calculation

For the tee, Equations 34 and 35 of Chapter 6 are used to calculate the error in a traverse downstream of the disturbance. In this case Equations 34 and 36 of Chapter 6 are used because the measurement is upstream of the tee before the flow diverges. The data for example 1 and the flow rate calculated in example E.3 is for one of several points measured with LabView. The flow rates of all the points are averaged and the result ($Q_{SCFM}(\text{Standard})$) is used to determine the measurement standard.

$$Q_{SCFM}(\text{Standard}) = Q_{SCFM}(\text{Nozzle Bank}) \quad \textbf{(E.21)}$$

$Q_{SCFM}(\text{Standard})$ = 7197.9 SCFM

The measurement standard along with the traverse flow rate determined in E.4.1 is used to determine the error in the traverse. The result is the same as in the data presented in Appendix B Figure B.24.

$$\text{Error} = \frac{Q_{SCFM}(\text{Traverse}) - Q_{SCFM}(\text{Standard})}{Q_{SCFM}(\text{Standard})} 100\% \quad \textbf{(E.22)}$$

Error = -1.87%

E.5 Example FMS Calculation

This FMS example is based on data for example 2 presented in E.1.2 above. The FMS calculation uses the FMS calibration curve and equations discussed in Chapter 3. The air density is assumed to be the same as the density at the nozzle chamber calculated with Equation (E.10) prior to the pressure correction. The viscosity is assumed to be the same as at the nozzle chamber. The following constants apply to the FMS.

- d_{tube} = 9/16" = 0.0143 m
- A_{ratio} = 1.1034

An initial guess of the Reynolds number is determined from the measured velocity pressure at the FMS assuming a flow coefficient (C) of 1 with Equation 8 of Chapter 3.

$$\text{Re} = \frac{\rho_o d_{tube}}{\mu_o}\left(\frac{2P_v}{C\rho_o}\right)^{\frac{1}{2}} \quad \textbf{(E.23)}$$

Re (Initial Guess) = 22918.5

The initial guess of the flow coefficient is then determined by Equations 10 and 12 of Chapter 3.

$$C = C^* A_{ratio}{}^2 \quad \textbf{(E.24)}$$

$$C^* = -1.36\ e-4\left(\frac{Re}{10^3}\right)^2 + 8.20e-3\left(\frac{Re}{10^3}\right) + 9.06997e-1 \quad \textbf{(E.25)}$$

C^* (1^{st} Iteration) = 1.0235

C (1^{st} Iteration) = 1.2461

An iterative process with Equations (E.23) and (E.25) are used to determine the final flow coefficient and Reynolds number. Two iterations were used to determine the final Reynolds.

Re (1^{st} Iteration) = 20531.0

C^* (2nd Iteration) = 1.0180

C (2nd Iteration) = 1.2394

Re (2nd Iteration) = 20586.4

The final Reynolds number is used to determine the average velocity of the FMS.

$$V_{FMS} = \frac{Re\mu_o}{\rho_o d_{tube}} \quad \textbf{(E.26)}$$

V_{FMS} = 22.431 m/s = 4415.6 fpm

The average velocity along with the nominal area of the FMS of 1 ft^2 can be used to determine the flow rate through the FMS.

$$Q_{FMS} = V_{FMS}\left(\text{FMS Area}\right) \quad \textbf{(E.27)}$$

Q_{FMS} = 4415.6 CFM

A correction must be made to standard density with Equation 14 of Chapter 3.

$$Q_{SCFM} = Q_{ACFM}\left(\frac{P}{T}\right)\left(\frac{21.1+273.15}{101.325}\right) \quad \textbf{(E.28)}$$

Q_{SCFM}(FMS) = 4295.6 SCFM

E.6 Example 2 Traverse Flow Rate and Error Calculations

E.6.1 Example 2 Traverse Flow Rate Calculation

The traverse flow rate is simply calculated from the average of the velocity measurements in the traverse and the duct area which is 2 ft^2 in this case. The anemometer has already given the velocity measurements at standard density. The average velocity of the traverse points in Figure E.2 is the following:

V_{AVG} = 1492.9 SFPM

$$Q_{Traverse} = V_{AVG} A_{duct} \quad \textbf{(E.29)}$$

$Q_{Traverse}$ = 2985.8 SCFM

E.6.2 Example 2 Traverse Error Calculation

For the tee, Equations 34 and 35 of Chapter 6 are used to calculate the error in a traverse downstream of the disturbance. The nozzle bank flow rate provided in E.1.2 and the FMS flow rate calculated in section E.5 are used to determine the measurement standard.

$$Q_{SCFM}(\text{Standard}) = Q_{SCFM}(\text{Nozzle Bank}) - Q_{SCFM}(\text{FMS}) \quad \textbf{(E.30)}$$

$Q_{SCFM}(\text{Standard})$ = 2922.7 SCFM

The measurement standard along with the traverse flow rate determined in E.6.1 is used to determine the error in the traverse. The result is close to the data presented in Appendix B Figure B.24. There is a slight difference due to rounding in this example.

$$\text{Error} = \frac{Q_{SCFM}(\text{Traverse}) - Q_{SCFM}(\text{Standard})}{Q_{SCFM}(\text{Standard})} 100\% \quad \textbf{(E.31)}$$

Error = 2.16%

Appendix F - LabView Files

A computer using LabView 7 and Microsoft Windows XP was used in conjunction with the Hewlett Packard 34970A Data Acquisition / Switch Unit to take measurements. Two LabView VIs were used for the project, one for non-tee measurements and one for tee measurements. The reason for the two is that tee VI includes measurements for the FMS and the non-tee does not. Figures F.1 and F.2 show the front panels of the Vis where the user inputs information and can see the output. The white boxes are inputs and the gray shaded boxes are outputs. The user inputs a 1 or 0 for each nozzle to indicate if the nozzle is plugged (0) or open (1). Figures F.3 and F.4 show the block diagrams for non-tee and tee measurements respectively. The details of the block diagrams are difficult to read because of the large size. The remaining figures separate the block diagrams into quadrants making it easier to see details.

F.1 LabView Front Panels

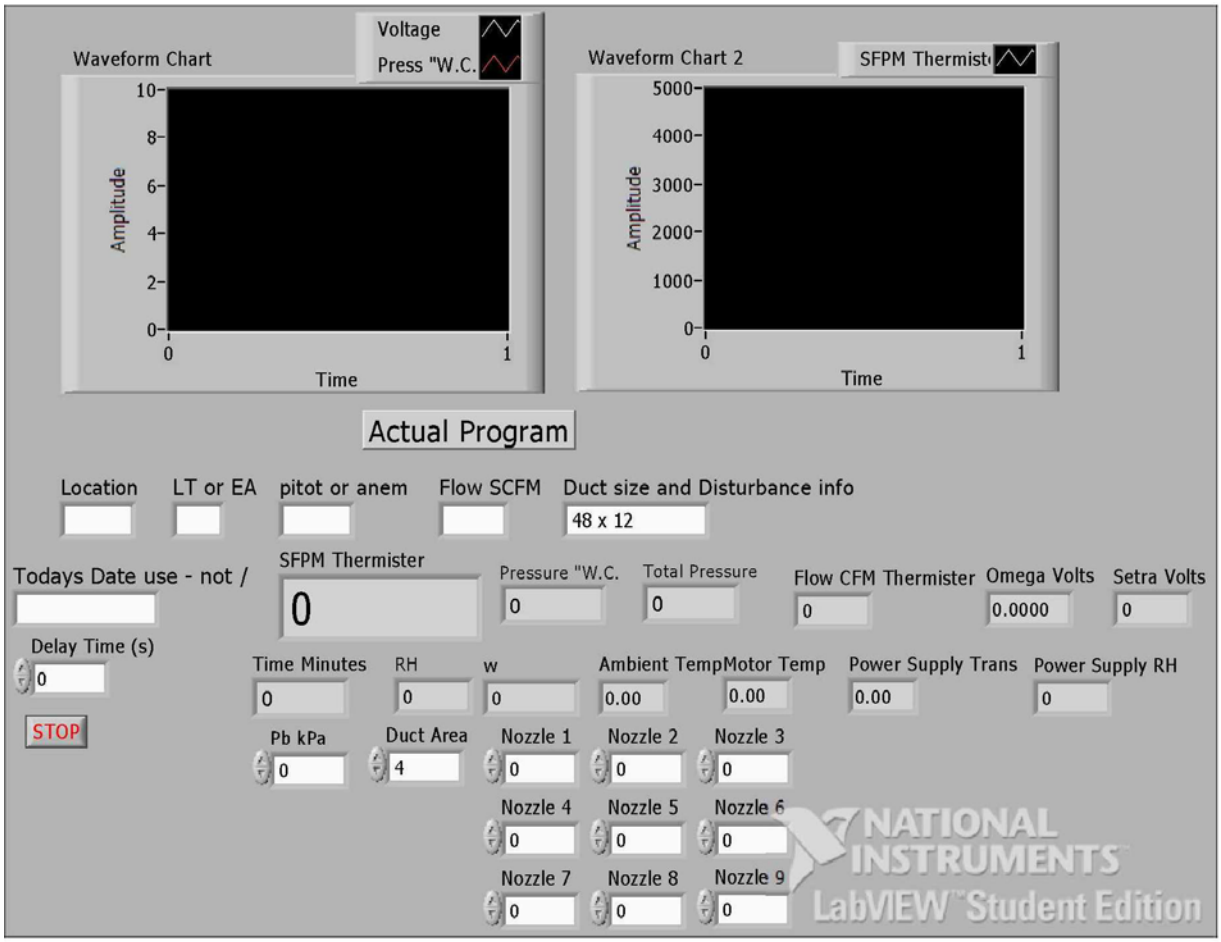

Figure F.1 LabView Front Panel, Non-Tee Measurements

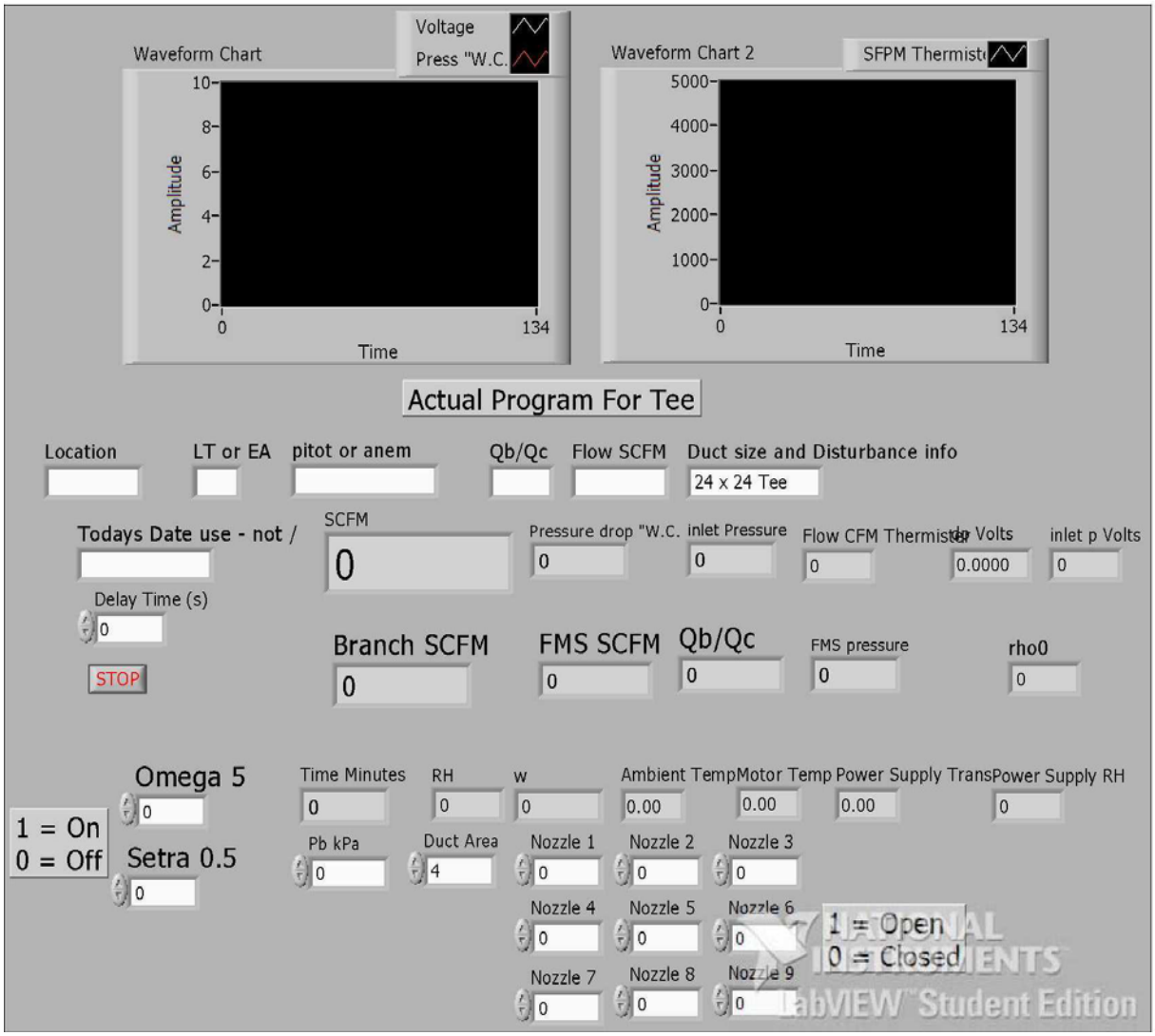

Figure F.2 LabView Font Panel, Tee Measurements

F.2 LabView Block Diagrams

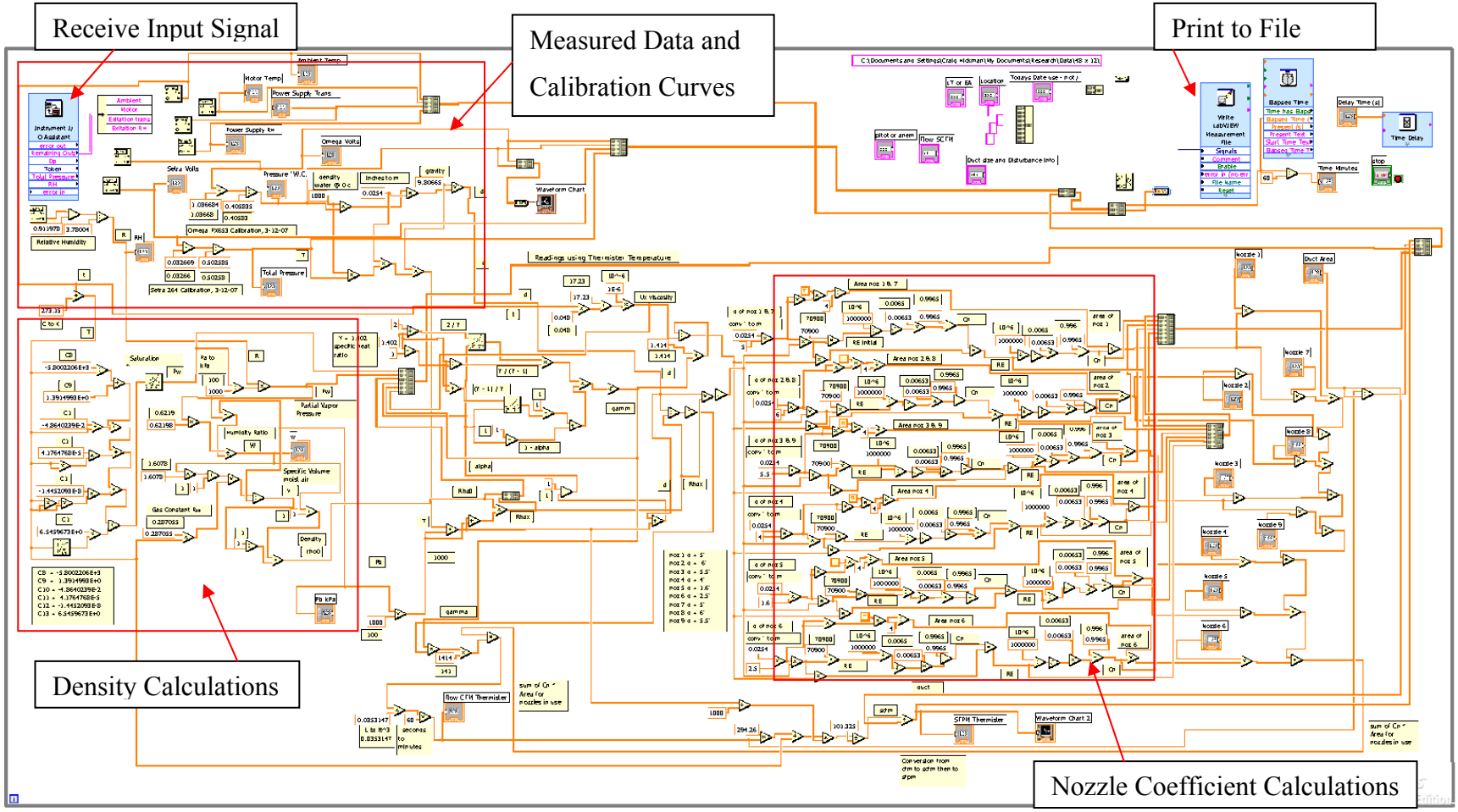

Figure F.3 LabView Block Diagram, Non-Tee Measurements

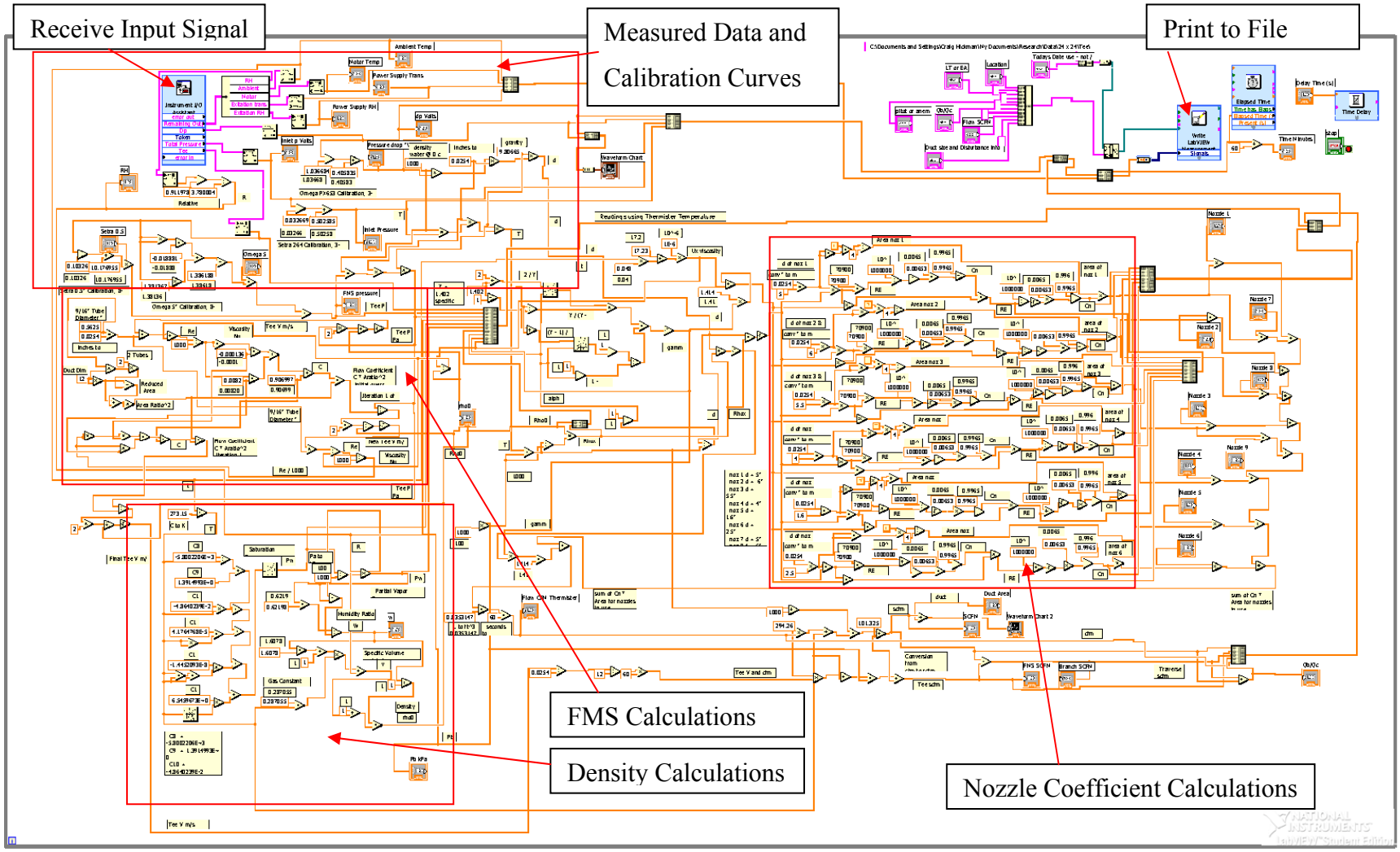

Figure F.4 LabView Block Diagram, Tee Measurements

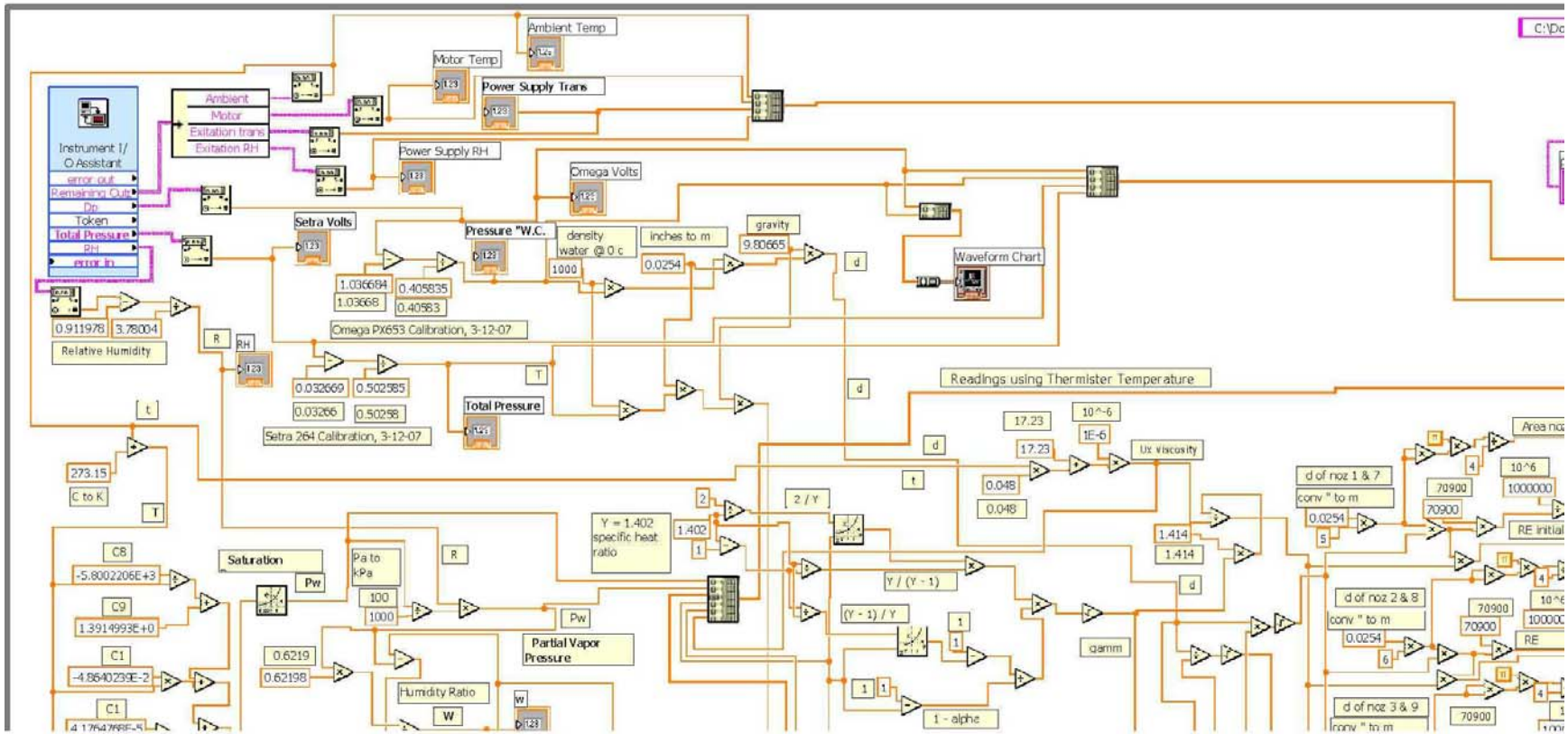

Figure F.5 LabView Block Diagram for Non-Tee, Upper Left Corner

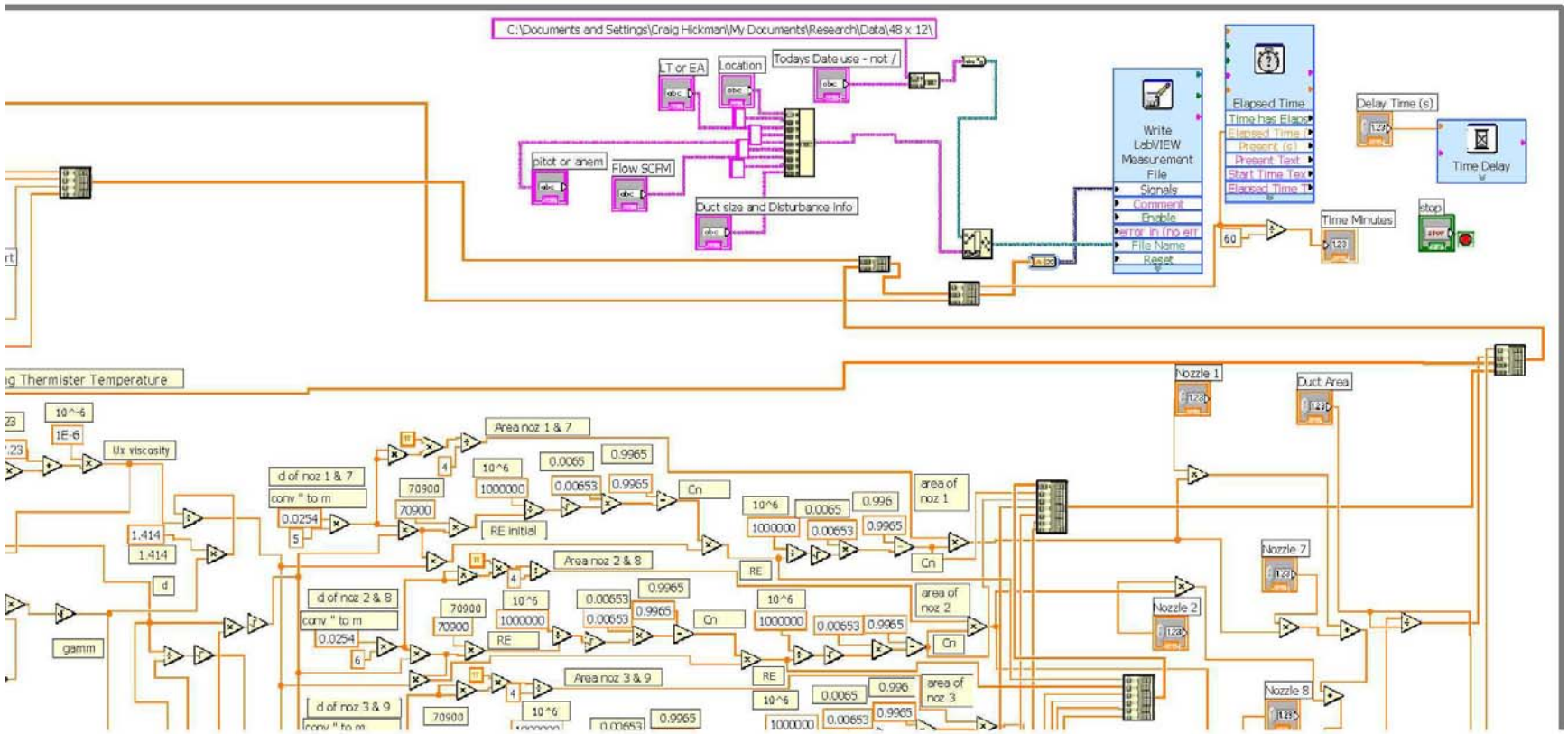

Figure F.6 LabView Block Diagram for Non-Tee, Upper Right Corner

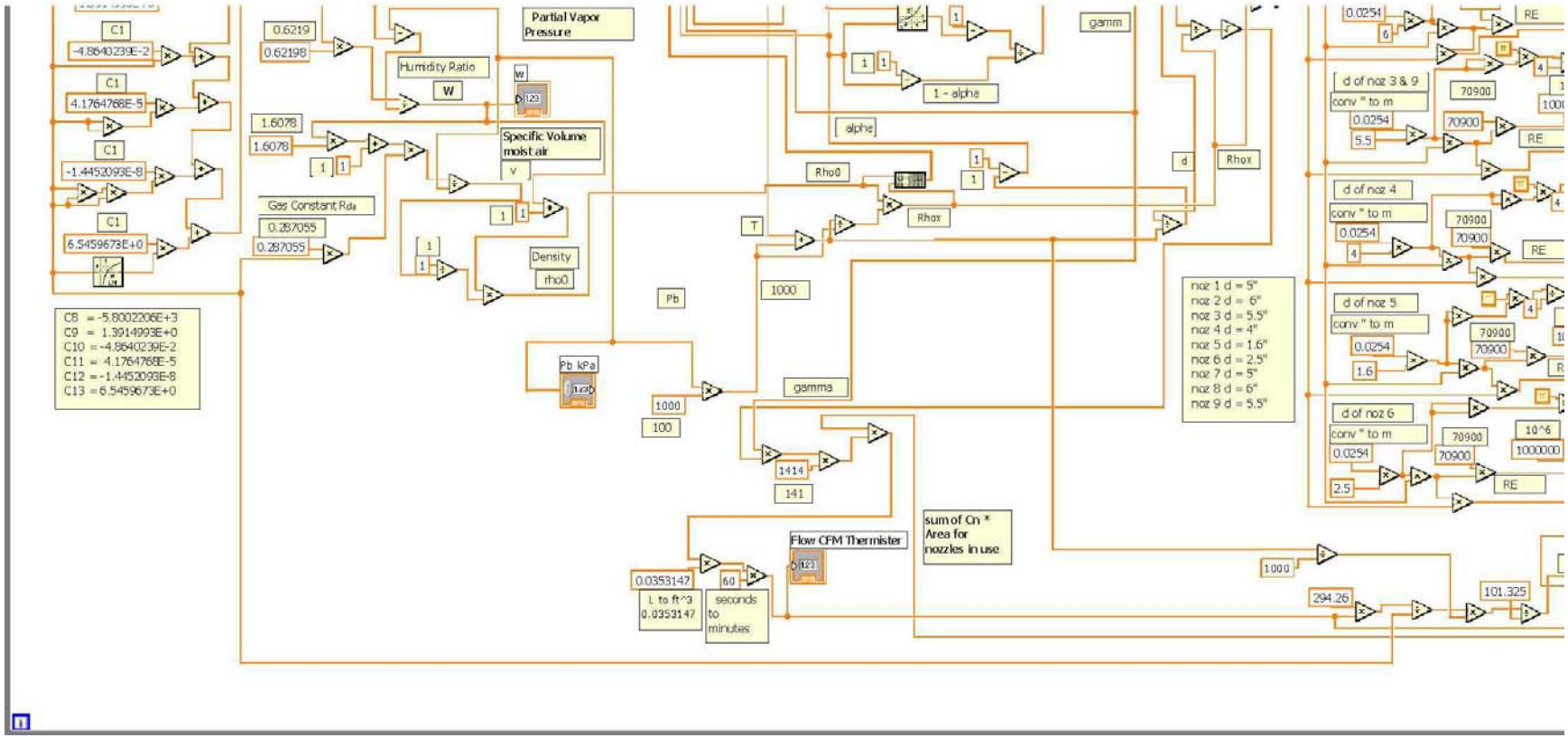

Figure F.7 LabView Block Diagram for Non-Tee, Lower Left Corner

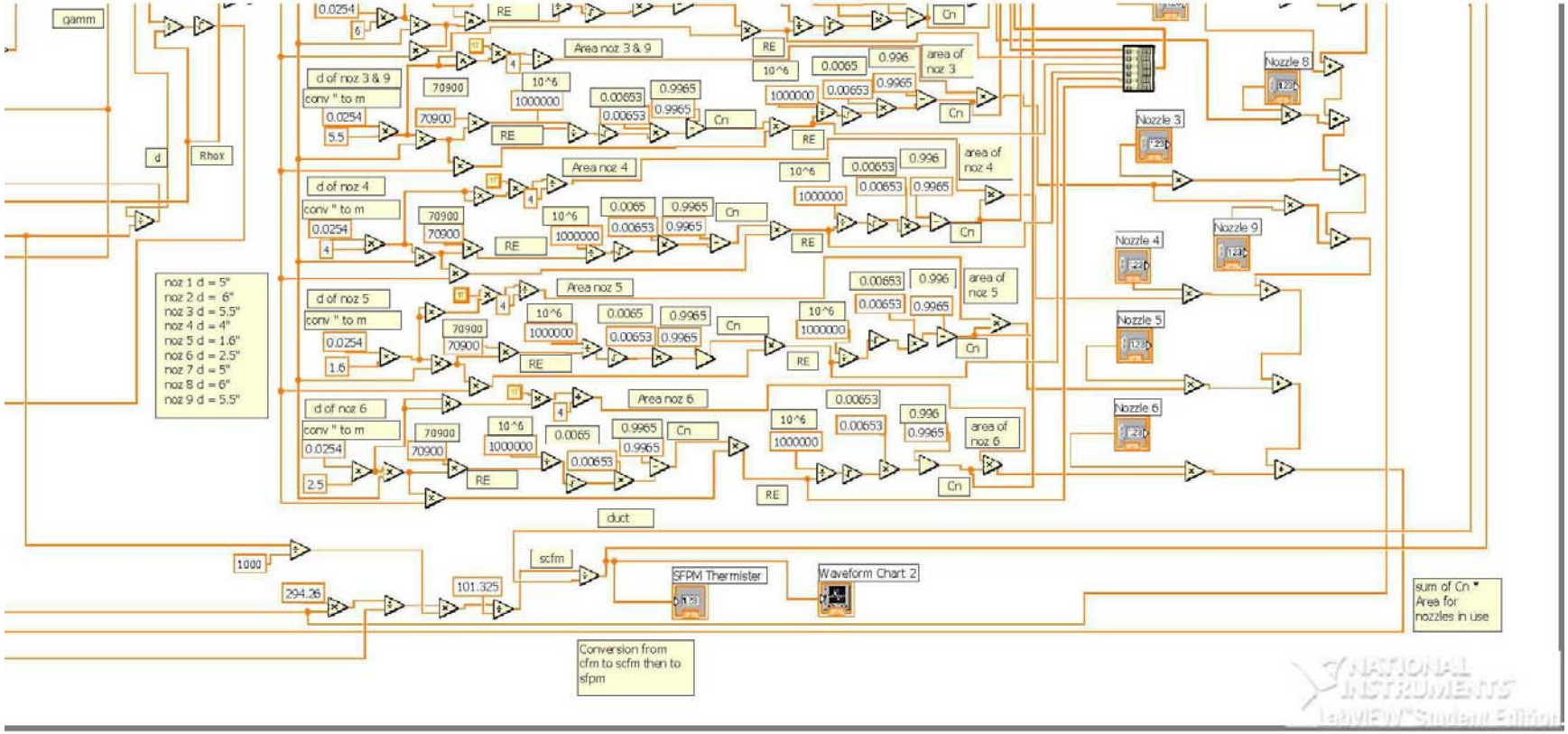

Figure F.8 LabView Block Diagram for Non-Tee, Lower Right Corner

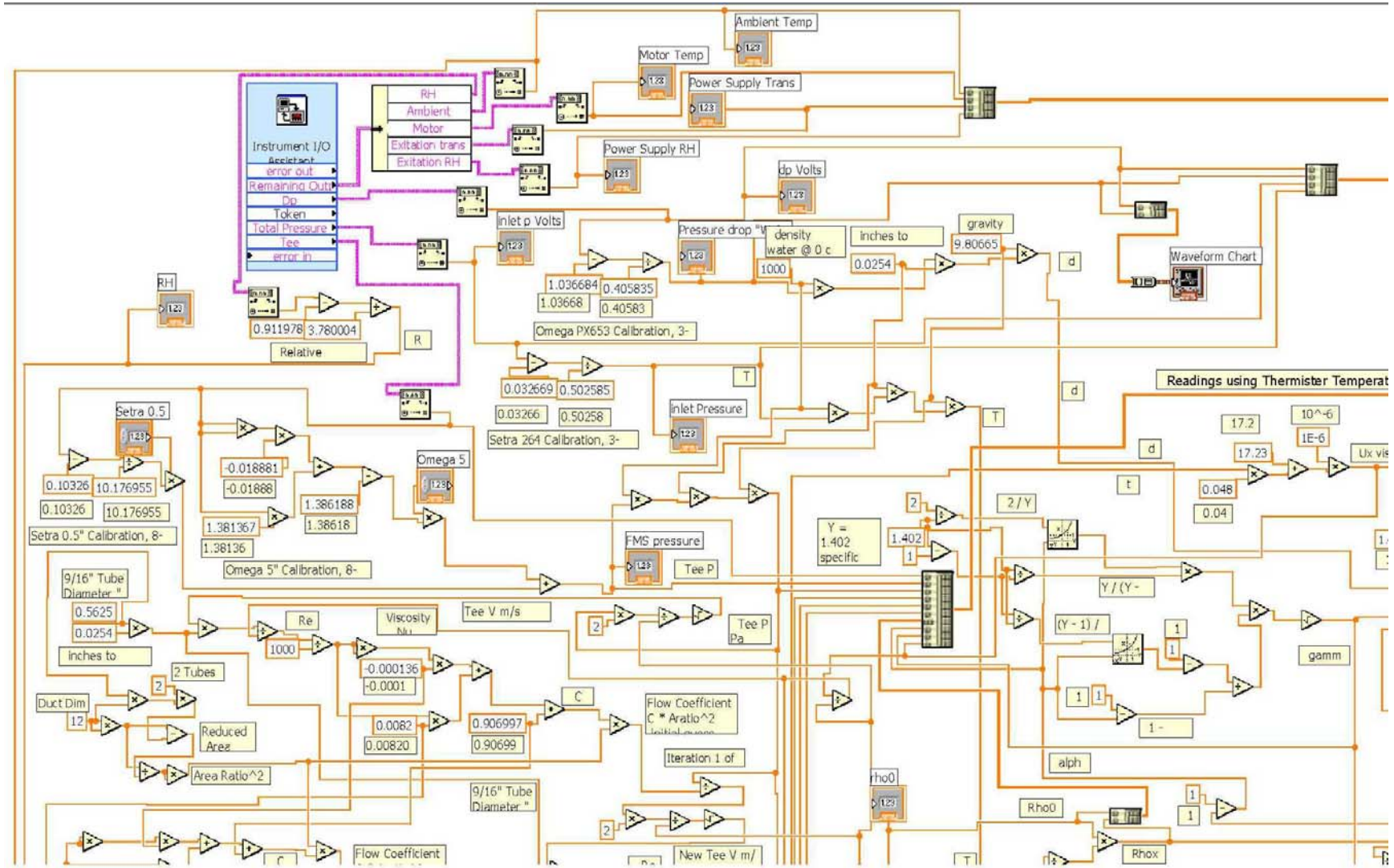

Figure F.9 LabView Block Diagram for Tee, Upper Left Corner

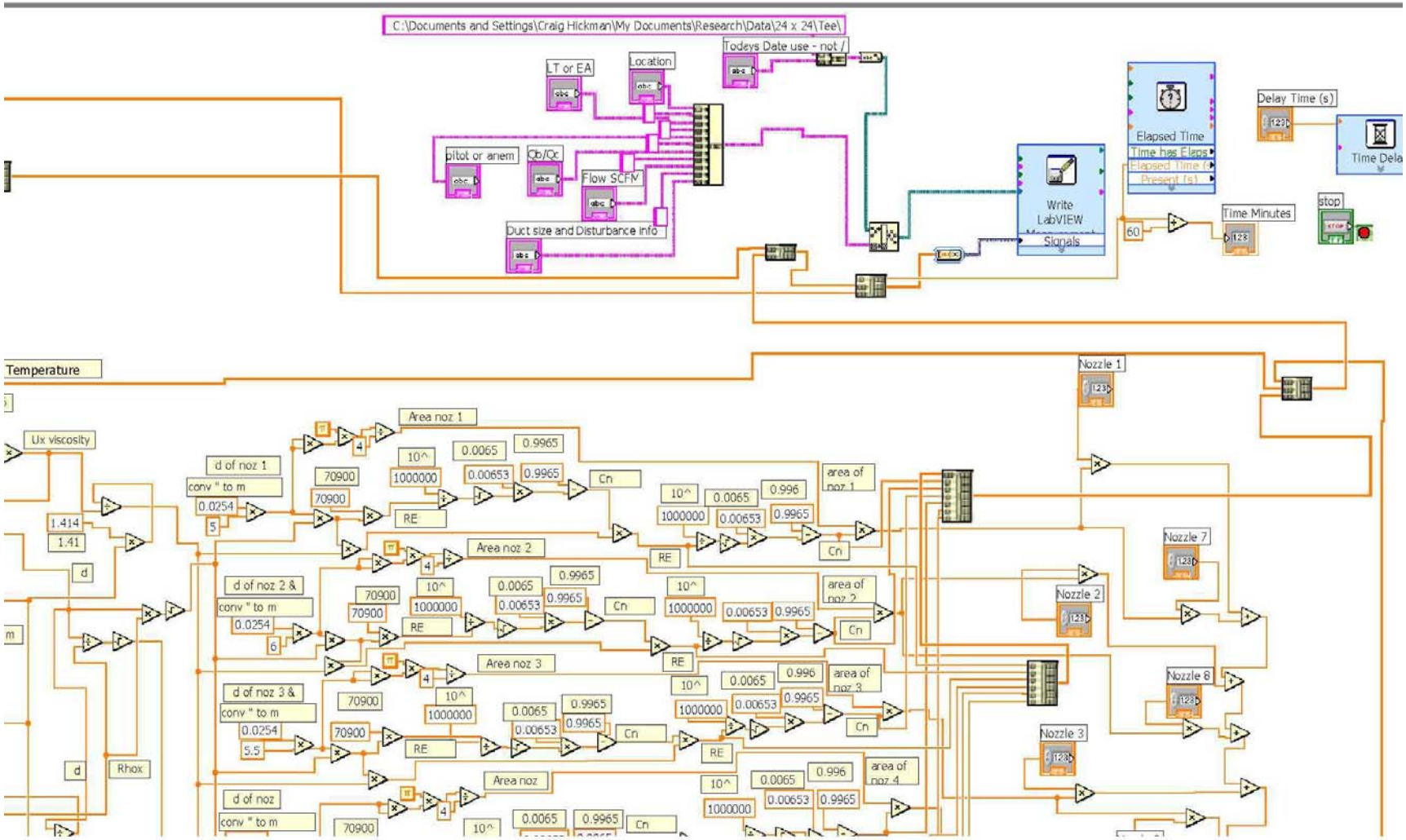

Figure F.10 LabView Block Diagram for Tee, Upper Right Corner

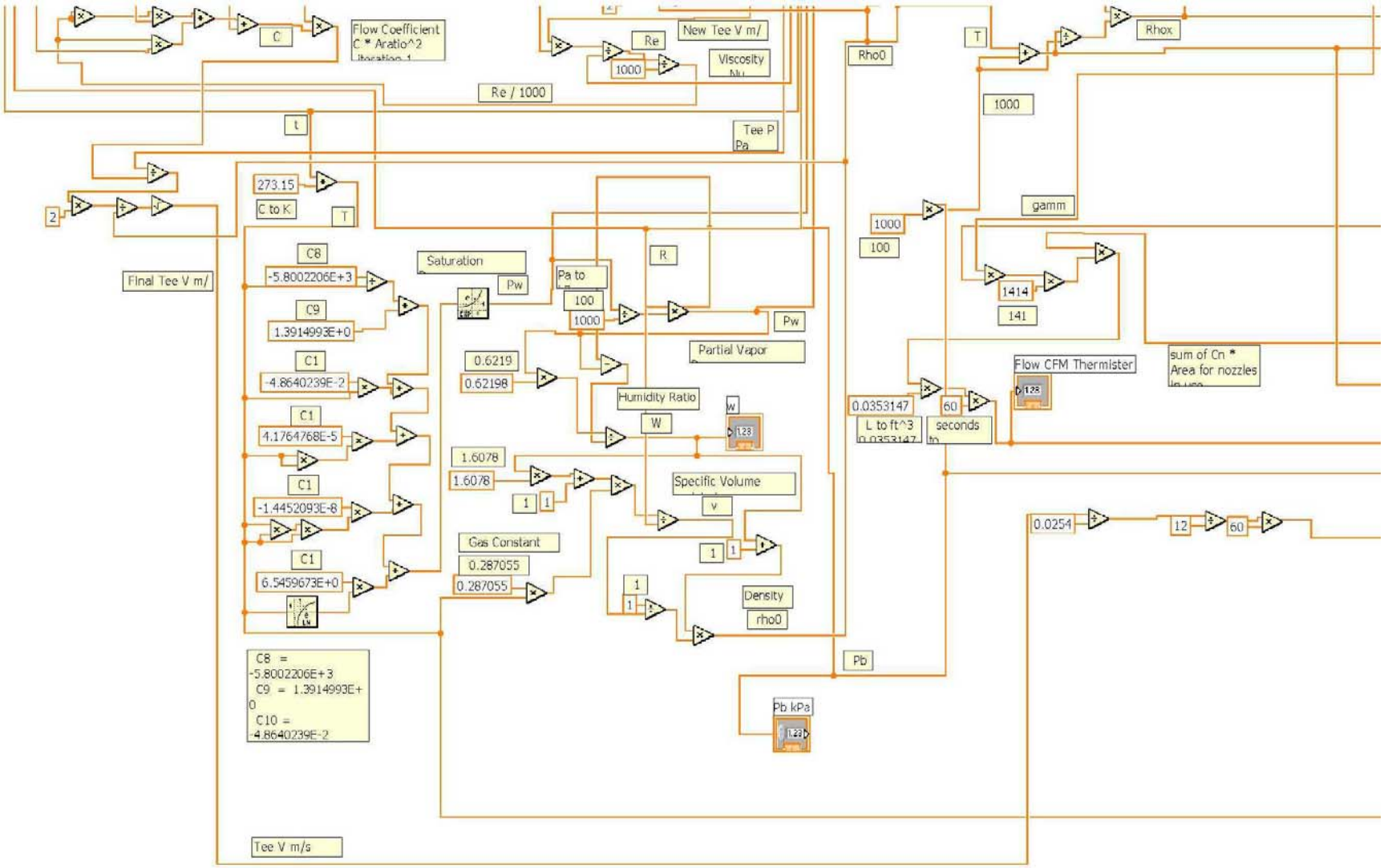

Figure F.11 LabView Block Diagram for Tee, Lower Left Corner

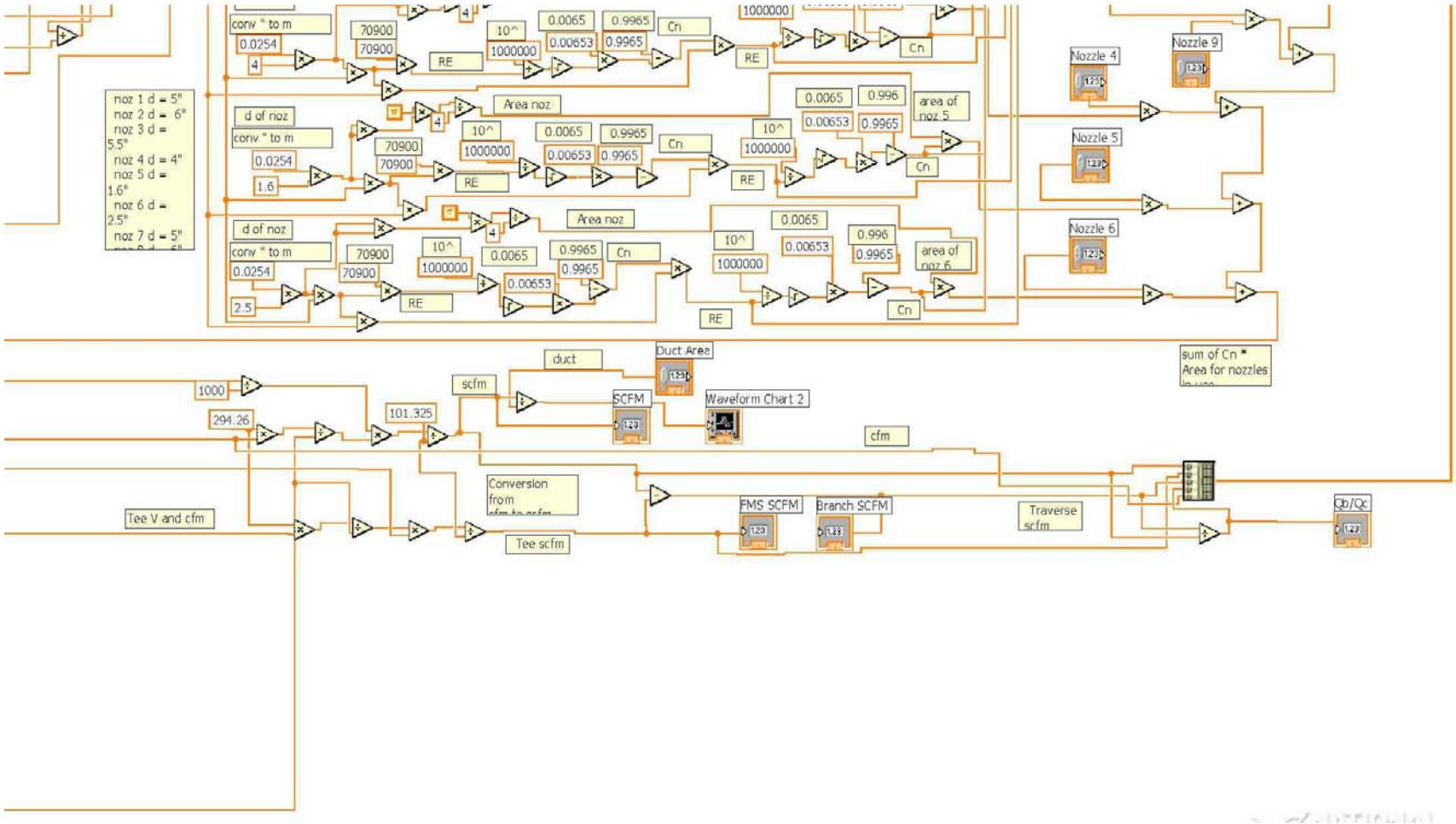

Figure F.12 LabView Block Diagram for Tee, Lower Right Corner